

Master Thesis in Geosciences

**Paleogene depositional conditions and
climatic changes of the Frysjaodden
Formation in central Spitsbergen
(sedimentology and mineralogy)**

Lars Riber



UNIVERSITY OF OSLO
FACULTY OF MATHEMATICS AND NATURAL SCIENCES

**Paleogene depositional conditions and
climatic changes of the Frysjaodden
Formation in central Spitsbergen
(sedimentology and mineralogy)**

Lars Riber



Master Thesis in Geosciences

Discipline: Petroleum geology and Petroleum geophysics

Department of Geosciences

Faculty of Mathematics and Natural Sciences

UNIVERSITY OF OSLO

June 2nd, 2009

© **Lars Riber, 2009**

Tutor(s): Henning Dypvik and Jenö Nagy, UIO

This work is published digitally through DUO – Digitale Utgivelser ved UiO

<http://www.duo.uio.no>

It is also catalogued in BIBSYS (<http://www.bibsys.no/english>)

All rights reserved. No part of this publication may be reproduced or transmitted, in any form or by any means, without permission.

Abstract

In this study the transgressive-regressive developments and depositional environment of the Frysjaodden Formation in the Central Tertiary Basin, Spitsbergen have been reconstructed. The depositional environment has been analyzed combining sedimentary field data, XRD and geochemical analyses. Special emphasis has been on clay minerals as an indicator of paleoclimate and the presence of one of the most abrupt and dramatic climatic events in the Cenozoic era; the Paleocene Eocene Thermal Maximum.

The studied section, core BH 9/05, displays a shallowing upwards development from the Grumantbyen Formation to the Gilsonryggen Member of Frysjaodden Formation. The maximum flooding zone has been identified in the basal Gilsonryggen Member based on shale characteristics, pyrite content and Th/U ratio. The upper parts of the section display a regressive development from the dark gray, laminated shales of lower/middle Gilsonryggen Member to the soft-sediment deformed siltstones and hummocky cross-stratified sandstones of the upper Gilsonryggen Member/Lower Battfjellet Formation.

The PETM has been identified just below maximum transgression in the lower parts of Gilsonryggen Member. The presence of PETM is based on kaolinite/(kaolinite + chlorite) and kaolinite/(kaolinite + illite) ratios and benthic foraminifera extinction coinciding with earlier $\delta^{13}\text{C}$ studies. Furthermore, the stratigraphic position coincides with the position of PETM in other studies from the Arctic and Antarctic.

Keywords: Svalbard, Frysjaodden Formation, PETM, sedimentology, XRD, clay mineralogy, kaolinite peak

Contents

Abstract	5
1 Introduction	8
2 Regional setting	9
2.1 <i>Tectonostratigraphic development</i>	9
2.2 <i>Lithostratigraphic setting</i>	13
2.3 <i>Paleogeography</i>	16
3 Paleoclimate	17
3.1 <i>Paleocene- Eocene Thermal Maximum (PETM)</i>	18
3.2 <i>Consequences of the PETM</i>	19
3.3 <i>Mechanisms of climate warming</i>	20
4 Methods and material	21
4.1 <i>Sedimentological core logging</i>	21
4.2 <i>Sampling</i>	21
4.3 <i>Facies description and facies associations</i>	21
4.4 <i>Mineralogical and petrographical analysis</i>	23
4.4.1 <i>Thin sections</i>	23
4.4.2 <i>XRD analysis</i>	24
4.5 <i>Geochemical Analyses</i>	29
4.6 <i>Sequence stratigraphy</i>	31
5 Sedimentological description	32
5.1 <i>Facies description</i>	33
5.2 <i>Facies associations</i>	41
5.2.1 <i>FA1: Upper Grumantbyen sandstone association (560 – 551,60 m)</i>	41
5.2.2 <i>FA2: Shales of lower/middle Gilsonryggen (551,60 m -280,00 m)</i>	41
5.2.3 <i>FA3: Upper Gilsonryggen siltstones (280 m – 150 m)</i>	44
5.2.4 <i>FA4: Upper Gilsonryggen / Lower Battfjellet sandstones (150,00 m – 110,00 m)</i>	45
6 Mineralogical and petrographical description	46
6.1 <i>Thin section analysis</i>	46
6.1.1 <i>Sandstones of Grumantbyen Formation (560,00 m -551,60 m)</i>	46
6.1.2 <i>Lower Gilsonryggen shales (part one): (551,60 m – 532,00 m)</i>	47
6.1.3 <i>Lower Gilsonryggen shales (part two), (532,00 m – 500,00 m)</i>	49
6.1.4 <i>Middle Gilsonryggen shales (part one), (500,00 m – 408,00 m)</i>	50
6.1.5 <i>Middle Gilsonryggen shales (part two), (408,00 m – 280,00 m)</i>	51
6.1.6 <i>Siltstones of upper Gilsonryggen (280,00 m– 150,00 m)</i>	52
6.1.7 <i>Sandstones of upper Gilsonryggen Member (150,00 m – 110,05 m)</i>	53
6.2 <i>XRD analysis</i>	55
6.2.1 <i>Bulk analysis</i>	55
6.2.2 <i>Clay separation</i>	67
6.2.3 <i>Removal of iron oxide by Na-Citrate:</i>	69
7 Geochemical analysis	71
7.1 <i>Rock-Eval analysis</i>	71
7.2 <i>TOC, CaCO₃ and Th/U analysis</i>	73
7.2.1 <i>CaCO₃</i>	73

7.2.2 TOC	73
7.2.3 Th/U.....	73
8 Discussion of data and reconstruction of depositional environment	75
8.1 <i>Lowstand systems tract (560 m - 551,60 m)</i>	77
8.1.1 Sandstones of Grumantbyen Formation (560,00 m -551,60 m)	77
8.2 <i>Transgressive systems tract (551,60 m –500 m)</i>	80
8.2.1 Shales of Gilsonryggen Member	80
8.3 <i>High stand systems tract (500 m-110 m)</i>	84
8.3.1 Shales of middle Gilsonryggen Member (500 m -280 m)	84
8.3.2 Siltstones of upper Gilsonryggen Member (280 m -150 m)	85
8.3.3 Sandstones of upper Gilsonryggen Member/Lower Battfjellet Formation (150 m – 110 m)	86
9 Conclusion.....	88
References	91
Appendices	100
Acknowledgments.....	112

1 Introduction

This master thesis is based on sedimentological and petrophysical analysis of early Cenozoic sedimentary strata from the Tertiary Basin of Central Spitsbergen. The focus will be on the Paleogene succession, and especially the Paleocene – Eocene transition (55 Ma.). At this time a dramatic and abrupt climatic change occurred, the Paleocene – Eocene Thermal Maximum (PETM). This thesis is part of a larger project, pACE (<http://www.wun.ac.uk/pACE/index.html>), which aims to undertake broad paleoenvironmental studies of Paleogene formations in the sedimentary strata at Svalbard and in the Arctic. The study provides information of dramatic climatic and oceanographic changes in the past and may have relevance to the present discussion of climatic changes.

The contribution to this project by the Oslo subgroup will focus on sedimentological descriptions and sampling for basic petrographic, micro paleontological and some geochemical analyses. In august 2007 outcrops of the lower Frysjaodden Formation and Hollenderdalen Formation were studied in detail by Burca (2008) and R  ther (2007) (Figure 1). The present study of core BH 9/05 comprises the entire Frysjaodden Formation with the absence of Hollenderdalen Formation (Figure 1)

In this master thesis the aim will be to collect and analyze sedimentary logs and mineralogical data (thin sections, XRD- analysis and SEM) of core BH 9/2005 (SNSK, Longyearbyen) (Figure 1). Based on this the thesis will give a description of the sedimentary succession and discussion of the depositional environments and the climatic conditions. There will be special emphasis on the analysis of clay minerals as climatic indicators.

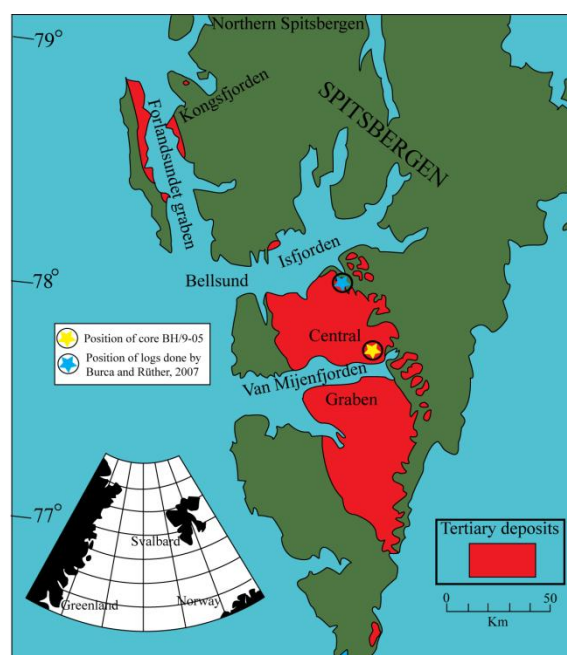


Figure 1: Map of Svalbard and Tertiary deposits (in red) (modified from Nagy,2005). Sites of field work of Burca and R  ther in 2007 and Jargvoll and Riber in 2008 are marked with yellow and blue star.

2 Regional setting

Svalbard is an archipelago in the Arctic Ocean, situated half way between Norway and the North Pole and east of Greenland (Figure 1). Spitsbergen is the largest island. The other islands of some size are Nordaustlandet, Edgeøya, Kvitøya, Bear Island, Hope Island, Barentsøya and Kong Karls land.

2.1 Tectonostratigraphic development

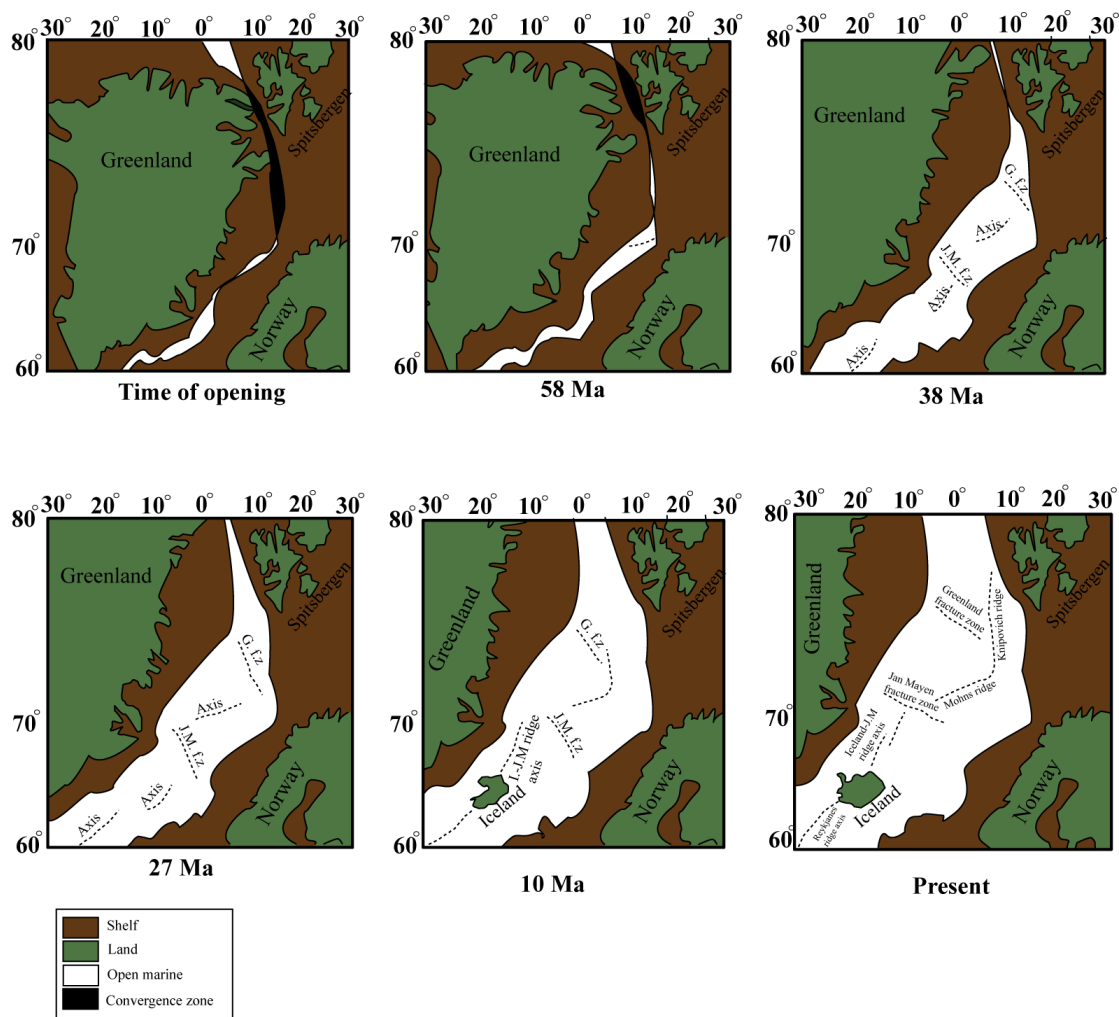


Figure 2: Evolution of the Norwegian-Greenland seas (modified from Talwani and Eldholm, 1977)

The mid oceanic ridge can be followed north of Iceland, consisting of the following segments: Iceland – Jan Mayen ridge, Mohns Ridge and the Knipovich Ridge (Talwani and Eldholm, 1977), with Spitsbergen situated east of the latter (Figure 2). Several studies have been carried out explaining the strike-slip movement which caused the separation between Greenland and Svalbard in early Cenozoic (Talwani and Eldholm, 1977, Olesen et al., 2007). This thesis will focus on the Cenozoic successions that are confined to depositional basins at

The development of the Central Basin on Svalbard has passed two major tectonic settings phases (Steel et al., 1985) (Figure 3). The central basin started as a rift basin in a transtensional regime in the early to mid Paleocene (Figure 3). Steel et al. (1985) lists three evidences for this theory. The first is the considerable thickness of the sedimentary succession and the thickening of this towards the De Geer Line. In addition the number of volcanic ash layers in the early Paleocene deposits of the Firkanten Formation indicates volcanic activity as a result of rifting (Major and Nagy, 1972). The third reason is that there is no evidence of western uplift in the west at this time. During the late Paleocene there are evidence suggesting significant change in the tectonic setting from a transtensional to a transpressional regime (Figure 3).

The Central Basin eventually got the architecture of a foreland basin in front of the West Spitsbergen mountain chain (Steel et al., 1985). This resulted in a drainage reversal, indicated by the sandstones of the Hollenderdalen Formation and Battfjellet Formation which are clearly displaying a western source area, in contrast to the eastern derived deposits from the early Paleocene succession. The theory of two tectonic regimes has been challenged by Bruhn and Steel (2003), claiming that the evolution of the Central Spitsbergen basin can be incorporated into a single compressional, foreland-basin scenario (Figure 4). Bruhn and Steel (2003) and Helland-Hansen (1990) state that the Tertiary fold belt reflects predominant compressional deformation, with little impact from the strike-slip movement suggested by Steel et al. (1985). The eastern source of sediments to the basin in the Paleocene is explained by the creation of a peripheral bulge in early foreland-basin evolution (Bruhn and Steel, 2003). Later in the basin evolution the peripheral bulge migrates away from the thrust belt and is gradually eroded (Figure 4).

Spitsbergen Tertiary Basin evolution

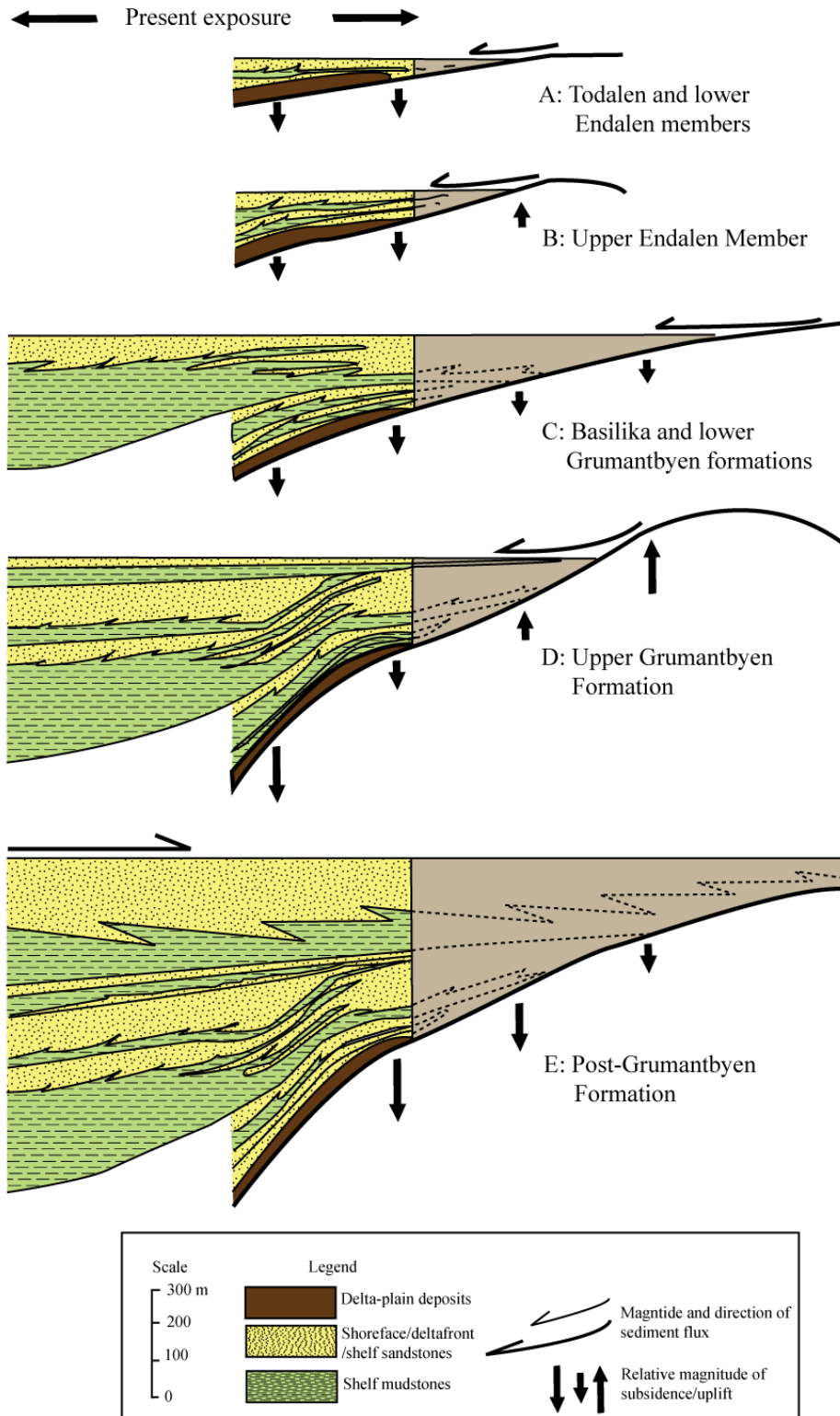


Figure 4: Depositional model (modified after Bruhn and Steel, 2003). The formation of a peripheral bulge in the early evolution of the foreland basin act as an eastern source of sediments.

2.2 Lithostratigraphic setting

The Cenozoic deposits at Svalbard are restricted to mainly five depocenters (Dallmann et al., 1999). These are: Bellsund, Forlandsundet, Kongsfjorden, Central Tertiary basin and Northern Spitsbergen (Figure 1). The Central Basin is the largest of these and also represents the most complete succession of early Cenozoic deposits at Spitsbergen (Nagy, 2005). The Cenozoic deposits in the Central Basin is made up of the van Mijenfjorden Group, which can further be divided into the Firkanten, Basilika and Grumantbyen Formations of the Paleocene and the Frysjaodden, Hollenderdalen, Battfjellet and Aspelintoppen Formations of the Eocene (Figure 5) (Dallmann et al., 1999).

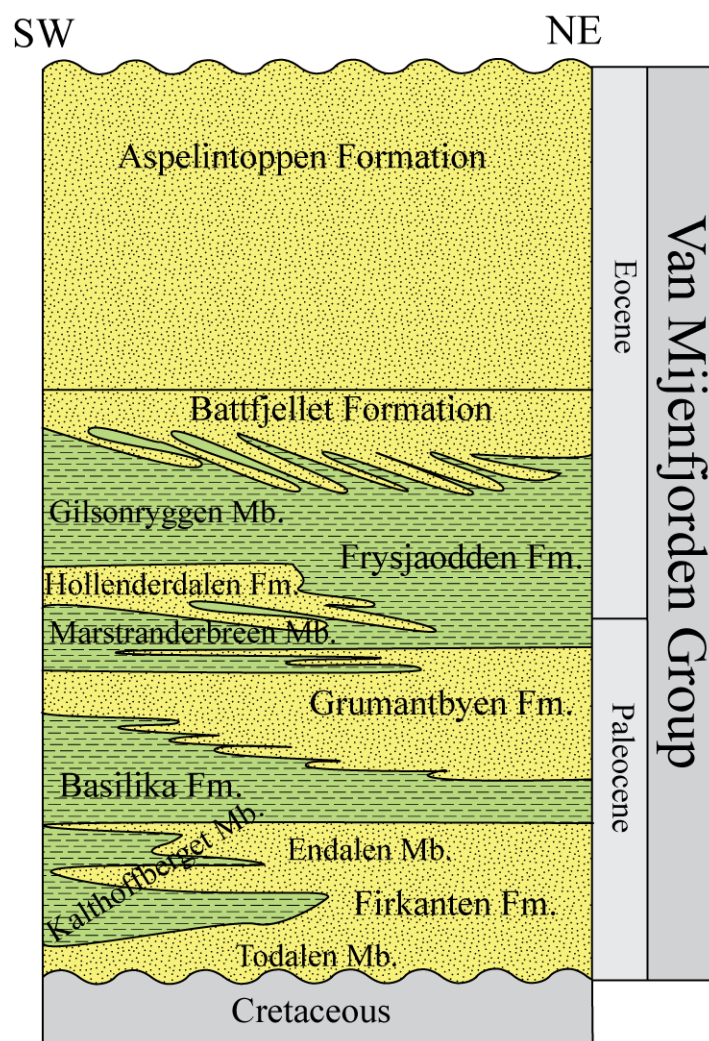


Figure 5: The Van Mijenfjorden Group (Modified from Helland-Hansen, 1992).

1. **Firkanten Formation** (Figure 5): The early Paleogene deposits of the Firkanten Fm. rests on a ravinement surface resulting from subaerial Late Cretaceous erosion (Nagy, 2005). The Firkanten formation shows an overall transgressive trend from delta plain to prodelta/outer shelf facies (Müller and Spielhagen, 1990). However, within this transgressive development several smaller, individual regressive cycles can be identified, as shown by Nagy, (2005), Bruhn and Steel (2003), Steel et al. (1981). The formation spans over a period of maximum 7 million years and it has been subdivided into three members (Bruhn and Steel, 2003):
 - a. **Todalen Member** (Figure 5): Represents the lowermost member in the Firkanten Formation and exhibit a transgressive trend from a deltaic coastal plain facies to barrier island facies (Nagy, 2005). Fluvial conglomerates are found at the base (Dallmann et al., 1999) overlain by non-marine mudstones and coals (Bruhn and Steel, 2003). At the top well-sorted sandstone is found, characterizing a barrier bar system, sheltering lagoonal waters (Nagy, 2005).
 - b. **Kolthoffberget Member** (Figure 5): The Endalen Member develops into prodelta deposits of the Kolthoffberget Member to the south-west (Steel et al., 1981). This represents a lateral development towards the south west, reflecting a paleotransport pattern from east to west.
 - c. **Endalen Member** (Figure 5): The maximum flooding surface has been located in the mid Endalen Member (Bruhn and Steel, 2003). The rest of the member represents an upward coarsening succession formed by a prograding delta-front (Nagy, 2005). At the top of the Endalen Member fluvial conglomerates are found (Steel, 1981), forming the upper most sequence boundary (Nagy, 2005).
2. **Basilika Formation** (Figure 5): The transition from the Endalen Member of top of Firkanten Formation to the Basilika Formation is locally marked by a sharp boundary between sandstones and shale (Nagy, 2005) which show a shift from regressive to transgressive trend. The deposition of the Basilika Formation has been interpreted as an outer shelf mud complex by Steel et al. (1985). It mainly consists of shales and siltstones (Bruhn and Steel, 2003) and is characterized by the scarcity of bioturbation and marine faunas. The abundance of pyrite indicates anoxic environments (Müller and Spielhagen, 1990).

3. **Grumantbyen Formation** (Figure 5): The origin of Grumantbyen Formation has been problematic due to its massive character and high degree of bioturbation (Steel et al., 1981). It represents a regressive phase culminating in conglomeratic sandstone at the top (Kellogg, 1975). Most probably the formation was deposited in a lower shoreface environment (Müller and Spielhagen, 1990). The thinning of the formation westward indicates that the paleotransport pattern continued to be from east to west. Within the formation five major sandstone wedges or sheets have been recognized (Bruhn and Steel, 2003).
4. **Frysjaodden Formation** (Figure 5): Forms the interval between the sandstones of the Grumantbyen Fm. and the first well-developed sandstones of the Battfjellet Fm. (Kellogg, 1975). The transition between the Frysjaodden and the underlying Grumantbyen Formations is a sharp boundary from sandstones/conglomerate into shales. The Frysjaodden formation is divided into two members by the sand wedge of the Hollenderdalen Formation which was building eastwards from the west (Steel et al., 1985).

The Frysjaodden Formation mainly comprise dark gray claystones and shales (Kellogg, 1975), but some turbidite deposits has been recognized, building out from west and thinning out eastward (Steel et al., 1981). This demonstrates the shift in sediment input from east to west. Dispersed bentonite layers are also present in the formation (Dallmann, 1999). The Frysjaodden formation has been interpreted as a prodelta/shelf system deposit (Steel, 1985). The Frysjaodden Formation has been divided into two members:

- a. **Marstranderbreen Member** (Figure 5): The lowermost member of the Gilsonryggen Formation. It is only defined in regions where the Hollenderdalen Formation is developed (Dallmann, 1999). The succession has been interpreted to be a deep water shale deposit (Dallmann, 1999) accumulated in a restricted basin environment (Burca, 2008).
- b. **Gilsonryggen Member** (Figure 5): Strictly speaking the Gilsonryggen Member is only defined where the Hollenderdalen occurs as an underlying development (Dallmann, 1999). In this thesis the term Gilsonryggen Member will be used comprising the entire Frysjaodden Formation deposit. The Gilsonryggen Member exhibits the same characteristics as the

Marstranderbreen Member, and is interpreted to be a deep water shale deposit (Dallmann, 1999). There is a gradual change from the shales of Gilsonryggen Member into the sandstones of Battfjellet Formation.

5. **Hollendardalen Formation** (Figure 5): The Hollendardalen Formation is a possible tidal-dominated, deltaic sand wedge in between the two members of the Frysjaodden Formations (Dallmann, 1999). R  ther (2007) and Burca (2008) interpreted the formation to be an offshore transition and foreshore deposit. The formation varies in thickness from 150 m in the north-western part of the basin to absence in the south-eastern part (Steel et al., 1981). According to M  ller and Spielhagen (1990), the high content of rock fragments and the mineral chloritoid points to a proximal source of eroded metamorphic rocks. This source probably corresponds to the West Spitsbergen mountain chain.
6. **Battfjellet Formation** (Figure 5): The increased supply of coarse grained material result in the gradual transition from the Gilsonryggen Member to the Battfjellet Formation. The Battfjellet Formation consists of siltstones and sandstones, and an abundance of wave dominated structures, e.g. hummocky cross stratification (Steel, 1985). Together with Frysjaodden it makes up a coarsening-upwards mega sequence (Steel, 1981), which ends in the first coals of the Aspelintoppen Formation (Dallmann, 1999). The eastwards dipping sandstone clinothems described in detail by Helland-Hansen (1992), demonstrate clearly that the sediments are derived from the western side of the basin. Steel et al. (1985) interpret the formation to be the product of a prograding deltaic and barrier coastline.
7. **Aspelintoppen Formation** (Figure 5): This formation represents the youngest unit of the Tertiary succession in the Central Basin, and it has a thickness of >1000 m. The Aspelin Formation represents the final basin fill and consists of terrestrial influenced deposits such as distributary channels, crevasse splays and swamp deposits (Dallmann, 1999).

2.3 Paleogeography

In Eocene time, a Svalbard latitude of 71  -72   N has been suggested by electromagnetic data (Dalland, 1976). Before the widening of the Norwegian – Greenland Sea, only a narrow sea path separated Svalbard and Greenland, resulting in continental climate conditions. In these climatic conditions Dalland (1976) suggest cold winters with existence of snow and ice and

warm summers. Later in the Eocene, after widening of the Norwegian-Greenland Sea, coastal climate conditions most likely have prevailed, with less seasonal temperature difference (Dalland, 1976). This view is contradicted by a study of conifers from two Tertiary horizons, early Paleocene and early Eocene respectively (Schweitzer, 1980). By determining the lowermost temperature by the most frost-sensitive conifer, an annual mean temperature of 15-18°C has been suggested (Schweitzer, 1980).

3 Paleoclimate

From late Cretaceous to Neogene there was a change in the earth's climate from ice-free and relatively warm conditions in late Cretaceous to the ice covered poles and relatively cold conditions of the Neogene (Savin et al., 1975, Corfield, 1994, Zachos et al., 1993). This large-scale cooling trend were driven by tectonic processes (in cycles of $10^5 - 10^7$ years), which included the North Atlantic rifting and the isolation of the Antarctic continent (Zachos et al., 2001). The so-called Milankovitch cycles are also contributing. These cycles describe the earth's orbital parameters controlling the distribution and amount of solar energy to the earth. These parameters vary with a cyclicity of $10^4 - 10^6$ years (Berger, 1988). The late Cretaceous to Neogene transition from a "greenhouse" to "icehouse" was for long thought to have developed gradually through the Paleogene, based on $\delta^{18}\text{O}$ measurements (Savin et al. 1975). The DSDP (Deep Sea Drilling Project) and the ODP (Ocean Drilling Project) in the 1970's and 1980's yielded more detailed paleoclimatic information of the Paleogene and it was shown that the transition was not gradual, but punctuated by several steps of rapid climate change (Kennett and Stott, 1991, Zachos et al., 1993). These early geochemical and sedimentological studies were mainly based on analyses of sedimentary sequences from high latitude on the southern hemisphere. The growing consciousness of the impact the extent of ice in the Arctic have on the Earth's climate resulted in The Integrated Ocean Drilling Program Expedition (IODP) (Arctic Coring Expedition (ACEX)) in 2004 (Moran et al., 2006). The aim of this expedition was to increase the knowledge of the palaeoceanographic record. Due to the difficulties of working in a harsh, ice-covered environment earlier work had only been able to contribute with sedimentary record from the last 200 – 500 000 years (Moran et al., 2006). ACEX provided a 400 m sediment core containing Cenozoic strata from the Lomonosov ridge in the Arctic Ocean (Figure 6).

The results from studying this record have revealed one abrupt and dramatic climatic event, namely the boundary between Paleocene and Eocene (Zachos et al., 2001, Sluijs et al. , 2006,

Moran et al. , 2006), hereafter referred to as The Paleocene Eocene Thermal Maximum (PETM).

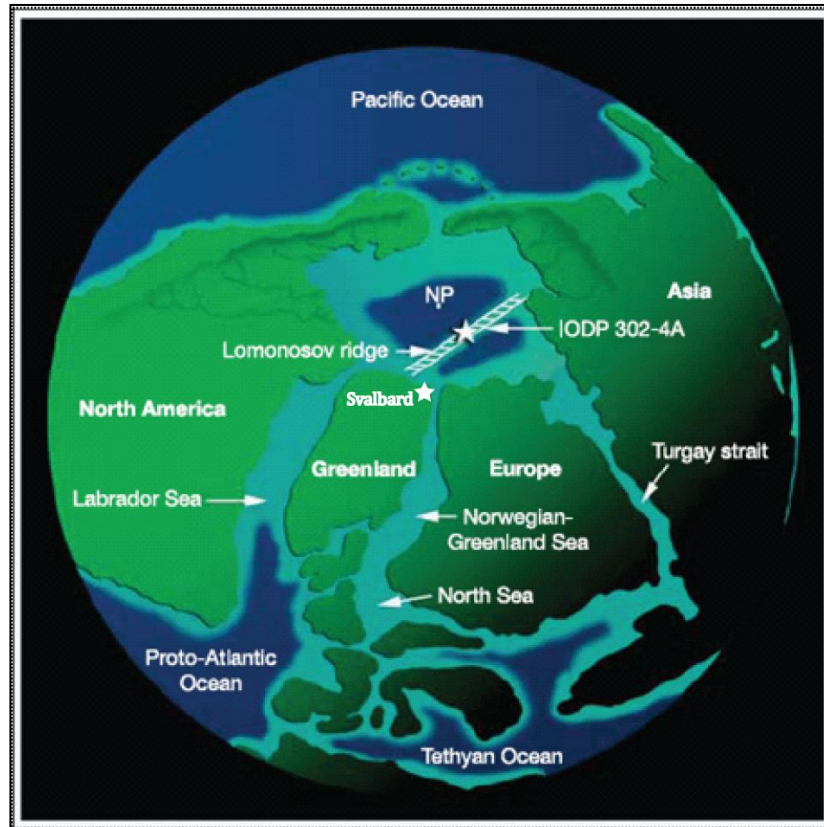


Figure 6: Reconstruction of Arctic Basin at the Paleocene - Eocene boundary and the Lomonosov ridge (modified from Sluijs et al. 2006).

3.1 Paleocene- Eocene Thermal Maximum (PETM)

The Paleocene-Eocene boundary (~ 55 Ma) is characterized by an abrupt climatic change, which lasted only 210-220 k years (Röhl et al., 2000) and had global consequences (Zachos et al., 1993). In less than 10 k years there was a rise in deep sea temperatures of 5-6°C and an increase in sea surface temperatures by as much as 8°C close to the poles and less at lower latitudes (Zachos et al., 2001). At the PETM peak, surface water in the Arctic Ocean could have been as high as 24°C implying ice free poles and a much lower temperature gradient between equator and the poles than today (Sluijs, 2006). The main evidences for this global temperature rise come from the isotopic records. Both the $\delta^{18}\text{O}$ and $\delta^{13}\text{C}$ ratio is temperature dependant. Figure 7 is based on isotopic data from more than 40 different localities and both $\delta^{18}\text{O}$ and $\delta^{13}\text{C}$ shows a large excursion corresponding to the PETM (Zachos et al., 2001).

Both graphs also display the general cooling trend from 70 Ma until present. Recent studies, based on pollen analysis, indicate that annual mean air temperature across the PETM, in the Arctic, increased from 16 -18° C to 25° C and dropping to 18-20° C at the end of the PETM (Weijers et al., 2007).

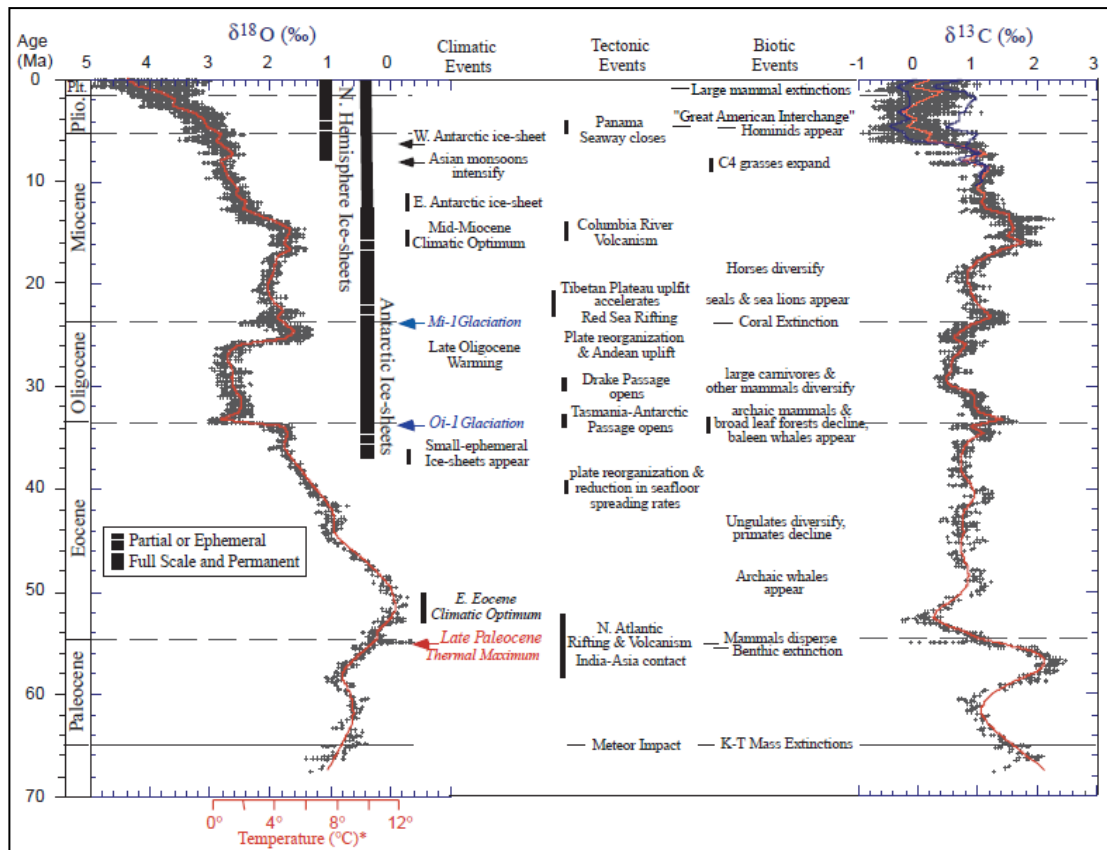


Figure 7: Isotopic oxygen and carbon excursions (Zachos et al., 2001)

3.2 Consequences of the PETM

The environmental implications after such an abrupt increase in global temperature are severe. There are indications of a rise in the eustatic sea level and the development of anoxic and euxinic conditions in the bottom waters at high latitudes (Sluijs et al., 2006). Warmer climate also resulted in an intensification of the hydrological cycle (Pagani, 2006). As a consequence of the increased precipitation chemical weathering of rocks escalated and the result was sedimentation rates in the Arctic 3 – 5 times higher during the PETM, than before and after the event (Brinkhuis et al., 2006). Major biotic changes include dramatic species reduction, (about 35-50%) of benthic foraminifera taxa during the PETM (Kennett and Stott, 1991). The Paleocene –Eocene transition has also been considered an important boundary in mammalian evolution, with the entry of modern mammalian species in North America right at the time of the PETM. This can be explained by the warmer climate allowing migration of

modern species to new areas. The immigrant taxa permanently changed the ecological framework of local mammalian communities (Clyde and Gingerich, 1998).

3.3 Mechanisms of climate warming

The isotopic record shows a rapid injection of ^{13}C -depleted carbon into the atmosphere possibly in the form of CO_2 or CH_4 (Sluijs et al., 2008). Most explanations relating the causes for the global warming at the end of Paleocene lean towards the release of massive amounts of methane from destabilization of methane hydrates at the seafloor (Dickens et al., 1995, Zachos et al, 2001, Bains et al., 1999). Methane is a very effective greenhouse gas (Bains et al, 1999) and has a ^{13}C depleted signature, when biogenic (Whiticar, 1999). Several mechanisms have been suggested causing this release of methane and hence being responsible for the global warming at Paleocene-Eocene boundary. One explanation is proposed by Dickens et al. (1995). They suggest that volcanism, caused by rifting in the North Atlantic, injected large amounts of CO_2 to the atmosphere. The subsequent climatic warming lead to a rise in deep sea temperatures until a threshold was reached. At this threshold the methane hydrates were no longer stable and enormous amounts of CH_4 were released, causing the rapid increase in temperature. This view has been supported by Svensen et al. (2004) suggesting that the destabilization of methane hydrates at the continental shelf was triggered by intrusions of mantle-derived melts into carbon-rich sedimentary strata. A huge magmatic complex dating from before and during the Atlantic break-up 55 Ma ago has been localized in the Norwegian Sea. Kent et al. (2003) introduce the idea that a comet impact could be responsible trigger mechanism. They argue that the extraterrestrial carbon is a potential source of ^{13}C depleted carbon, and that the impact could also destabilize the methane hydrates. A study carried out by Higgins and Schrag (2006) implies that the carbon addition to the atmosphere was too large to be accounted for by the release of methane. Instead they suggest the oxidation of 5000 Gt C of sedimentary organic carbon as a possible mechanism. A possible scenario is isolation of large epicontinental seaway by tectonic uplift followed by desiccation and bacterial respiration of the aerated organic matter (Higgins and Schrag, 2006). Together with the effect from the intrusive complex discovered by Svensen et al. (2004) this hypothesis could explain the rapid injection of CO_2 to the atmosphere during the PETM.

4 Methods and material

In the following chapter the methods and material used in this master thesis will be presented.

4.1 Sedimentological core logging

The logging of core BH 9/05 was carried out in the summer of 2008, from 30/6 – 7/7, at Svalbard. It took place in Store Norske's core storage just outside Longyearbyen. During these days, the writer and David Jargvoll logged 450 m (560 m – 110 m core depth) under the supervision of Professor Henning Dypvik and Professor Jenő Nagy, and with the assistance of Jonna Poikolainen.

Each core box contained five pieces of core, each at the length of one meter. They were cleaned with a water wet sponge before they were inspected closely with the aid of a hand lens. The entire core was logged on logging sheets (shown in the appendices) in the scale of 1:50. The interval 560 m – 547,20 m was logged in the scale of 1:20.

In addition to the core logging and samples, pictures were provided from the entire core. Pictures of the core in boxes were taken, both water wet and dry, by H. Dypvik. Close-up photographs were taken by J. Nagy and the writer.


4.2 Sampling

During field work 429 samples, each 4-6 cm, were collected from core BH 9/05. The sampling was mainly performed by Professor Jenő Nagy and Jonna Poikolainen. Different intervals between the samples were used. From 110 m – 140 m: 1 sample every 2 meters. From 140 m -160 m: 1 sample every 1 meter. From 160 m – 475 m: 1 sample every 2 meter. From 475 -500: 1 sample every 1 meter. From 500 – 554,72: 3 samples every 1 meter. From 551,41 – 560: 1 sample every 1 meter. In addition 36 special samples were taken. When referring to one sample, it is named using only the lower depth. E.g. sample 530,35-530,40 will hereafter be called 530,40.

4.3 Facies description and facies associations

In this thesis the classification of shales and siltstone according to Potter, Maynard and Pryor (Boggs, 2006) will be used. Shales are defined as sedimentary rocks where more than 50% of the grains are less than 0,062 mm. Fine-grained siliciclastic rocks that contain less than 33 % clay size constituents are defined as siltstones (Boggs, 2006). The division of different types of shales and siltstones are presented in Table 1.

Table 1: Classification of shales and siltstone (Boggs, 2006)

Percentage clay-size constituents:		0-32	33-65	66-100
Field adjective:		Gritty	Loamy	Fat or slick
NONINDURATED	Beds > 10 mm	Bedded silt	Bedded mud	Bedded claymud
	Laminae < 10 mm	Laminated silt	Laminated mud	Laminated claymud
INDURATED	Beds > 10 mm	Bedded siltstone	Mudstone	Claystone
	Laminae < 10 mm	Laminated siltstone	Mudshale	Clayshale
METAMORPHOSED	Degree of metamorphism: Low  High	Quartz Argillite	Argillite	
		Quartz Slate	Slate	
		Phyllite and/or Mica Schist		

Facies definitions are based on field logs, pictures and thin sections. The division into the respective facies is determined by lithology, texture and structures. The prominent characteristics of the rock are emphasized and a certain tolerance of movement is allowed in order to group similar rock intervals into the same facies. Where transition between two facies is gradual the boundary is set approximately in the middle of the transition zone. Consecutive facies have been grouped into different facies associations, representing certain depositional environments.

Grain sizes are defined according to Wentworth size-classes (Boggs, 2006):

Clay: < 0,004 mm

Silt: 0,004 - 0,063 mm

Very fine sand: 0,063 mm – 0,125 m

Fine sand: 0,125 mm – 0,25 mm

Medium sand: 0,25 mm – 0,5 mm

4.4 Mineralogical and petrographical analysis

The mineralogical and petrographical analysis has been performed using both thin sections and XRD.

4.4.1 Thin sections

Thin sections were prepared at the Naturhistorisk Museum. Small slabs of rock were molded in blue epoxy and glued to a 2,5 cm x 4,5 cm glass slide. In order to make the sample transparent the rock were polished down to 30 μm thickness.

Thin section description:

Thin sections were studied in order to yield detailed information about rock texture and mineralogy. 35 samples were selected from the 429 samples in order to give a representative image of the core. A denser sampling interval was used in the varied sandstones towards the upper part of the section, than in the shales of the middle and lower part. From the thin sections, information about lithology, framework configuration, predominant structures, average grain size, grain shape and sorting has been obtained. These results are summarized in Appendix 2.

Table 2: Thin sections (35 pcs.). Thin sections where point counting was conducted are given in italic bold.

Thin section no.	Depth	Thin section no.	Depth	Thin section no.	Depth	Thin section no.	Depth
1	<i>110,05</i>	10	180,05	19	290,05	28	<i>530,99</i>
2	<i>115,90</i>	11	187,00	20	<i>330,05</i>	29	532,37
3	<i>120,05</i>	12	<i>190,05</i>	21	380,05	30	534,37
4	<i>130,05</i>	13	220,05	22	410,05	31	544,63
5	138,80	14	<i>230,05</i>	23	439,93	32	548,35
6	<i>140,05</i>	15	250,05	24	<i>490,05</i>	33	<i>551,43</i>
7	<i>150,05</i>	16	264,59	25	500,05	34	<i>552,43</i>
8	<i>160,05</i>	17	270,05	26	517,08	35	<i>557,58</i>
9	170,05	18	<i>282,05</i>	27	525,05		

Counting of minerals

Mineral content has been determined by point-counting 400 points using a Swift automatic counter. A representative selection of 16 thin sections was subject to counting (Table 2), using a Nikon Optiphot-Pol petrographic microscope both with plain polarized and cross polarized light.

4.4.2 XRD analysis

XRD-analysis has been carried out both to make qualitative and semi-quantitative analysis.

Table 3: XRD samples. Clay separated samples are in italic bold

XRD no.	Depth	XRD no.	Depth	XRD no.	Depth	XRD no.	Depth
5614	110,05	5624	230,05	5645	511,10	<i>5743</i>	<i>531,35</i>
5651	115,90	5625	250,05	5646	517,00	<i>5744</i>	<i>531,68</i>
5615	120,05	5647	264,59	5635	517,08	<i>5745</i>	<i>531,99</i>
5616	130,05	5626	270,05	5636	525,05	<i>5746</i>	<i>532,05</i>
5650	132,50	5627	282,05	<i>5734</i>	<i>528,45</i>	<i>5638</i>	<i>532,37</i>
5649	138,80	5628	290,05	<i>5735</i>	<i>528,75</i>	<i>5747</i>	<i>532,70</i>
5617	140,05	5629	330,05	<i>5736</i>	<i>529,05</i>	<i>5748</i>	<i>533,07</i>
5618	150,05	<i>5732</i>	<i>350,05</i>	<i>5737</i>	<i>529,35</i>	<i>5749</i>	<i>533,38</i>
5619	160,05	5630	380,05	<i>5738</i>	<i>529,75</i>	<i>5750</i>	<i>533,71</i>
5620	170,05	5631	410,05	<i>5739</i>	<i>530,05</i>	5639	534,37
5621	180,05	5632	439,93	<i>5740</i>	<i>530,40</i>	<i>5751</i>	<i>536,36</i>
5648	187,00	<i>5733</i>	<i>469,58</i>	<i>5741</i>	<i>530,65</i>	5640	544,63
5622	190,05	5633	490,05	<i>5637</i>	<i>530,99</i>	5641	548,35
5623	220,05	5634	500,05	<i>5742</i>	<i>531,05</i>	5642	551,43
						5643	552,43
						5644	557,58

Bulk analysis

To get an overview of the mineralogical composition 38 samples were chosen to represent the entire section in first batch.

To get a detailed view of the mineralogical composition of the section around the PETM , and additional 20 samples were picked close to the PETM boundary in the second batch

Clay separation

The clay fraction of 20 samples has been separated. This was done with the 20 samples from the second batch, plus two samples from the first batch (Table 3). The separation procedure was carried out as followed:

- Samples were crushed in an agate mortar to a size of 1-2 mm.
- Approximately 8-10 grams of each sample were placed in recipients.
- 300 ml of distilled water was added to each of the recipients and the mixtures were stirred for about 1 min.
- Each sample underwent a 10 min ultrasound treatment in a Bandelin Sonorex RK102 transistor, in order to accelerate the dispersion of clay particles.

- Samples were then left for 24 hours.
- Each sample was stirred for 1 minute and then 100 ml of distilled water was added. In order to prevent flocculation roughly 15 ml of calgon was added to the samples.
- Samples was now left in suspension for 3 ½ hours and then the clay fraction (the upper 200 ml) was transferred to new recipients.

The next step was to filter the clay fraction samples in a vacuum suction through millipore filter.

- 20 ml of the solution was run through the filter, treated with 0,1 M MgCl₂ and finally washed with distilled water.
- The filtered samples were placed on silica glass slides which were put in aluminum holders.

Now the samples were ready for XRD analysis. Three different treatments were applied:

- In the first XRD run. Samples were analyzed air-dried.
- In the second run, samples were treated with ethylene glycol vapor, and then put into an exsiccator for 12 hours. This was done in order to identify possible swelling clays.
- In the third run samples were heated to 550°C for two hours. At this temperature kaolinite becomes amorphous to X-rays and its diffraction pattern disappears. Thus comparing EG-solvated diffractograms and diffractograms which have undergone heating to 550°C will provide a positive identification of kaolinite in the sample.
- An additional slow scan was conducted across the 3,54 -3,58Å reflection.

Removal of iron oxide by Na-Citrate

There are no suspicion of iron oxide in these samples, but in order to compare the results from this thesis with the XRD-results of Florin Burca`s thesis (Burca, 2008), there have been decided to follow the same procedure as him. The procedure was carried out on 4 samples for comparison. Using a Cu-target X-ray tube can cause problems if samples are rich in iron oxide (Moore and Reynolds, 1997). The removal of iron oxides can be done chemically, treating the sample with citrate-bicarbonate-dithionite (CBD) (Mehra and Jackson, 1960). The basic concepts of this method:

- 2 grams of samples are placed in a 100 ml centrifuge tube.
- 40 ml of 0,3 M Na-citrate solution and 5 ml of 1 M NaHCO₃ solution are added.
- The tubes are placed in a water bath and the temperature is brought to 80° C.
- Tubes are taken out of the water bath, and ½ grams of Na₂S₂O₄ is added.
- The mixture is stirred for 1 min and then occasionally for a total of 15 min.
- At the end of the 15 min, 10 ml of saturated NaCl solution and 10 ml of acetone is added to the tube, to prevent flocculation.
- The suspension is then mixed, warmed in a water bath and centrifuged for 5 min at 2000 rev/min.
- The clear supernatant is decanted, and the tubes are filled with distilled water and centrifuged one more time before the water is removed.
- The clay fraction is now ready to be separated and then the samples are filtered as described above.
- In addition to the treatments applied to the clay fraction samples, an extra heat treatment (350° C) were applied to these 4 samples

Qualitative analysis

Methods suggested by Moore and Reynolds (1997) and Bergaya (2006) have been used in the identification procedure. Minerals identified are shown in Figure 8

Bulk (Figure 8 (uppermost diffractogram))

- **Clay minerals:**
 - *Illite*: 001 reflection identified at 10,0 Å.
 - *Kaolinite/Chlorite*: The 001 reflection for kaolinite and 002 reflection for chlorite are coinciding at 7,00 Å. Thus the kaolinite 002 reflection at 3,58 and chlorite 004 reflection at 3,54 are identified and their internal ratio applied on the reflection at 7,00 to obtain a semi-quantification of kaolinite and chlorite.
- **Quartz**: the 002 reflection at 4,26 is utilized instead of the 001.
- **Feldspars:**
 - *K-feldspar*: The 001 reflection at about 3,24 Å is used.
 - *Plagioclase*: The 001 reflection at about 3,19 Å is used.
- **Carbonates:**
 - *Calcite*: 3,03 Å reflection is used.

- *Dolomite*: 2,89 Å reflection is used.
- *Siderite*: 2,79 Å reflection is used.
- *Pyrite*: Reflection at 2,71 Å is used.

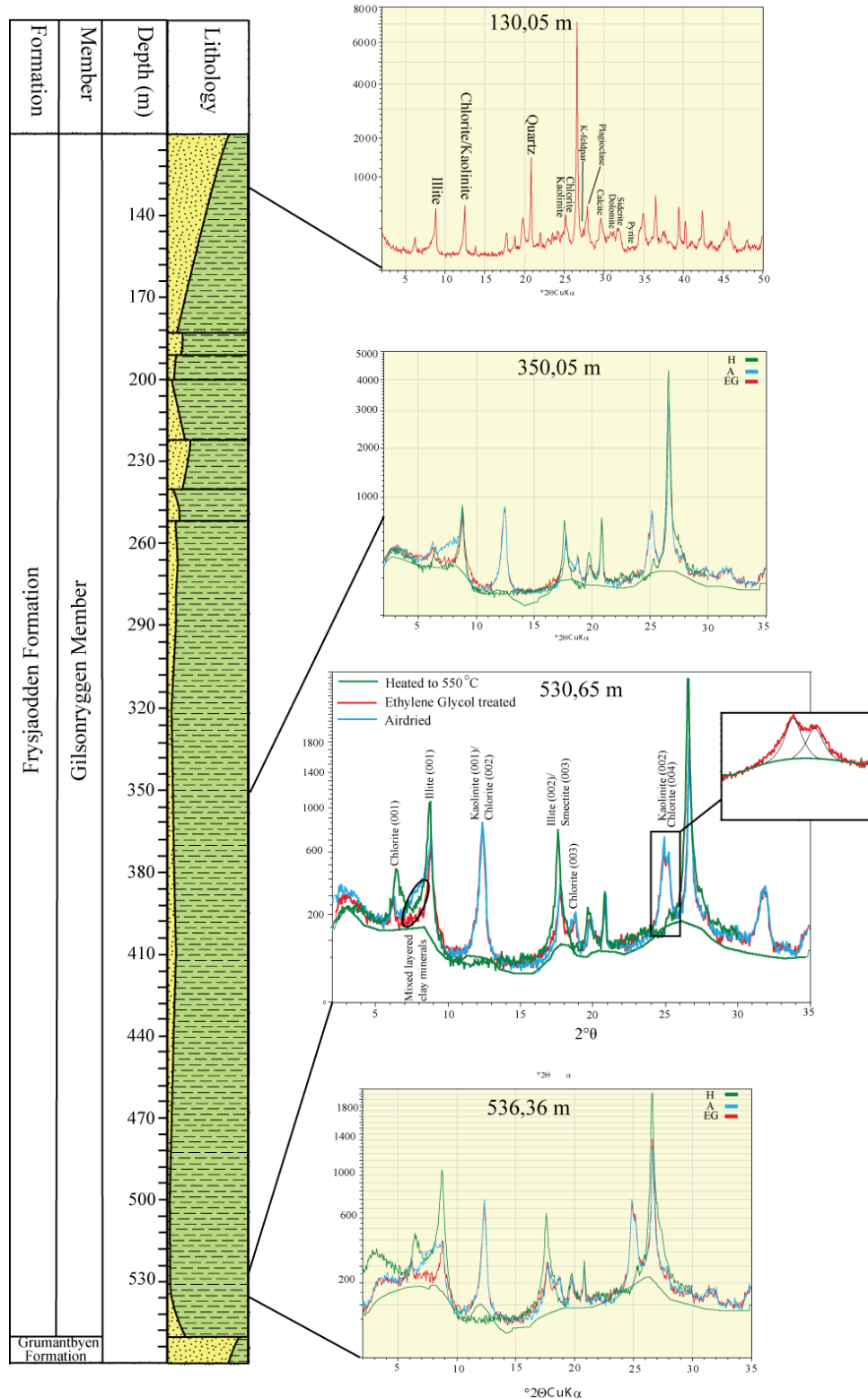


Figure 8: Diffractograms for bulk (the upper most diffractograms) and clay separated samples (the three lower most)

Clay separated samples (Figure 8 (three lowermost diffractograms))

- **Clay minerals:**
 - *Illite*: 001 reflection identified at 10,0 Å.
 - *Kaolinite/Chlorite*: using the same method as in the bulk analysis splitting the 7 Å reflection into kaolinite and chlorite. Distinguishing between Fe-chlorite and Mg-chlorite is accomplished by the method suggested by Moore and Reynolds (Moore and Reynolds, 1997) claiming that a weakening of the 001 and 003 reflections relative to the 002 and 004 reflections indicate an Fe-rich chlorite.
 - *Vermiculite*: Burca (2008) identified small amounts of vermiculite, where the identification of vermiculite was based on the reflection at 14,2 Å. In order to determine the origin of the 14,2 Å reflection, a comparison of diffractograms from EG-saturated and heated samples was undertaken. (Bergaya et al., 2006) state that if vermiculite is present the 14,2 Å reflection will collapse to 10 Å after heating. In case of chlorite the 14,2 Å reflection will experience a slight decrease from 14,2 Å to 13,8 Å – 13,9 Å after heating.
 - *Smectite*: possible smectite can be identified comparing the air-dried and ethylene glycol-solvated preparations. If smectite is present the EG-solvated preparation will give a strong reflection at about 16,9 Å which shifts to about 15 Å in the air-dried (Moore et al., 1997).
 - *Mixed-layered clay minerals*: to decide the properties of mixed-layered clay minerals the area between 10 – 13 Å has been subject to close inspection. If this area experience significant changes in the diffraction pattern after EG treatment, an expandable (smectite) component is present. If illite is the other component, a reflection will be present in the 5,5 – 5 Å region. (Moore and Reynolds, 1997).
- **Other minerals:**
 - *Pyrite*: reflection at 2,71 Å.
 - *Siderite*: reflection at 2,79 Å.

Semi quantitative analysis

The XRD-analysis has been carried out using the Macdiff software. For the bulk analysis the quantitative analysis was conducted by using the maximum intensities for the respective mineral reflections.

For clay minerals Moore and Reynolds (1997) recommend using the integrated intensities. This has been done using the Pseudo Voigt function in Macdiff which states that the intensity at a given θ_i , Int_p , can be expressed as:

$$Int_p = \omega \times Int_{p(Lorentz)} + (1 - \omega) \times Int_{p(Gauss)}$$

$$Int_p = \text{intensity at a given } \theta_i \text{ [counts]}$$

$$\omega = \text{weighted factor}$$

$$\theta_i = 2 \text{ Theta of a given point } (^{\circ}2\theta)$$

The quantification of clay minerals has been conducted on the ethylene glycolated diffractograms, except the quantification of mixed layered clay minerals. For mixed layered clay minerals the quantification was obtained by measuring the area between the airdried reflection and ethylene glycolated reflection in the interval between 10-13 Å.

4.5 Geochemical Analyses

Several geochemical analyses have been conducted (see below). Rock-Eval analysis was carried out in order to decide maturation history and type of organic matter. Total organic carbon (TOC) and calcium carbonate ($CaCO_3$) content have been analyzed to assist the environmental interpretation. Thorium and Uranium content have been used as a measure of oxic vs. anoxic conditions.

Total organic carbon and calcium carbonate

These analyses were carried out by Mofak Naoroz at the University of Oslo on a total number of 69 samples. A CR-412 Carbon Analyser was used in the treatment of 0,35 g pulverized material to determine the carbon content.

Rock-Eval analysis

Rock-Eval pyrolysis was conducted on 30 samples (Appendix 6) which had previously undergone geochemical analysis (TOC, TC, TIC, CaCO₃). The Rock-Eval analysis was conducted by Geolab Nor in Trondheim.

Rock-Eval pyrolysis has been developed to provide a rapid evaluation of prospective source rock by identifying quantity, type and thermal maturation of the associated organic matter (Espitaliè et al, 1977). The basic idea is to gradually heat a pulverized sample under an inert atmosphere. This heating distills the free organic compounds, then cracks pyrolytic products from the insoluble organic matter (kerogen) (Peters,1986). Key parameters measured in this process are (Peters and Cassa, 1994):

- S1: the amount of free hydrocarbons that can be volatilized out of the rock without cracking the kerogen.
- S2: the amount of hydrocarbons after cracking of kerogen. Provides a more realistic measure of source rock potential than TOC, which also contains “dead carbon”.
- Production index (PI), S1/(S1+S2): generally increase with depth and can together with T_{max} be used as a maturation parameter.
- Hydrogen index (HI), S2/TOC [HC/g C_{org}]: indicate the amount of hydrogen in the kerogen and provides information on the potential of the rock to generate oil.
- Oxygen index (OI), S3/TOC [CO₂/g C_{org}]: indicate the amount of oxygen in the kerogen. HI vs. OI plots (modified van Krevelen diagram) can be used to determine kerogen type in the sample.
- T_{max}: corresponds the pyrolysis oven temperature at maximum S2 generation, and is used as a thermal maturity indicator.

Uranium and Thorium

The geochemical analysis conducted in order to determine the uranium and thorium content were carried out by Activation Laboratories LTD (ACT LAB, Canada) on 68 samples.

Detection limit for both Uranium and Thorium was 0,1 ppm.

In oxic conditions Uranium is behaving conservatively as the unreactive uranyl-carbonate complex [U₂(CO₃)₃⁴⁺], (U(VI)) (Calvert and Pedersen, 1993). In chemically reducing conditions U(VI) can be reduced to the much less soluble U(IV) which may then precipitate

from solution as discrete U minerals (Anderson et al., 1989). Thus enrichment of Uranium in the stratigraphic record may be used as a proxy of anoxic conditions.

4.6 Sequence stratigraphy

Sequence stratigraphy has been defined as “the subdivision of sedimentary basin fills into genetic packages bounded by unconformities and their correlative conformities” (Emery and Myers, 1996). The infilling of a basin is controlled by the interaction of tectonics, eustasy and climate. Together, tectonics and eustasy control the space available to accommodation. Rate of sediment supply to the basin is controlled by tectonics, eustasy and climate (Emery and Myers, 1996). The evolution of basin architecture is controlled by the balance between accommodation space and sediment supply. If sediment supply exceeds accommodation space available progradational geometry will be the result. If accommodation space and sediment supply are roughly balanced aggradational geometries occur. When sediment supply is less than the creation of accommodation space retrogradational geometries occur (Emery and Myers, 1996).

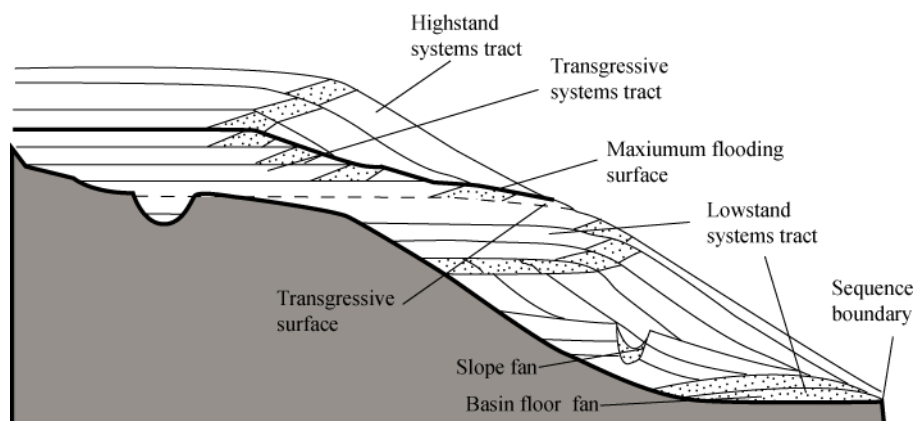


Figure 9: Type 1 sequence (Emery and Myers, 1996).

The stratigraphic sequence illustrated in Figure 9 is divided into different depositional cycles bounded by surfaces recognized on seismic as reflection terminations. The lowermost depositional package is the lowstand systems tract. It is bounded by a lower sequence boundary and an upper transgressive surface (Figure 9). The lowstand systems tract is deposited during an interval of relative sea-level fall with a subsequent slow relative sea-level rise (Emery and Myers, 1996). The middle depositional sequence is the transgressive systems tract. It is deposited in a period where sediment supply is less than the creation of accommodation space. The transgressive systems tract is bounded by the transgressive surface and the maximum flooding surface (Emery and Myers, 1996) (Figure 9). Following the

maximum transgressive surface is progradational system, the highstand systems tract (Figure 9). It is characterized by an initial aggradation deposit, formed in a time of decelerating rate of relative sea-level rise and followed by progradational deposit architecture. The highstand systems tract is bounded at the top by a sequence boundary (Emery and Myers, 1996).

5 Sedimentological description

During field work in June 2008, field logs were collected from core BH 9/05 (Figure 10). The following chapter will present the sedimentological features which have been identified based on these field logs and supported by photographs. The logging and photography was done on uncut, round core stringers.

The entire core (450 m) has been separated into three sedimentological logs represented by a lower part (Figure 11a), middle part (Figure 13a) and an upper part (Figure 14a). Also one log spanning the entire interval has been made.

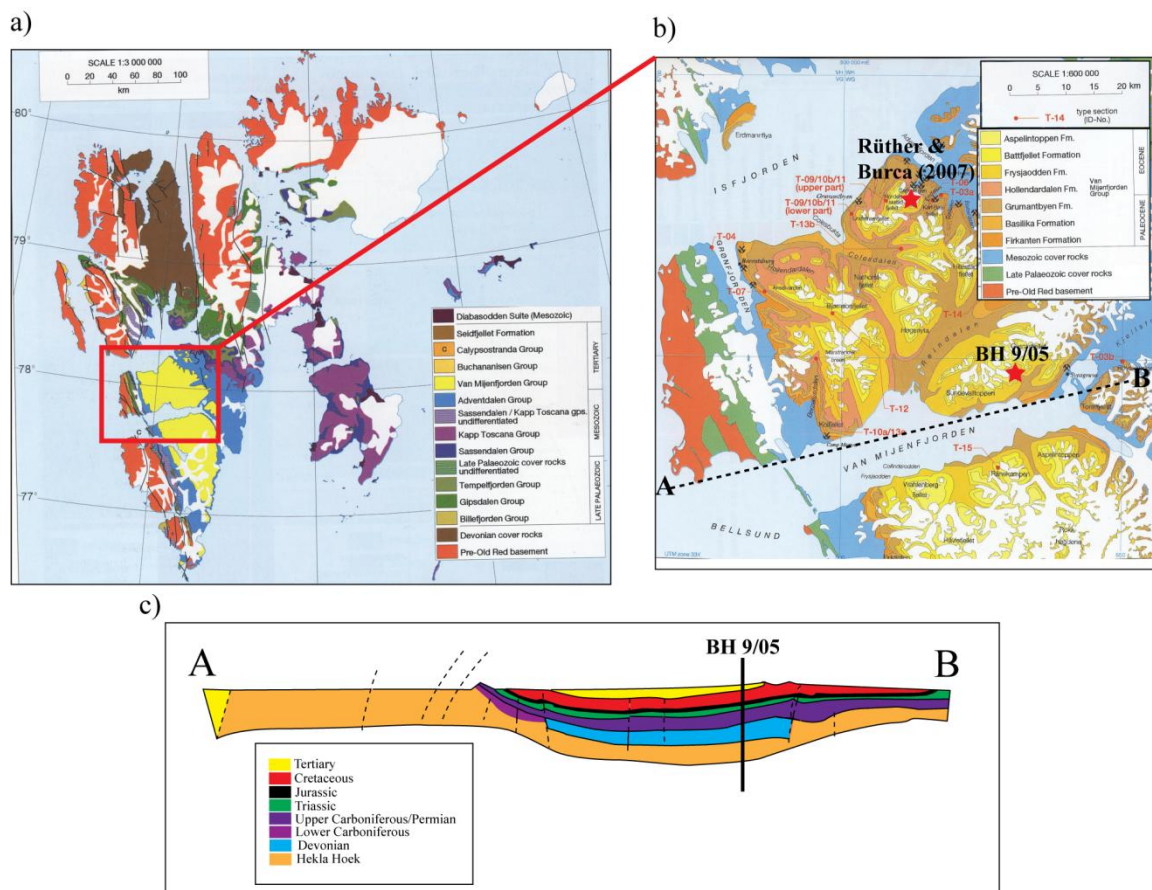


Figure 10: a) and b) Geological maps modified from Dallmann 1999). On b) the position of BH 9/05 and the studies conducted by Burca and Rütter in 2007 are marked. Profile A-B is marked on (b) and shown in c) Profile modified from Steel et al. (1985)

5.1 Facies description

Based on criteria mentioned in chapter 4.3, ten different facies has been recognized and are listed in Table 4. This chapter will explain the main characteristics of the ten facies.

Table 4: Sedimentary facies in core BH 9/05.

Facies nr	Facies	Grain size	Physical/ biological structures	Presence in BH 9/05	Figures
i	Highly bioturbated siltstone/sandstone.	Silt to very fine sand.	All bedding destroyed by bioturbation, Horizontal burrows. Plant materials, shell fragments, dropstone. Good sorting.	<ul style="list-style-type: none"> • 560,00 – 556,20 m • 553,00 – 551,60 m 	Figure 11 b-d
ii	Laminated siltstone	Clay to silt	Shaly laminated siltstone with siderite layers. Some bioturbation. Light gray color.	<ul style="list-style-type: none"> • 556,20 – 553,00 m 	Figure 11c
iiia	Conglomerate	Pebbles	Grain supported, Rounded clasts of pebble.	<ul style="list-style-type: none"> • 551,60 – 551,55 m 	Figure 12a
iiib	Conglomerate	Gravel	Grain supported (a lot of matrix in between grains).	<ul style="list-style-type: none"> • 548,40 – 558,25 m 	Figure 12c
iv	Claystone	Clay to silt	No lamination, poor/moderate sorting, moderate bioturbation, agglutinated foraminifera. Pyrite and siderite nodules. Medium gray color.	<ul style="list-style-type: none"> • 551,55 – 548,40 m • 548,25 – 535,00 m • 304,00 – 280,00 m 	Figure 12b Figure 13d
v	Clayshale	Clay	Parallel laminated shale, some siderite bedding, small upwards fining, silty sequences (1-2 cm). Dark gray color.	<ul style="list-style-type: none"> • 532,00 – 498,00 m • 410,00 – 280,00 m • 280,00 – 249,00 m • 249,00 – 242,00 m • 216,00 – 200,00 m 	Figure 12 e-f Figure 13b
vi	Siderite rich claystone	Clay	High abundance of siderite (bedding and concretions). Light reddish gray colored.	<ul style="list-style-type: none"> • 535,00 – 532,00 m • 498,00 – 410,00 m • 325,00 – 304,00 m 	Figure 12a Figure 13c
vii	Soft sediment deformed siltstone	Clay to silt	Siderite beds moderately bioturbated. Ripples, convolute lamination and loadcasts.	<ul style="list-style-type: none"> • 242,00 – 231,00 m • 231,00 – 222,00 m • 222,00 – 216,00 m • 200,00 – 194,00 m • 194,00 – 190,00 m • 190,00 – 184,00 m • 184,00 – 178,25 m • 178,00 – 150,00 m 	Figure 14b Figure 18b
viii	Soft sediment deformed sandstone	Silt to very fine sand	Upwards coarsening siltstone with decreasing lamination and siderites towards the top and increasing soft sediment deformation.	<ul style="list-style-type: none"> • 150,00 – 140,00 m 	
ix	Low angle ripple laminated sandstone	Silt to very fine sand	Increasing bioturbation towards top, vertical burrows. Plant materials, ripple marks toward the top.	<ul style="list-style-type: none"> • 178,25 – 178,00 m • 140,00 – 132,00 m • 132,00 – 127,00 m 	Figure 14c Figure 19
x	Cross-stratified sandstone	Very fine sand	Through cross- and hummocky cross-stratification. Bioturbation, plant materials and load casts.	<ul style="list-style-type: none"> • 127,00 – 121,00 m • 121,00 – 110,00 m 	Figure 14d

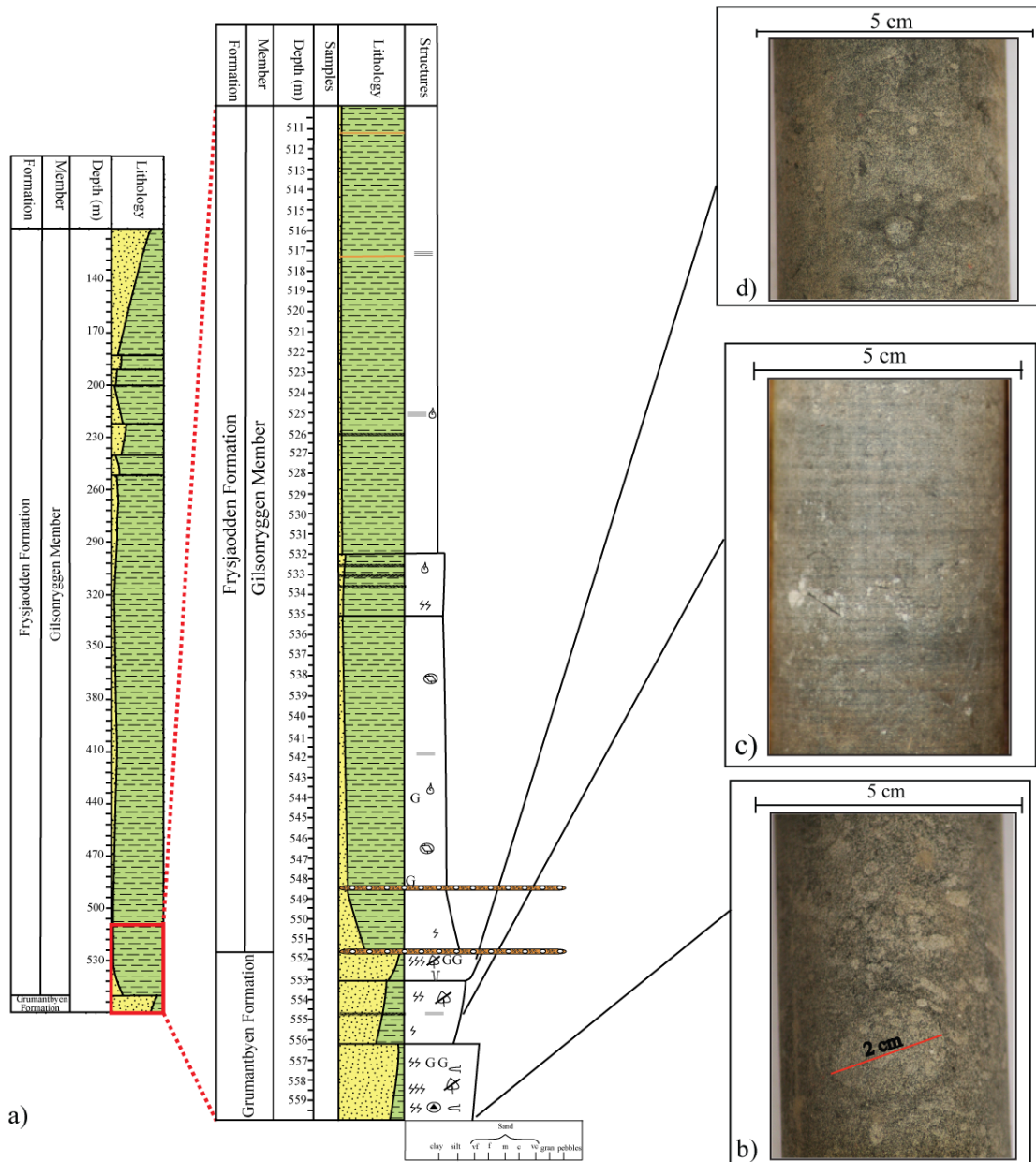
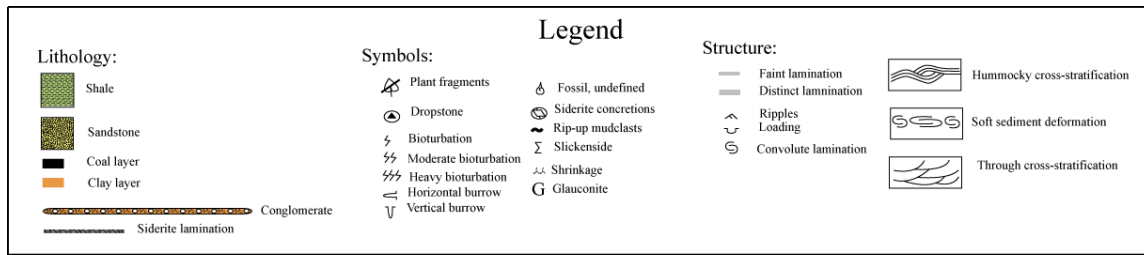


Figure 11: a) Enlarged lower part of core BH /05. b) Example of highly bioturbated sandstone at level 559,40 m. Large burrow: *Thalassinoides*, Small burrows: *Planolites*. c) Example of laminated siltstone at level 555 m. d) Burrow with thin clay rim identified possibly as the trace fossil *Ophiomorpha*.

- i. **Highly bioturbated sandstone** (Figure 11b-d): This facies is present in the Grumantbyen Formation and comprises the first 380 cm of the core (560 – 556,20 m). It contains a silty sandstone of very fine sand. In this upwards coarsening sequence most bedding and structures are destroyed by a high amount of bioturbation, increasing upwards. The burrows are mainly horizontally oriented and they vary in shape and size. Small pieces of organic matter, possibly leaves are present mostly in the lower part of the sequence. Rip-up mud clasts are visible through the whole sequence. This facies is also visible in the last 150 cm of the Grumantbyen Formation, where it ends abruptly in a conglomerate layers at level 551,60.
- ii. **Laminated siltstone** (Figure 11c): In between the two highly bioturbated sandstone facies in the Grumantbyen Formation a parallel laminated siltstone is deposited as a 320 cm thick sequence (556,20 – 553 m).
- iii. **Conglomerate:**
 - a. An about 5 cm polymict conglomerate bed marks the top of the Grumantbyen Formation (551,60 m) (Figure 12a). This conglomerate contains rounded, pebble sized grains, with various origin and composition. It is clearly grain-supported. The conglomerate layer has a conformable base and shows no signs of aerial exposure.
 - b. This 15 cm thick conglomerate disrupts the clay sedimentation two meters above the first conglomerate (iiia) (548,40 m) (Figure 12c). The nature of this layer is quite different from the one below. The grains are subangular and have an average size around medium. The majority of clasts is quartzite, and although the conglomerate is grain supported it contains a high amount of matrix between the grains. The base is possibly erosional.
- iv. **Claystone** (Figure 12b and Figure 13d): Moderately bioturbated, medium grey shale, with small (1-1,5 cm) upwards fining sequences. Lack of lamination characterize this facies which comprise the first 15,50 meters of the Gilsonryggen Member (551,50 - 535 m), only disrupted by the iiib conglomerate. This facies is also repeated in the upper part of the core. The first interval is a 24 meter silty shale sequence at level 304 – 280 m. Silt content is increasing slightly upwards (Figure 13d). This sequence is followed by two contiguous intervals of claystone. The first sequence is represented by a 31 m thick succession ranging from 280 – 249 m (Figure 13d). The last appearance of this facies is a short level (249 – 242 m). Both intervals show a rapid, upwards-coarsening trend and increased intensity of 1-2 cm thick silt layers, with both

erosive and non-erosive base. Large amounts of forams are present in this facies (*Trochammina* aff. *Inornata* most common (Jargvoll, 2009)).

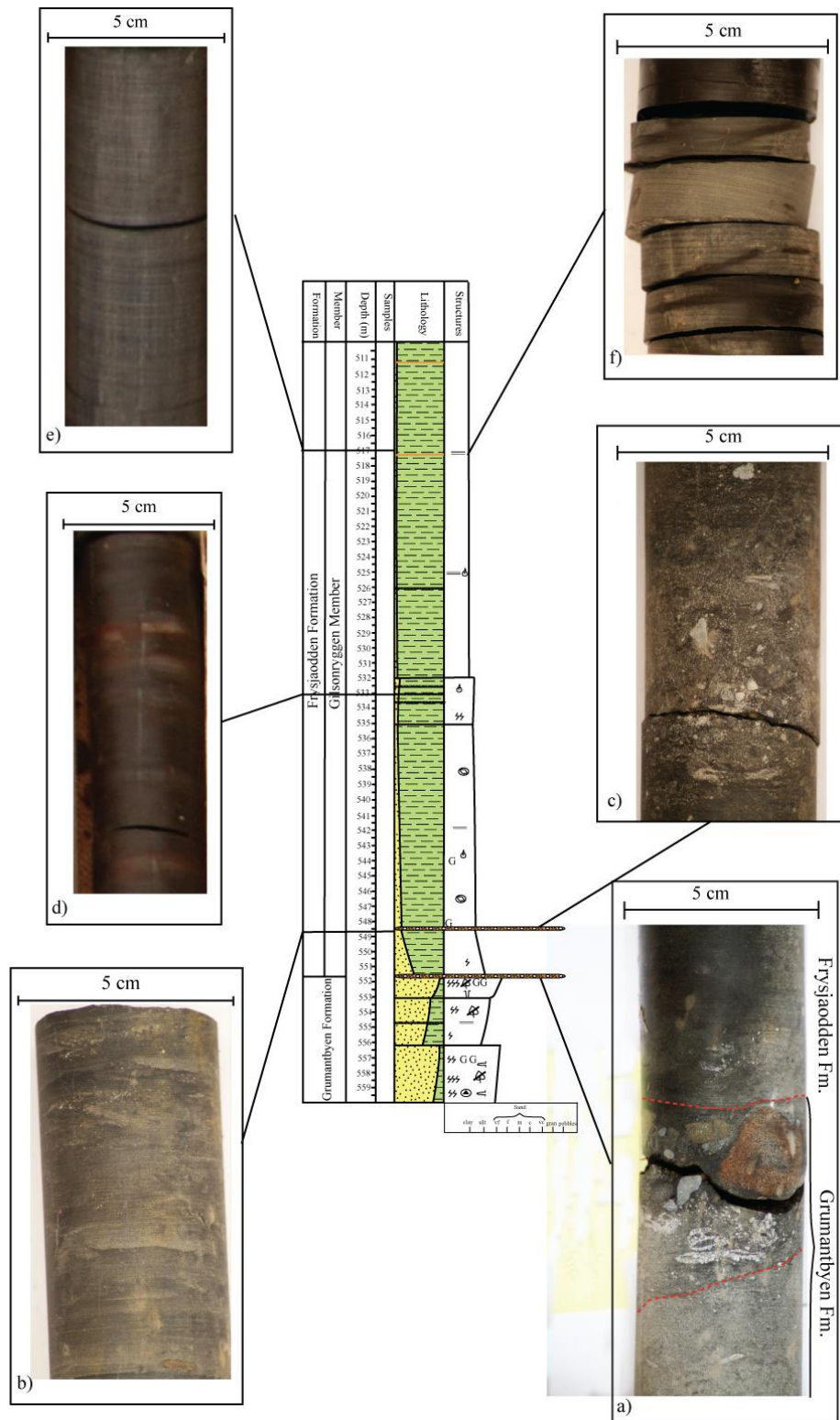


Figure 12 a) Conglomerate (iiiia) at level 551,60 m. b) Claystone at level 548,54 m. c) Conglomerate (iiiib) at level 548,40 m. d) Siderite rich claystone at level 533,20 m. e) Clayshale at level 518,70 m. f) Light gray clay layer in between clayshale at level 517 m.

- v. **Clayshale** (Figure 12e-f and Figure 13b): This facies dominates the lower and middle Gilsonryggen member, making up two large sequences. The lowest one covers 34 meters (532 - 498 m), with another large sequence of around 85 meters in the middle of the section (410 – 325 m) (Figure 13b). This dark gray shale is made up of parallel laminated clay, only disrupted by several upwards fining sequences ranging from 1-2 cm and varying degree of small siderite beds. Intervals with high pyrite content appear.
- vi. **Siderite rich claystone** (Figure 12d and Figure 13c): Claystone characterized by distinct siderite beds and concretions and moderate to high amount of bioturbation. Dispersed organic matter is present. This claystone has a light gray color and grain size lies between clay and silt. This facies comprise one 3 meters thick sequence in the lower part of Gilsonryggen (535 – 532 m), a 90 meters thick sequence in the middle of section (498 – 408 m) and a 20 meter thick succession from 325 – 305 m.
- vii. **Soft sediment deformed siltstone** (Figure 14b and Figure 18b): This facies includes 7 successions in the upper part of the Gilsonryggen Member (242 – 231 m, 231 – 222 m, 222 – 216 m, 200 -190 m, 190 -184 m, 184 – 178,25 m, 178 -150 m) (Figure 15 and Figure 18a). Thickness varies between 4 and 11 meters. The lowest succession (242 - 231 m) has an erosive base, while the others have conformable base. Six of the beds are upwards coarsening, while one is upwards fining (222 – 216 m). Facies viii contains ripple lamination and soft sediment deformation structures like convolute lamination. Also loading structures at the base of sand and silt beds. All beds are moderately bioturbated. The grain size of this facies is close to silt size.
- viii. **Soft sediment deformed sandstone:** Facies viii forms an upwards coarsening succession, where the lower part is a moderately laminated silty shale. Moving upwards the silt content increase, siderite beds decrease in intensity and convolute lamination appears near the top. This facies is moderately bioturbated and contains some organic matter. This facies is found in the upper part of the section (level 150 m – 140 m) (Figure 18a).

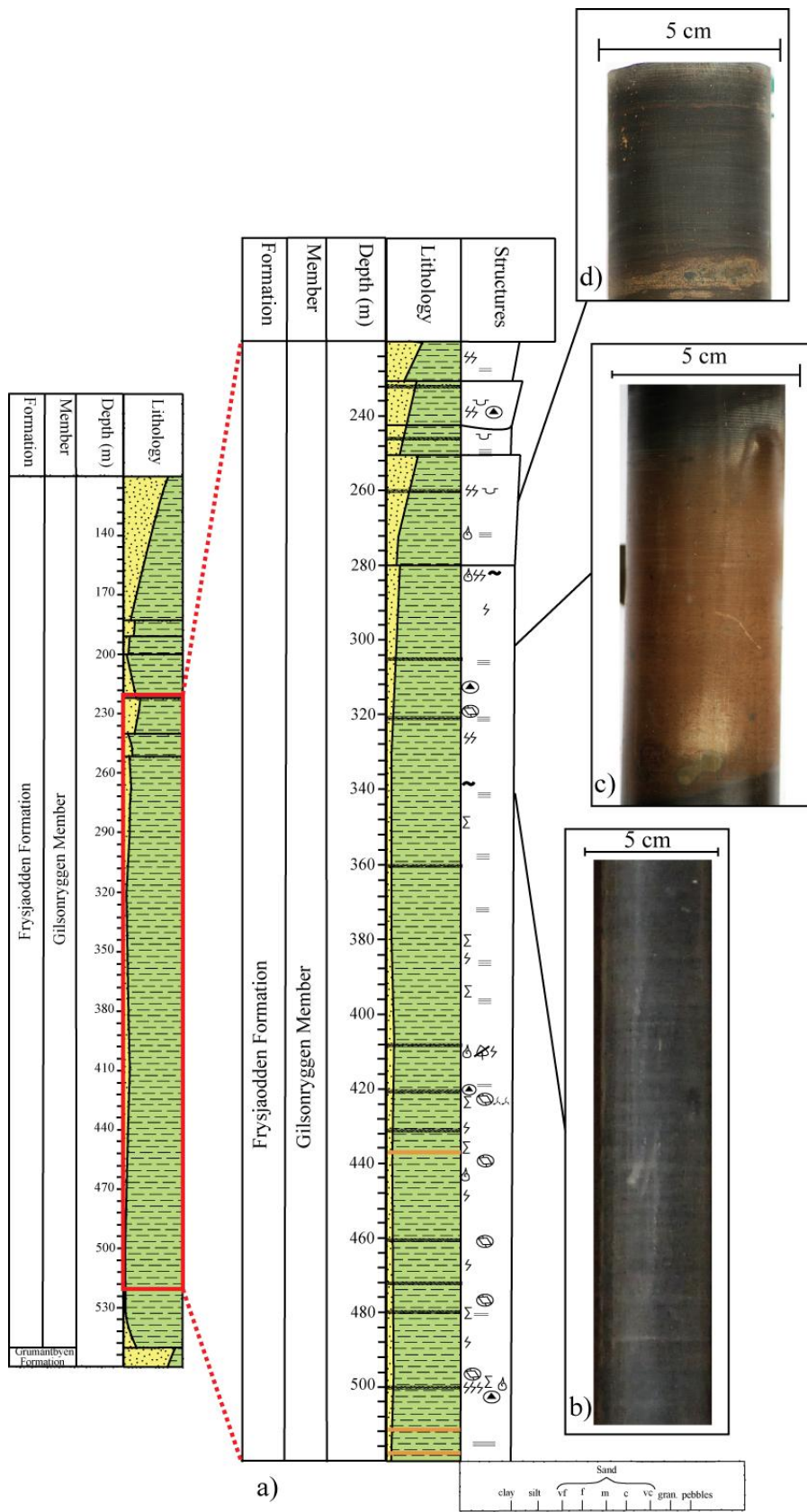


Figure 13: a) Enlarged middle part of core BH 9/05. b) Example of clayshale at level 338,60. c) Siderite rich claystone at level 304,60 m. d) Claystone at level 264,54. Note the coarse grained layer (1 cm) at the bottom.

- ix. **Low angle ripple laminated sandstone** (Figure 14c and Figure 19): Present as two contiguous sequences in the upper Gilsonryggen Member (140 m – 127 m). The lowermost bed (8 m) has an erosive base and is conformably overlaid by the upper 5 m thick bed (Figure 18a). Both sequences are moderately bioturbated, with mainly vertically oriented burrows. The grain size increases from silt to very fine. The top of both sequences are characterized by ripple laminated sandstone. Coal fragments are also present in all three. This facies also appears as a very fine sandstone bed in between soft sediment deformed siltstones beds as a 0,25 meter thick layer (178,25 m – 178,00m.)
- x. **Cross-stratified sandstone** (Figure 14d): The two upper most sequences in the core are made up of trough cross- and hummocky cross-stratified sandstone. One being 6 meters (127 m -121 m) and the other 11 meters (121 m -110 m) in thickness (Figure 18). Distinctive features identifying this facies are trough cross bedding structures and possible hummocky-cross stratification, loading structures and moderate to high grade of bioturbation. Increased intensities of sand beds appear towards the top of each sequence. The base of these beds is varying between being conformable and eroding into the background clay sedimentation. The grain size is changing from silt at the bottom to very fine sand at the top. Both sequences are rich in organic matter, both as individual fragments (0,5 -1 cm) and thin layers (2-3 mm thick).

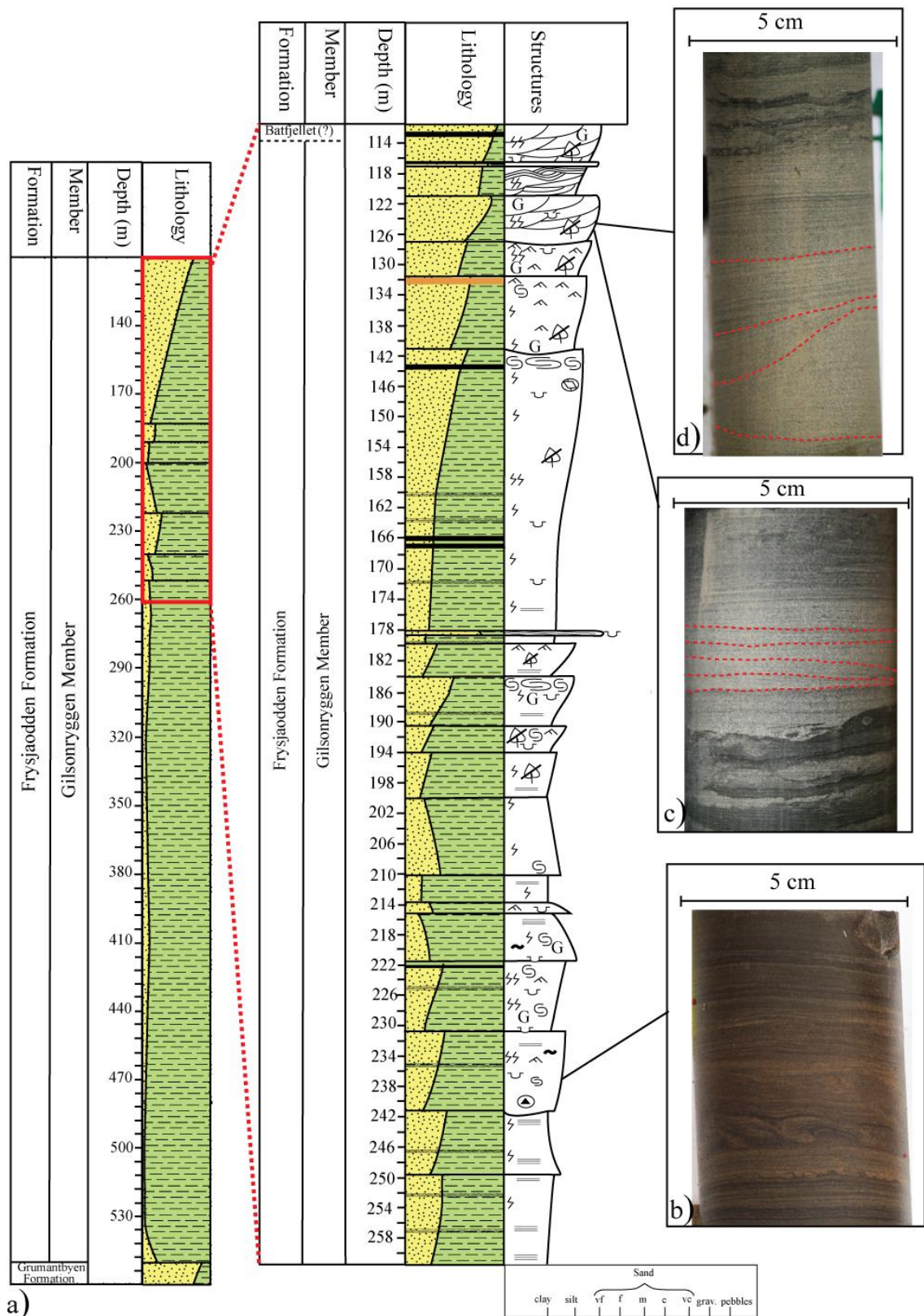


Figure 14 a) Enlarged upper part of core BH /05. b) Example of soft-sediment deformation structures (convolute lamination, ball-and-pillow, loading) at level 227,90 m. c) Ripple-laminated sandstone at level 125,20 m. d) Hummocky cross-stratified sandstone at level 124,30 m.

5.2 Facies associations

- **FA1:** Upper Grumantbyen sandstone association (560 m -551,60 m):
(Figure 15)
 - *Highly bioturbated sandstone (i), Laminated siltstone (ii), Conglomerate (Pebble) (iiia)*
- **FA2:** Shales of lower/middle Gilsonryggen (551,60 m -280,00 m)
(Figure 15)
 - *Claystone (iv), Siderite rich claystone (vi), Clayshale (v), Conglomerate (Gravel) (iiib)*
- **FA3:** Upper Gilsonryggen siltstones (280,00 m – 150,00 m)
(Figure 15 and Figure 18a)
 - *Claystone (iv), Soft sediment deformed siltstone (vii) and Low angle ripple laminated sandstone (ix)*
- **FA4:** Upper Gilsonryggen/ Lower Battfjellet sandstones (150,00 m - 110,00 m) (Figure 18a)
 - *Soft sediment deformed sandstone (viii), Low angle ripple laminated sandstone (ix) and Cross stratified sandstone (x).*

5.2.1 FA1: Upper Grumantbyen sandstone association (560 – 551,60 m)

The lower most facies association constitutes of two upwards coarsening sequences of highly bioturbated sandstone layers (i) where all bedding and structures have been destroyed (Figure 11 b-d). The two layers are separated by an episode of parallel laminated silt deposition (ii) (Figure 11c). This association represents an overall upwards coarsening trend and at the top ripple marks are visible. The upper Grumantbyen sandstones end in a conglomerate layer (iiia) (Figure 12a), indicating the transition between the Grumantbyen Formation and the Frysjaodden Formation.

5.2.2 FA2: Shales of lower/middle Gilsonryggen (551,60 m -280,00 m)

The shales of the lower/middle Gilsonryggen comprise the largest interval of the facies associations. It begins where the conglomerate of Grumantbyen ends (551,60 m), and extend up to where the siltstone interval starts, at 280,00 m.

The first 18,40 meters contain a claystone facies (iv) (Figure 12b) disrupted by a conglomerate layer (iiib) at 548 m (Figure 12c). The silt content rapidly decreases between the two conglomerates and the shale gradually becomes cleaner moving upwards. At 535 m a

more siderite rich claystone (vi) occupy the next 3 meters (Figure 12d). The lighter color of this rock might be due to a slight increase in grain size. The end of this siderite rich claystone, at 532 m marks the start of the laminated shales. A laminated shale facies, denoted “clayshale” (v), spans the interval from 532 m to 498 m (Figure 12e). The dark gray color and thin lamina implies clean shale, interrupted only by thin (1 cm) upward fining sequences. Two thin (1-2 cm), light gray layers are present at 517 m (Figure 12d) and 511 m and are possibly thin bentonite beds. The interval from 498 m to 409 m is covered by a moderately bioturbated, claystone (v) where siderite bands appears frequently (Figure 13d). Silt content appears to increase slightly from the clayshale below.

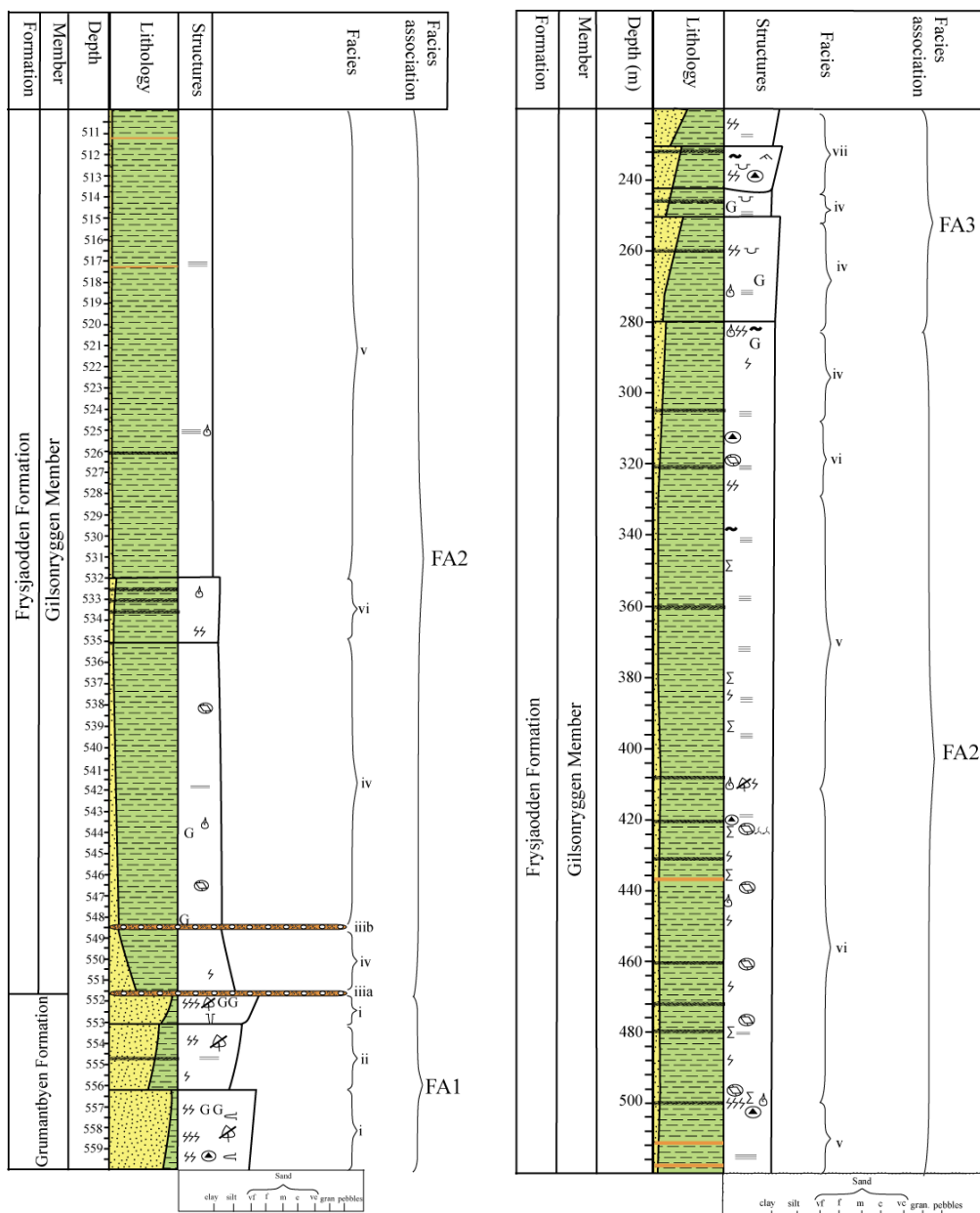
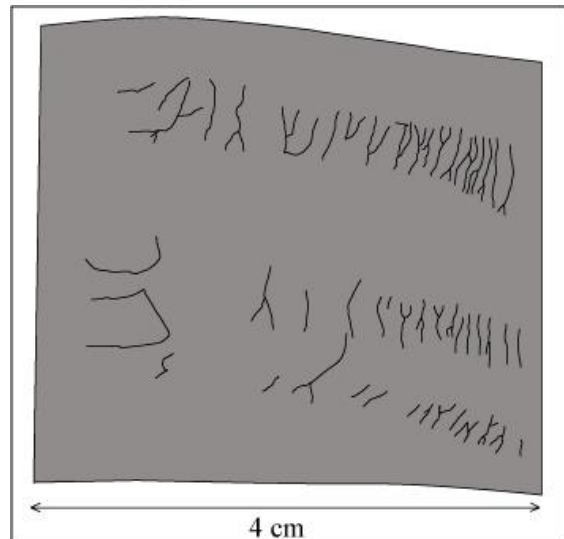


Figure 15: Facies and facies associations from level 560 to 220 m

At 436 m another light gray clay layers with a soapy consistence is observed. Around level 425 m there are several examples of sub-aqueous shrinkage structures. Sketch in Figure 16 illustrate one example of these structures.

Figure 16: Sketch of subaqueous shrinkage cracks in sample at level 426,90 m.



A large interval from 409 m to 325 m is made up of clayshale (v) (Figure 13). This section contains little but dark gray, laminated shale, pyrite concretions (Figure 17) and certain small upwards fining sequences. These small, coarser grained sequences are moderately bioturbated. The interval between 409 – 325 m shows similarities to the interval spanning the region 532 – 498 m.

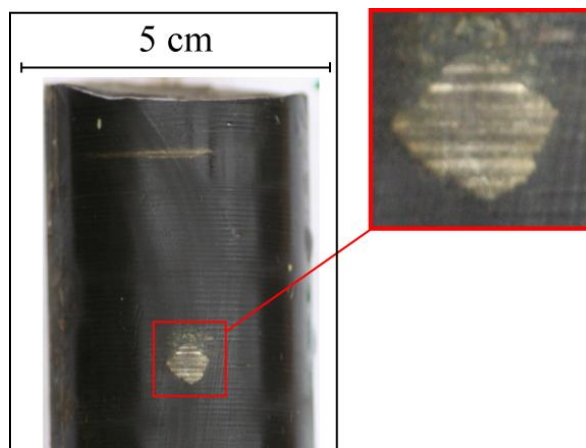


Figure 17: Example of pyrite from level 400,20 m.

From 325 m – 305 m a siderite rich claystone (vi) is observed (Figure 12d and Figure 13c). This interval also marks the start of an upwards coarsening mega sequence, which will continue through the rest of the core. It is overlain by a 15 meter thick, upwards coarsening claystone (iv) which ends FA2 and the shales of the middle part of Gilsonryggen at 280 m (Figure 15).

5.2.3 FA3: Upper Gilsonryggen siltstones (280 m – 150 m)

This facies association act as an intermediate between the shales below (FA2) and the sandstones above (FA4). Grain size increases from clay at the bottom to coarse silt at the top of the interval. The general trend is upwards coarsening, but the region from level 222 to 200 m represents a short episode of upwards fining deposits (Figure 18).

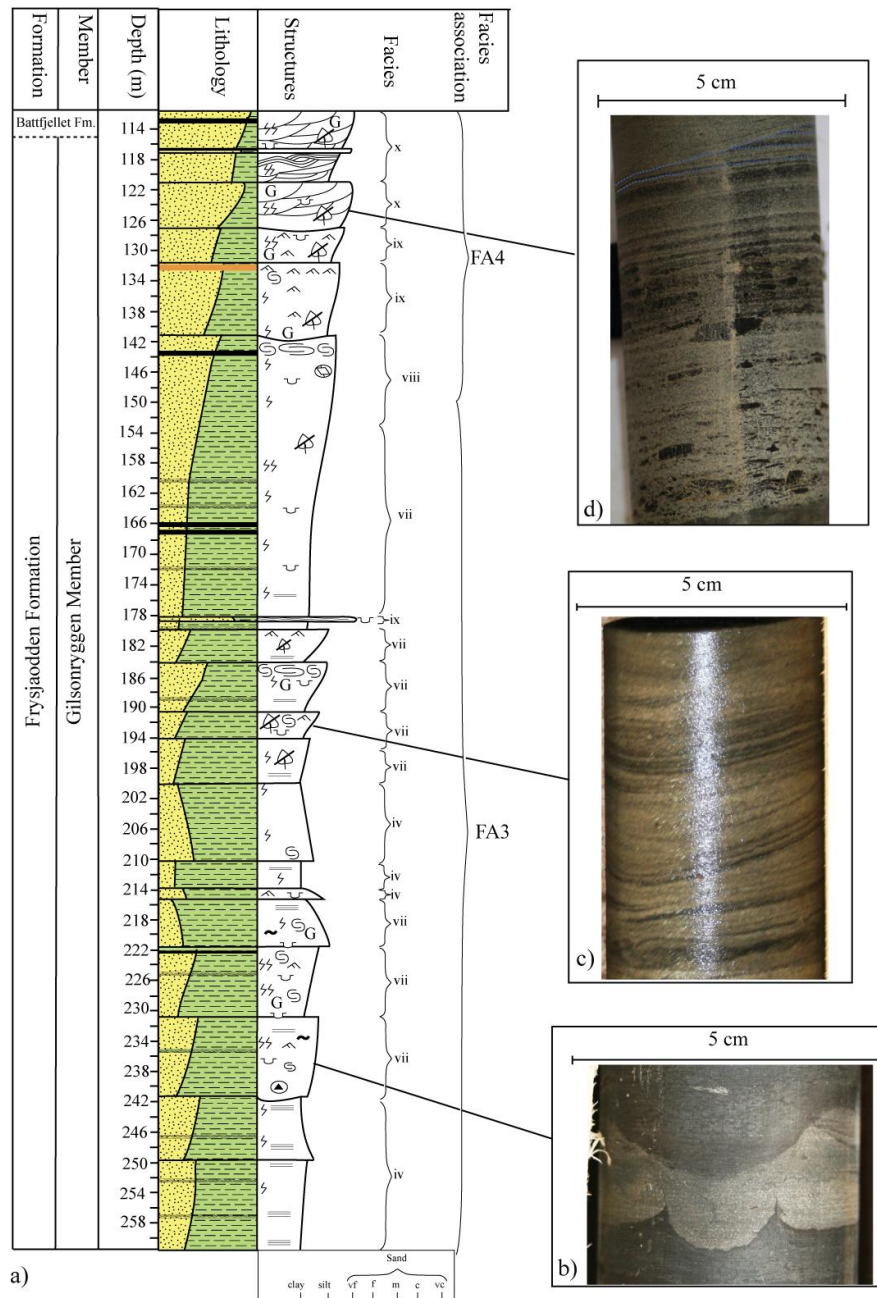
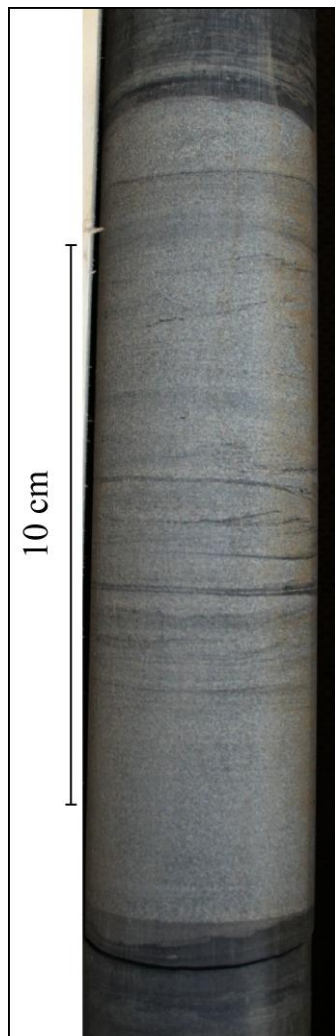


Figure 18: a) Facies and facies associations from level 260 – 110 m. b) Loading and flame structure at level 227,90. c) Ripple laminated siltstone at level 192,35. d) Wood fragments in sand layer. Note the eroding sand layers near the top (111,10 m).

This facies association begins with two upwards coarsening beds of claystone (iv) (Figure 15) similar to the first deposits of Gilsonryggen Member shales. This interval is overlain by an upwards coarsening, soft-sediment deformed siltstones (vii) (Figure 18a - b) with and erosive base. The interval continues with a similar bed with conformable base. From around 222 m core depth a period of upwards fining deposits begins. The first interval consists of a soft-sediment deformed siltstone. Above this interval three beds of upwards fining, poorly bioturbated claystone follow.

The siltstone facies continues with four upwards coarsening, rich in organic material, soft sediment deformed siltstones (vii), ranging from 200 m to 178,25 m (Figure 18a).

From 180 m an upwards coarsening, soft sediment deformed siltstone/sandstone facies



begins, which range up to 141 m (Figure 18a). At level 179,70 m a 15 cm thick, low angle ripple laminated sandstone is observed (Figure 19). The boundary between the siltstones of Gilsonryggen and the sandstones of Gilsonryggen is placed at 150 m.

5.2.4 FA4: Upper Gilsonryggen / Lower Battfjellet sandstones (150,00 m – 110,00 m)

There is a gradual transition from siltstones to a sandstone dominated succession. At around 150 m the grain size has increased to between silt and very fine sand, and the coarse grained intervals become more and more frequent. The first interval in this facies association is formed by soft sediment deformed sandstone. This silty sandstone package is eroded by a low angle ripple laminated (LARL) siltstone at level 141 m. Another LARL sandstone is deposited above this level ranging from 132 m to 127 m. The silt/sand content is increasing upwards along with bioturbation by larger organisms (*Thalassinoides* ichnofacies). The deposition of a cross-stratified sandstone start at level 127 m. This facies can be divided into two packages, the latter ranging from 121 m to 110 m. Heavy bioturbation (*Planolites*) and high energy structures such as trough cross and hummocky cross stratification is abundant (Figure 14d). Close to

Figure 19: Low angle ripple laminated siltstone at 179,70 m

the top there are indications of some layers with more planar bedding. Coaly fragments (0,5-1 cm) and thin coal layers (0,2 -0,5 mm) are numerous in the sand deposits (Figure 18d).

6 Mineralogical and petrographical description

This chapter will present the results from the mineralogical and petrographical description. These observations have been carried out by thin section studies and XRD analysis, as explained in chapter 4.

6.1 Thin section analysis

This chapter will present the results of thin section analysis. The results of point counting are summarized in Appendix 3, and the main lithological characteristics will be presented together with the petrographical properties.

6.1.1 Sandstones of Grumantbyen Formation (560,00 m -551,60 m)

From this formation two thin sections were studied. They both represent grain supported sandstones, where all the sedimentary structures have been destroyed by heavy bioturbation. Sand grains are of subangular to angular shape, with an average size of very fine. The grains are tightly packed with clays; illitic clay cement has been identified. Only isolated pockets of open pore space with no pore-pore interconnection are visible. Thus these rocks have moderate porosity and poor permeability. Elongated grains, such as mica (mostly muscovite) and mud clasts have non-preferred orientation. From the point counting muscovite appears to be the most abundant mineral of the micas, but biotite is also present (Appendix 3). Most of the larger mica grains (0,1-0,2 mm) have been bent and deformed between sandgrains. Contacts between grains appear to be tangential with prevailed concavo-convex and long contacts. The most striking mineralogical feature of these sandstones is the scarcity of quartz compared to feldspar (Figure 20a), the relation is 40/60 in favor of feldspar (Appendix 3). Some of the feldspar grains have partly dissolved into clay minerals, but most are visually unaltered (Figure 20b). The quartz grains are mostly monocrystalline, but there are some examples of polycrystalline quartz. Besides the rock forming minerals, this sandstone is rich in glauconite, chlorite and micas (muscovite and biotite) (Figure 20c). Organic matter, in form of wood particles (0,2-0,5 cm) is present.

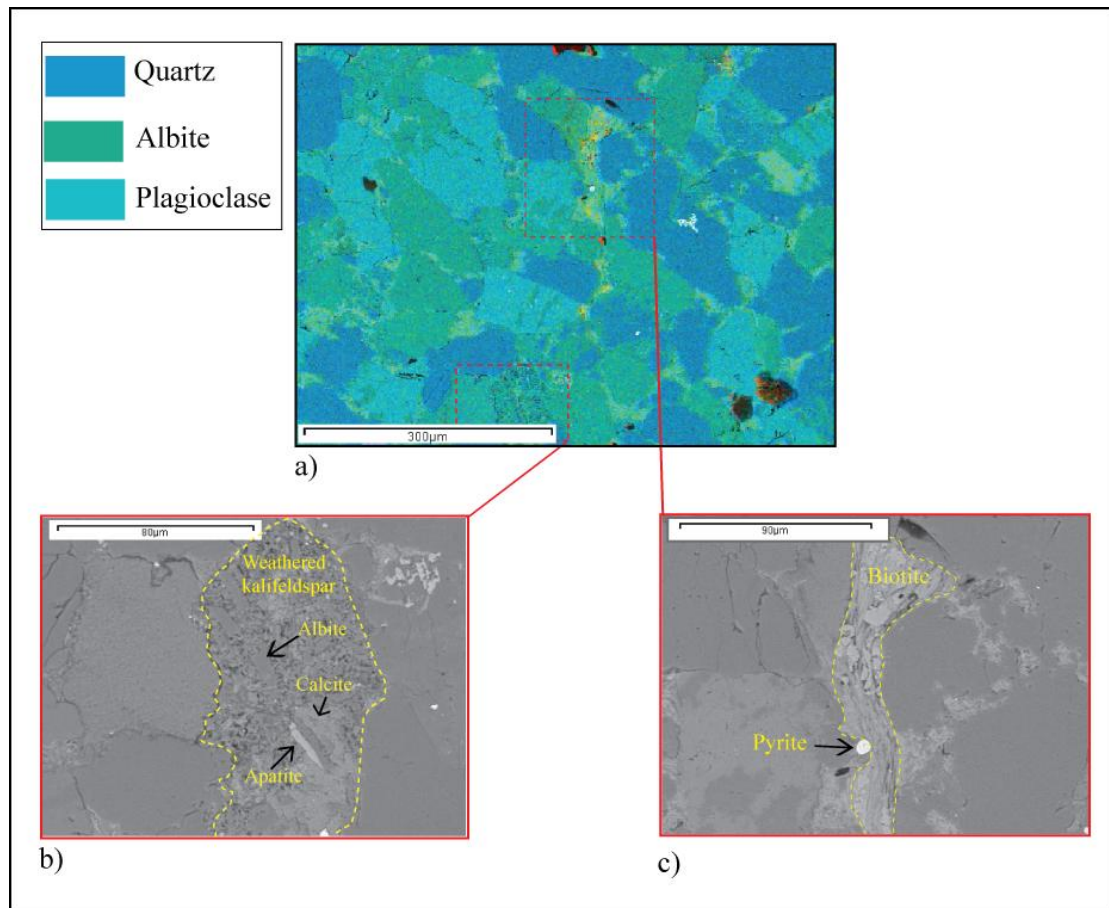


Figure 20: a) Cameo photography from SEM illustrating the high content of feldspar (552,43 m). b) Weathered kali-feldspar, with larger fragments of albite, calcite and apatite. c) Detrital biotite squeezed between grains. Also visible is a small pyrite.

6.1.2 Lower Gilsonryggen shales (part one): (551,60 m – 532,00 m)

This interval is represented by five thin sections. It starts with a poorly sorted siltstone (Figure 21a), situated just above the conglomerate separating the Grumantbyen Formation and Gilsonryggen Member (Figure 12a). The siltstone contains large amount of illitic clay matrix, but the overall impression is a grain supporting framework. The poor sorting is evident, as the sample is also rich in grains larger than 0,25 mm. From point counting it is evident that there is a change in the quartz/feldspar ratio at this level (Appendix 3). They are now present in equal amounts, together making up around 45 % of the rock. In this shaly siltstone is small amounts of chlorite, glauconite, micas (mainly muscovite) and some diagenetic pyrite are also present. Lamination has been destroyed by bioturbation.

The shales in the lowest part of Gilsonryggen are interrupted by a conglomerate at 548,35 (Figure 12c). The conglomerate matrix contains mostly subangular quartz, chert and feldspar grains, with monocrystalline quartz being the dominate one (Figure 21b). Average grain size in this conglomerate matrix is medium. Although this is a grain supported rock, there are a

high content of clay matrix between grains. A few examples of micas and glauconite grains are also observed.

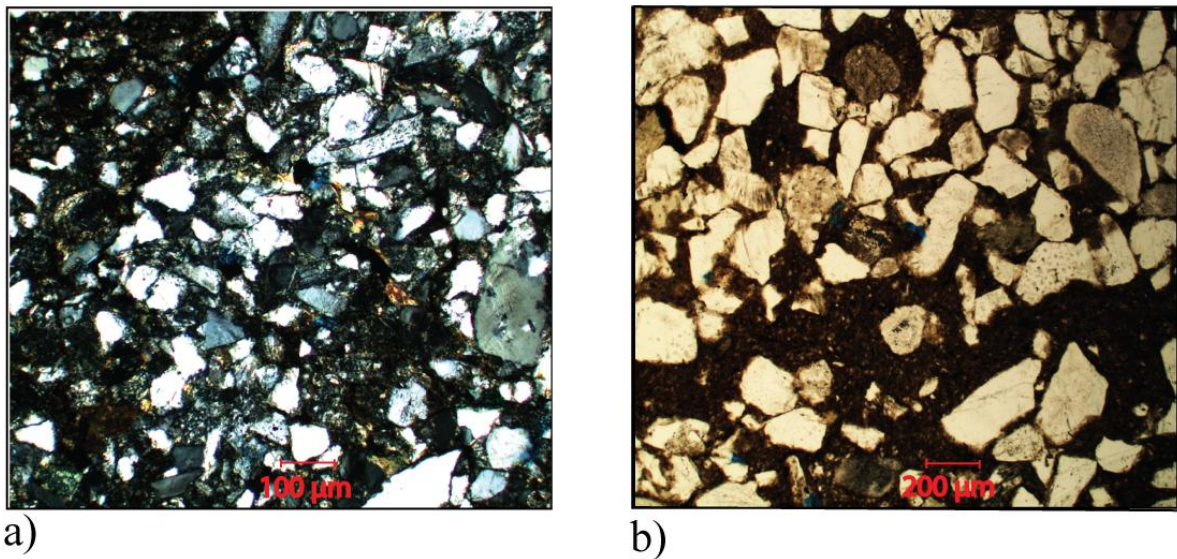


Figure 21: a) Poorly sorted, shaly siltstone at 551,43 m represents the transition from sandstones to shales (crossed nicol) b) Conglomerate matrix at 548,35 m.

The three samples above the conglomerate display an upwards fining trend (Figure 23). The most common grain shape changes from sub angular to rounded and the sorting from poor to good. The input of larger grains also decreases upwards along with decreasing level of bioturbation. A common feature in this interval is the high content of agglutinated foraminifera (Figure 22).

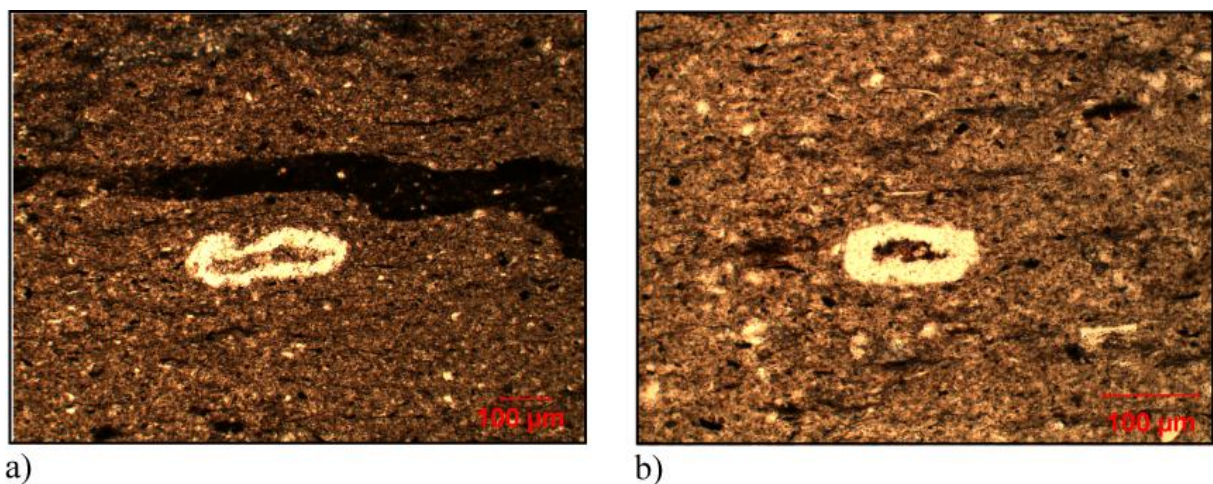
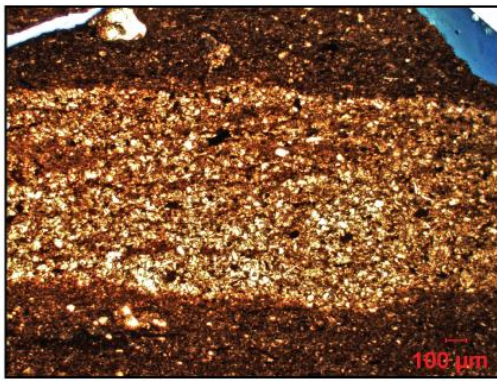


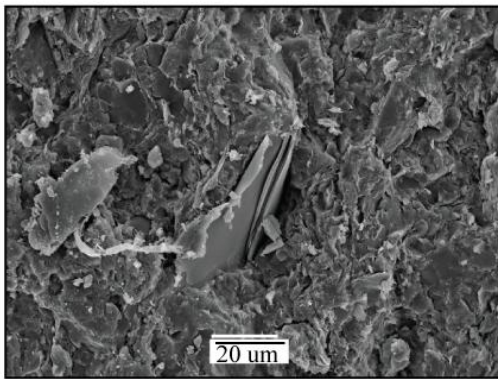
Figure 22: Two examples of agglutinated foraminifera from level 532.37. a) *Hyperammina* sp. b) *Hyperammina* Sp.



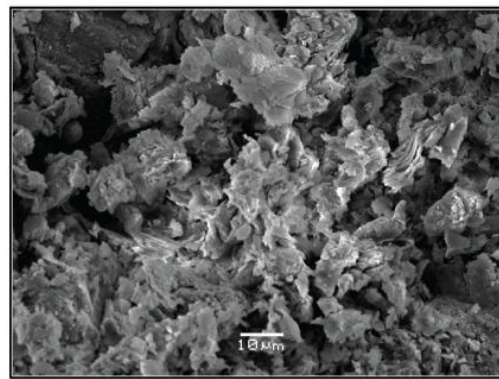
a)



b)



c)



d)

Figure 23: a) Thin upwards fining silt layer in clay matrix (544,63 m). b) Homogenous clay matrix, non-laminated (532,37 m). c) SEM picture of shale (536,36-6 m). The large clay particle in the centre of picture is a chlorite. d) SEM picture of clay matrix at level 536,66 m.

6.1.3 Lower Gilsonryggen shales (part two), (532,00 m – 500,00 m)

The lower middle part of shales in Gilsonryggen is covered by four thin sections. The main characteristics of this interval are parallel laminated shale (clayshale), with rounded to subrounded grains (Figure 24). Some thin, upwards fining silt layers interrupt the clay sedimentation. These layers are moderately to heavy bioturbated. There are a few examples of agglutinated forams present (*Hyperammina* Sp., *Trochammina* aff. *inortata* and *Birsteiniolla* Sp. (Jargvoll, 2009)) Two of the samples contain secondary cracks following the direction of the bedding.

In thin section this clayshale is almost exclusively clays and the only prominent non-clay mineral is pyrite, which appears both as single framboidal pyrites (Figure 24d) and in some cases as entire bands, made up of framboidal pyrite, crossing the entire thin section. Isolated quartz and feldspar grains are observed scattered in the clay matrix.

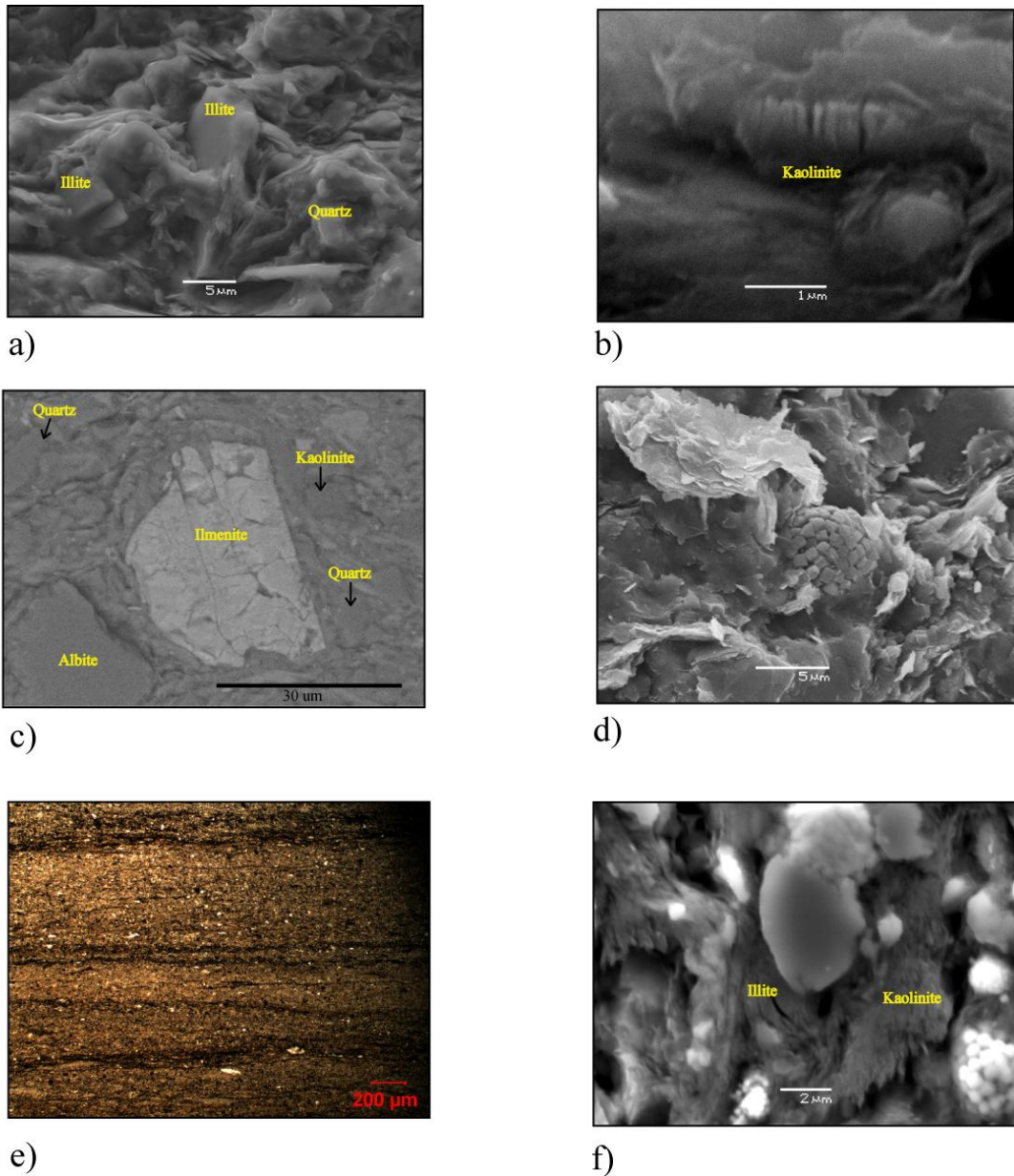


Figure 24: a) Detrital illite at 530,99 m. b) Possibly authigenic kaolinite (530,99 m). c) Possibly detrital kaolinite, large ilmenite and albite grain. d) SEM picture showing framboidal pyrite (528,75 m) e) Laminated shale from 525,05 m. f) Detrital illite and kaolinite (525,05 m)

6.1.4 Middle Gilsonryggen shales (part one), (500,00 m – 408,00 m

The three thin sections covering this interval exhibit similar textural features: alternating laminated shale and moderately bioturbated, upwards fining silt layers. Upwards in the interval coarse grains (>0,2 mm) and elements of organic material appears more frequent (Figure 25b). Agglutinated forams are present both in the lower and upper part (*Rheophax* aff. *metensis* and *Psammosphaera* aff. *Fusca*, (Jargvoll, 2009)).

This section contains, besides the clay matrix (close to 95%), some quartz, chert (Figure 25a) and feldspar grains (Appendix 3). Single, isolated glauconite grains are observed.

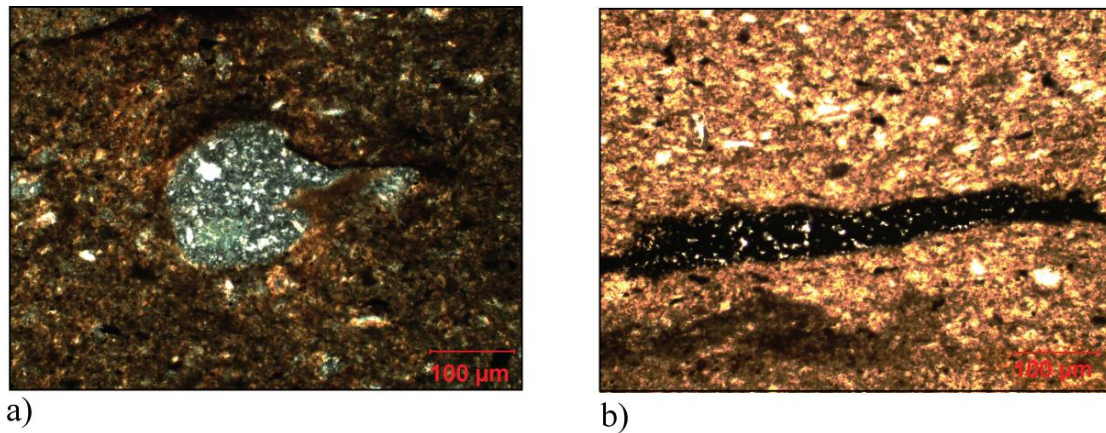


Figure 25: a) Chert pebble in clay matrix at 439,93 m. b) Organic material in clay matrix at 410,05 m.

6.1.5 Middle Gilsonryggen shales (part two), (408,00 m – 280,00 m)

The four thin sections from this interval indicate a trend moving from parallel laminated and moderate bioturbated shale into heavy bioturbated, non-laminated shale (claystone). Most grains are subangular in shape. In the lowest section there is evidence of a listric, normal fault with throw of about 5 mm. Upwards in the section thin layers (up to 3 mm) with increasing

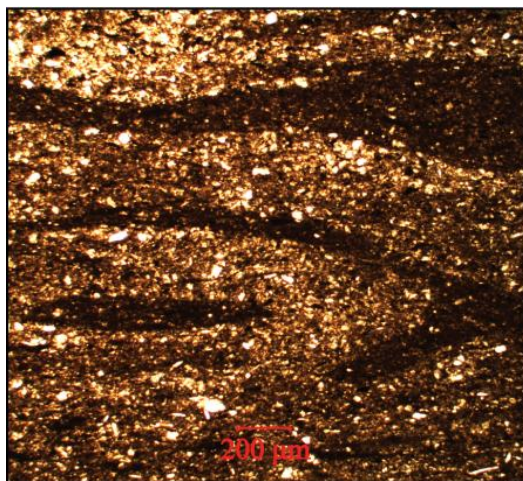


Figure 26: Possibly *Planolites* trace fossil, compressed during compaction (282,05 m)

grain size are interrupting the clay sedimentation with growing intensity. The lowermost layers contain clay sized particles in fining upwards developments. Higher up in the interval (E.g. level 380,05, 330,05, 290,05 and 280,05 m), grains of silt size dominate in the intervening layers. These layers are eroding into the mud layers below, ripping up mud clasts to be found in the succeeding beds

The layers are around 2-3 mm thick and fining upwards. In this part of the section the sediments are highly bioturbated (Figure 26).

These sediments also contain some agglutinated forams (*Rheophax* aff. *metensis* and *Psammosphaera* aff. *Fusca* , (Jargvoll, 2009)).

The mineralogical composition changes from the lower parts of the interval to the upper parts. Clay content is decreasing, from around 90% to around 80%, and minerals like glauconite, mica and chlorite become more common (Appendix 3). Small quartz grains, mainly monocrystalline, are apparent through the whole interval.

6.1.6 Siltstones of upper Gilsonryggen (280,00 m– 150,00 m)

This shaly siltstone succession is represented by eleven thin sections. It is characterized by shale alternations, both laminated and non-laminated, and coarse grained lamina are present (Figure 27). Grain size of these coarse grained layers varies from silt to very fine sand. The shape of the grains alternates between subangular and subrounded, but in the last thin section at 150,05, grain shape is clearly angular. The majority of grains are monocrystalline quartz. Feldspathic grains are less frequent but some examples have been observed.

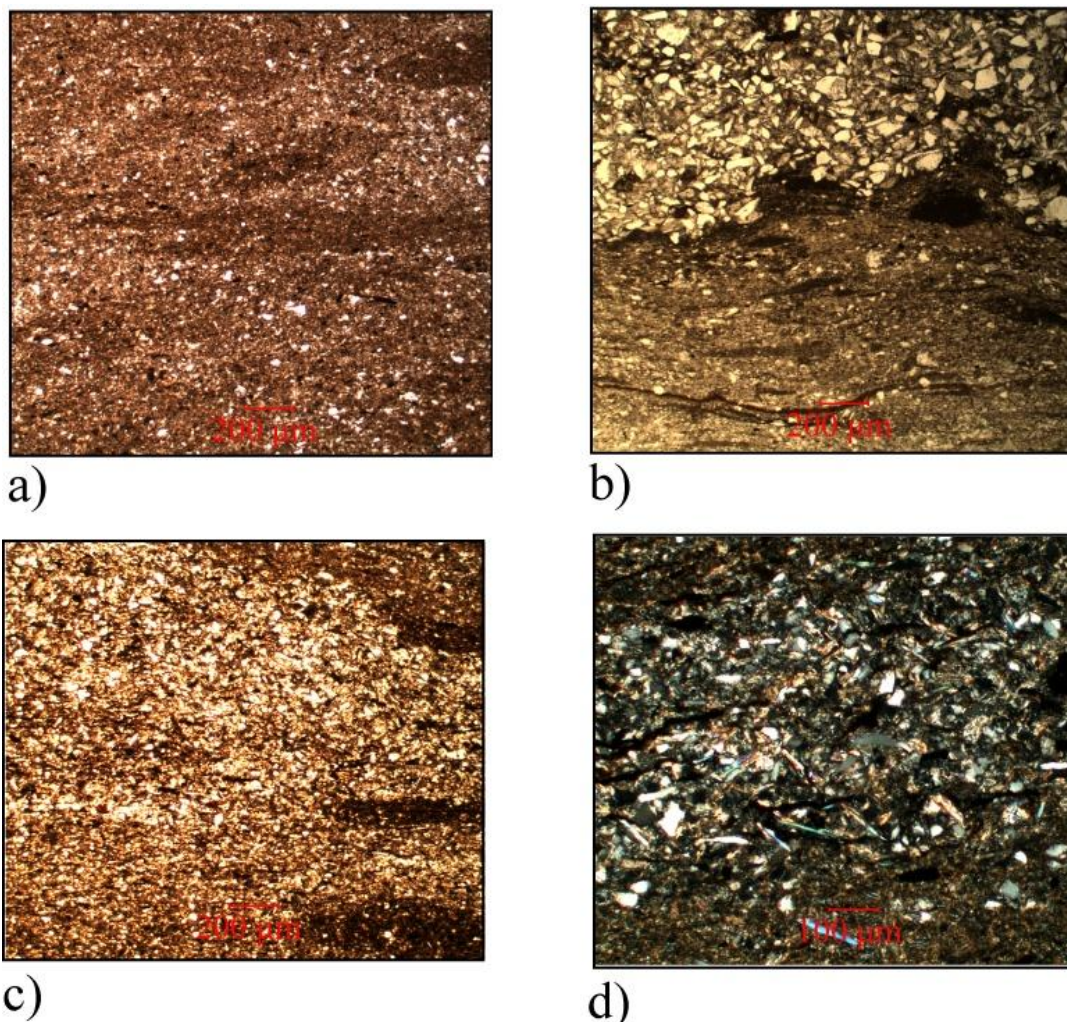


Figure 27: : Four micrographs illustrating the evolution of the siltstones in Gilsonryggen. At a) a bioturbated silty shale (270,05 m). b) Coarse grained silt layer above shale (264,59 m). c) Example of shaly silt at 190,05. d) Illustrates an organic rich siltstone with plant fragments at 150,05 m (crossed nicol).

The silt and sand amount increase upwards. The siltstone/shales are more illitic in the upper part of the interval, and micas and chlorite become more common. In the upper part of the succession the silt layers can be classified as beds since they exceed 10 mm thickness. Most of the silt layers are upwards fining containing rip-up mud clasts along the base, loading and soft sediment deformation structures and moderate degree of bioturbation. These silt beds contain what is believed to be ripple lamination. The silt beds also contain some organic matter and agglutinated forams. Pyrites are present in some sections and absent in others.

6.1.7 Sandstones of upper Gilsonryggen Member (150,00 m – 110,05 m)

This is the final part and marks the end of the Gilsonryggen Mb. Six thin sections are chosen to represent this succession. These sandstones are grain supported and have an average grain size varying from silt to very fine sandstone. The grains are sub-angular to sub-rounded and moderately sorted. Structures changes from heavy bioturbation in the lower parts to examples of cross lamination at the top. One example of spreiten trace fossil, *Rhizocorallium* type appears in the middle of the interval (Figure 28) .

The silt and sand beds alternate between being upwards fining and upwards coarsening. They contain rip-up mudclasts and large amounts of organic matter (up to 5%) (Appendix 3). Mud clasts and elongated grains vary between being parallel and obliquely oriented to the bedding.

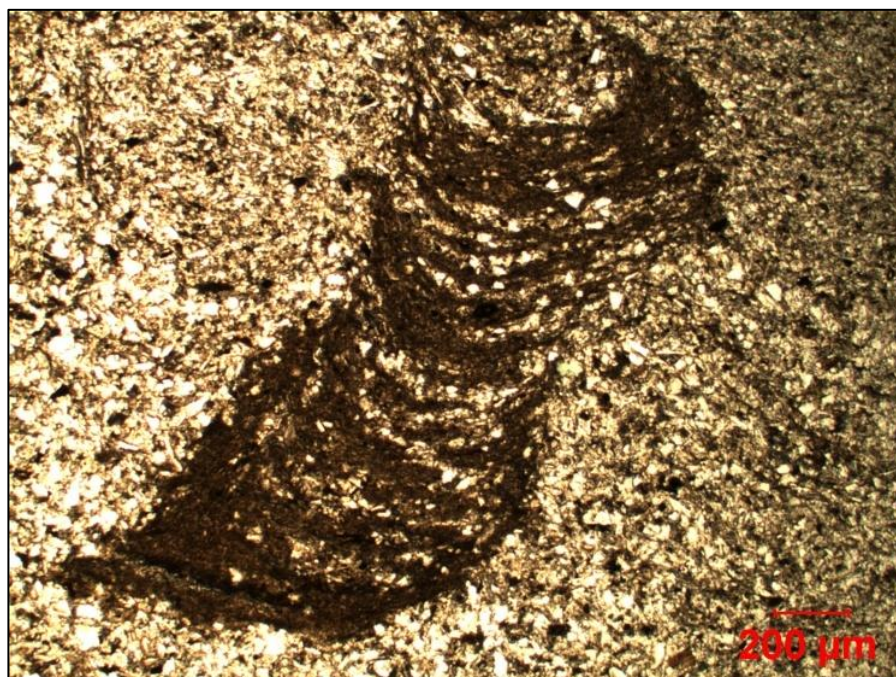


Figure 28: Spreiten trace fossil, *Rhizocorallium* type (130,05 m).

The sandstones contain both monocrystalline and polycrystalline quartz and feldspar (Figure 29). These sandstones differentiate from the Upper Grumantbyen sandstones. The quartz/feldspar ratio is now 60/40 in contrast of 40/60 near the core base (Appendix 3). Contacts between grains are in most part tangential. The pore space is mainly filled with a dominating illitic clay matrix (30-40% of total rock) and large amounts of bent and deformed micas (up to 10%). As for the Grumantbyen sandstones, the pores also here appear as isolated pockets and consequently with poor permeability. From point counting glauconite is identified (0,2 %), but not as frequent as in the Grumantbyen sandstones (around 1,5 %). Other secondary minerals are chlorite (up to 4 %) and pyrite (Figure 29b-c).

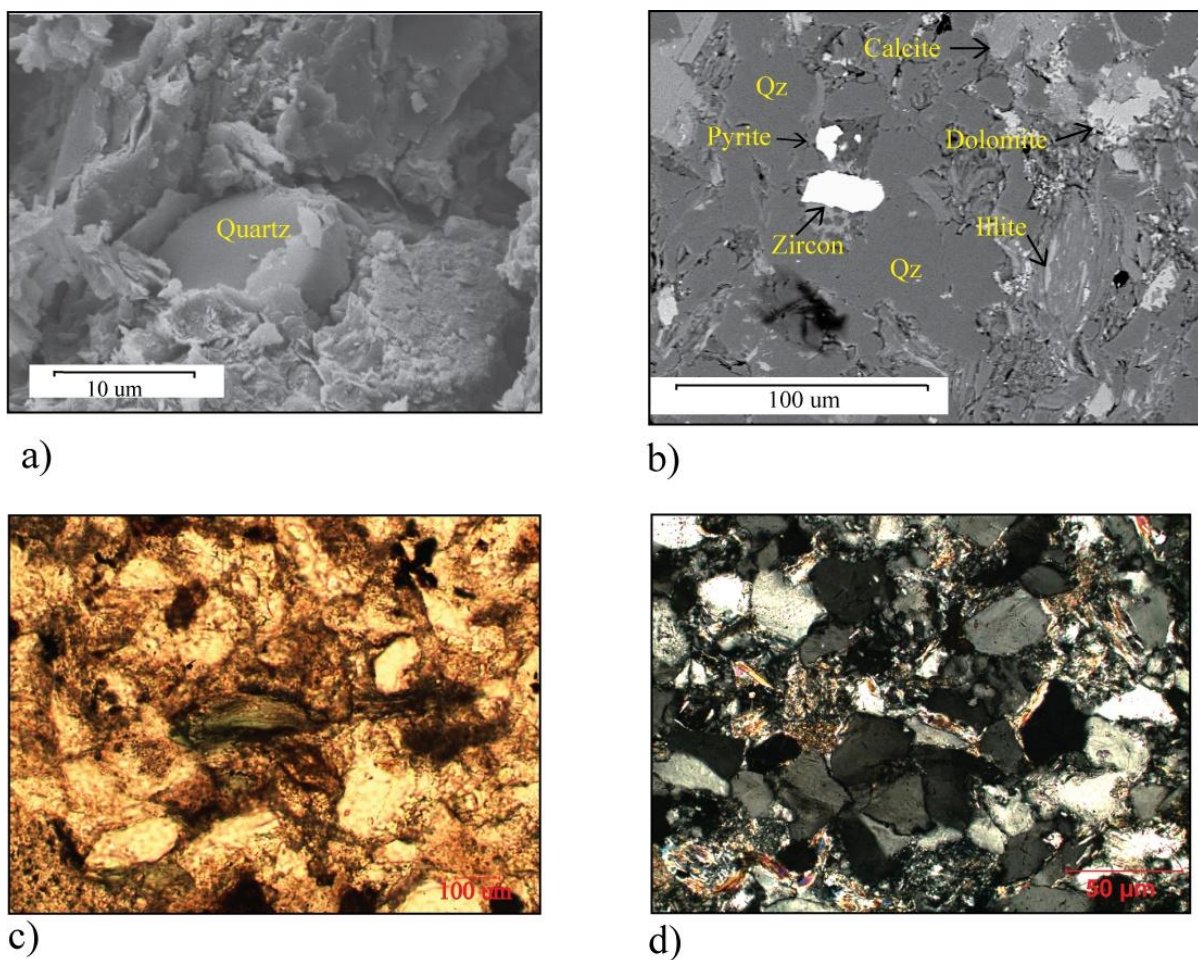


Figure 29: a) This picture shows SEM photography of a quartz grain embedded in shale matrix (140,05 m). b) This SEM picture illustrate variations of minerals in sandstone at 138,80. c) Micrograph of a chlorite grain at 120,05 m. d) Micrograph of a mica rich sandstone at 110, 05 m (crossed nicol).

6.2 XRD analysis

This chapter comprises the results from the XRD-analyses (bulk and clay fraction).

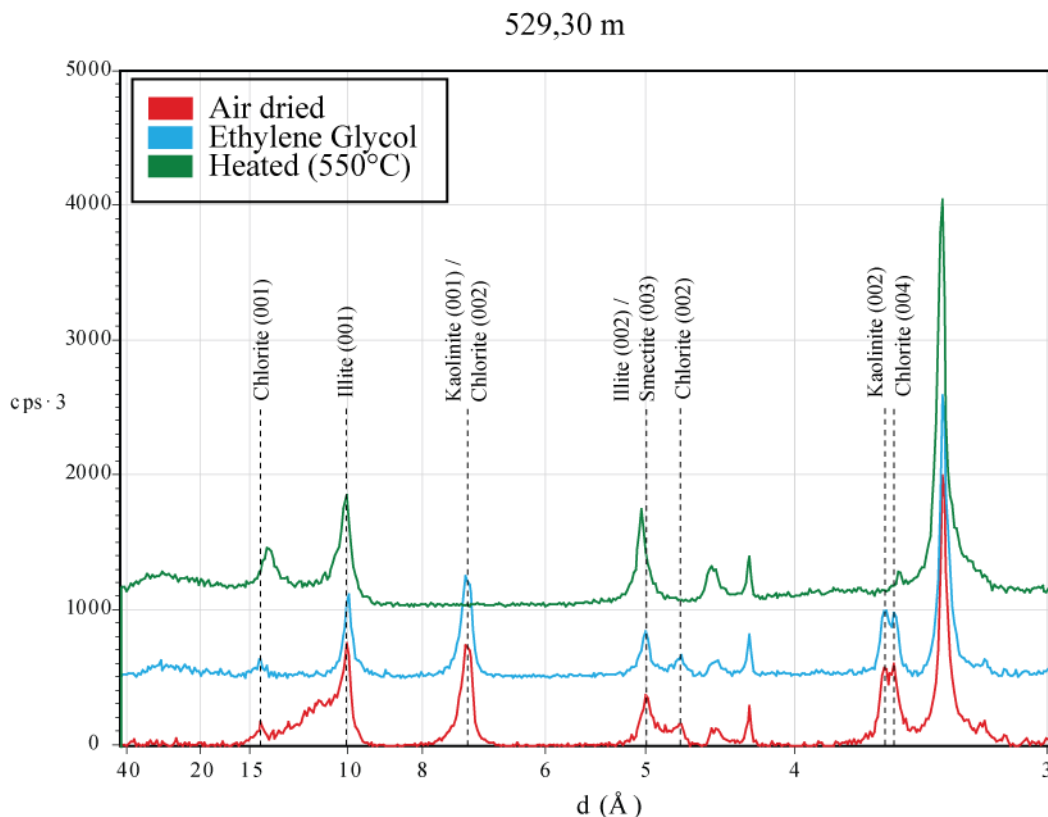


Figure 30: This figure is an example of three different diffractograms (airdried, ethylene glycol treated and heated) from sample at level 529,30 m. Dashed lines illustrate peak shifts and intensity variations. The area between 14 Å and 10 Å (mixed-layered clay minerals) suffers shifts in intensity after ethylene glycol solvation. The kaolinite (001)/chlorite (002), chlorite (002) and kaolinite (002) reflection collapses after heating to 550 °C. Chlorite (001) and illite (002)/smectite (003) reflection experiences a shift and increased intensity. While the chlorite (004) suffers a large decrease after heating to 550°C.

6.2.1 Bulk analysis

In the bulk XRD both clay minerals and non-clay minerals are identified and semi-quantified. The semi-quantification is carried out by simple peak height percentage calculations for the respective minerals. The results are presented in Figure 36, Figure 37 and Appendix 4.

Upper Grumantbyen Formation sandstones (560,00 m – 551,60 m)

The sandstones of the upper Grumantbyen formation has an average feldspar content of 55 XRD%, where plagioclase make up 38,3 XRD% and K-feldspar 16,7 XRD%. The average quartz content is 28,4 XRD% which yield an average quartz/feldspar of 0,34 (Figure 37). A similar observation was made in thin section analysis (Figure 20). Chlorite is the dominating clay mineral with 8,4 XRD%, while illite and kaolinite contribute with 3,1 and 0,7 XRD%. This results in a kaolinite/(kaolinite + chlorite) ratio of 0,08 and a kaolinite/(kaolinite + illite) ratio of 0,20 for the whole interval (Figure 31). The presence of chlorite is supported by

observations made in petrographic microscope (Appendix 3). The carbonates contribute with 4,4 XRD% of the total, with calcite being the most abundant. The pyrite content in this interval is close to neglectable (Figure 37).

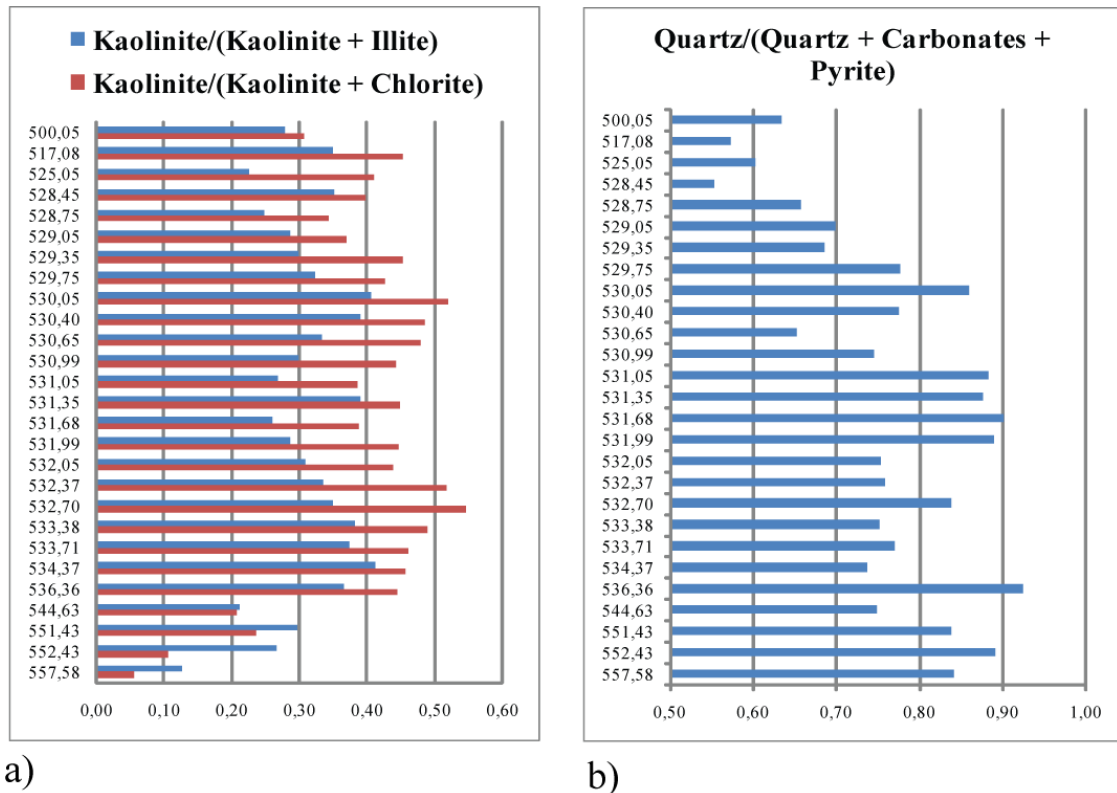


Figure 31: a) Kaolinite/(Kaolinite + Illite) and Kaolinite/(Kaolinite + Chlorite) ratios in the upper Grumantbyen sandstones, transition between Grumantbyen and Gilsonryggen and the shales of lower Gilsonryggen. b) Quartz/(Quartz + Carbonates + Pyrite) as a measure of allogenic vs. authigenic minerals in the same interval as a).

Transition interval between Grumantbyen Formation and the shales of lower Gilsonryggen Member (551,60 m – 550,00 m)

Only one sample is present in this interval. The most abundant mineral is feldspar, making up 46,7 XRD% (Plagioclase 33,4 XRD), with quartz contributing with 31,9 XRD% of the total (Figure 37). This results in a quartz/feldspar ratio of 0,41, which is close to the result obtained from point counting (Appendix 3).

Chlorite makes up 7,2 XRD%, while illite and kaolinite must be content with 5,3 and 2,3 XRD% respectively. These results yield a kaolinite/(kaolinite + illite) ratio of 0,30 and a kaolinite/(kaolinite + chlorite) of 0,24 (Figure 31).

The carbonate content in this sample is poor. All three minerals (calcite, dolomite and siderite) contribute with just around 1 XRD% each, while pyrite claims 3,4 XRD% (Figure 37). Pyrite has also been observed in microscope at this level (Appendix 3)

Shales of lower Gilsonryggen Member (550,00 m – 500,00 m)

In addition to the shales, two special samples were analyzed from the conglomerate at 548,35 m and the siderite layer at 533,07 m. The values from these two samples will be discussed separately and not included in the average fine grained values.

The conglomerate layer at 548,35 m (Figure 12c) explains the quartz (64,4 XRD%) and feldspar (23,8XRD%) contents in that sample (Appendix 3). Illite (5,5 XRD%) and chlorite (4,0 XRD%) dominate over the kaolinite (1,3 XRD%), also demonstrated by the kaolinite/illite of 0,19 and kaolinite/chlorite of 0,25 (Appendix 3).

At level 533,07 a prominent siderite layer is apparent. This has a high siderite content of 47,7 XRD% and a low quartz/(quartz + carbonates + pyrite) ratio of 0,33. At this level the kaolinite/chlorite is the highest in core with 0,71 which is also true for the kaolinite/illite with 0,45. The feldspar content is relatively low resulting in a quartz/feldspar content of 0,76 (Appendix 3).

Quartz is the dominating mineral of this interval with an average of 40,7 XRD%, values ranging from 48,2 XRD% at level 521,35 to 31,6 XRD% at level 500,05. Feldspar minerals make up 19,4 XRD%, reflecting 13,6 XRD% of plagioclase and 5,8 XRD% of K-feldspar. The total feldspar content is varying between 14,5 and 31,3 XRD% (Figure 37). The average quartz/feldspar ratio is 0,68, which is a representative value through the whole interval.

Illite is the most common clay mineral with an average content of 12,1 XRD%. This is however varying between 5,4 and 18 XRD%. The chlorite portion is ranging between 2,3 and 14,1 XRD%, giving an average of 7,4 XRD%. The kaolinite content also fluctuates, with a minimum value of 1,3 XRD% and a maximum value of 9,2 XRD%, resulting in an average of 5,5 XRD% across the interval. The trends representing the kaolinite/illite ratio and kaolinite/chlorite ratio are shown in Figure 31a. There is a similar trend in both ratios. The increase rapidly from around 0,2 in both ratios at 550 m to peak values at level 532 m, with kaolinite/(kaolinite + illite) values at around 0,4 and kaolinite/(kaolinite + chlorite) values close to 0,55. Both ratios experience a decrease from 532 m to 531 before again reaching almost peak values at 530 m. Then both ratios decrease moving upwards in the stratigraphy, except high ratios at 517,08 m.

Both ratios show similar trends as they display an increase from the start of the interval to around 528, and then a decrease towards the initial values (Figure 31a).

Both calcite and dolomite contents have average values around 1 XRD%. The dolomite contribution does not change much through the interval, while calcite displays a peak of 10,7 XRD% near the top (517,08 m). Siderite comprise the largest portion of the carbonates with an average of 5,5 XRD%. The values are either between 1-3 XRD% or between 9-16 XRD%, with no real trend corresponding to depth. On the other side, the pyrite content appears to vary from low values (<6 XRD%) at the beginning increasing upwards (10 -24 XRD%) in the section.

The quartz/(quartz + carbonates + pyrite) ratio is over 0,7 in the lower part of the interval but increase to almost 0,9 in the area around 530 m (Figure 31b). This is due to the low input of pyrite and carbonates. At the top (529,75 – 517,08 m), the pyrite portion is very high, and thus the ratio will be much lower (around 0,6). The thin sections from this interval also reveal high amounts of pyrite. The interval between 535 m and 532 m display increased siderite values (Figure 37) resulting in a lower quartz/(quartz + carbonates + pyrite) ratio (Figure 31b).

Shales of middle Gilsonryggen Member (500,00 m – 280,00 m)

Quartz is the main mineral in these shales. On average it constitute 43,0 XRD% of the total, with extreme values at 48,6 XRD% and lowest at 37,2 XRD% . Feldspar is the second most abundant mineral, making up 20,1 XRD% of the interval, with the plagioclase content generally about twice as large as the K-feldspar content (13,6 XRD% and 6,5 XRD%). Both minerals show only minor variations through the 253 m of this interval (Figure 36). The quartz/feldspar ratio is relatively constant all through this interval.

Illite and chlorite are the two major clay mineral contributors, with 12,4 XRD% and 11,1 XRD% respectively. The kaolinite content only correspond to 3,2 XRD% on an average. Both the kaolinite/(kaolinite + chlorite) and the kaolinite/(kaolinite + illite) display upwards decreasing values in the interval, reflecting decreasing kaolinite content relative to both chlorite and illite in the more silty intervals at shallower depths (Figure 32).

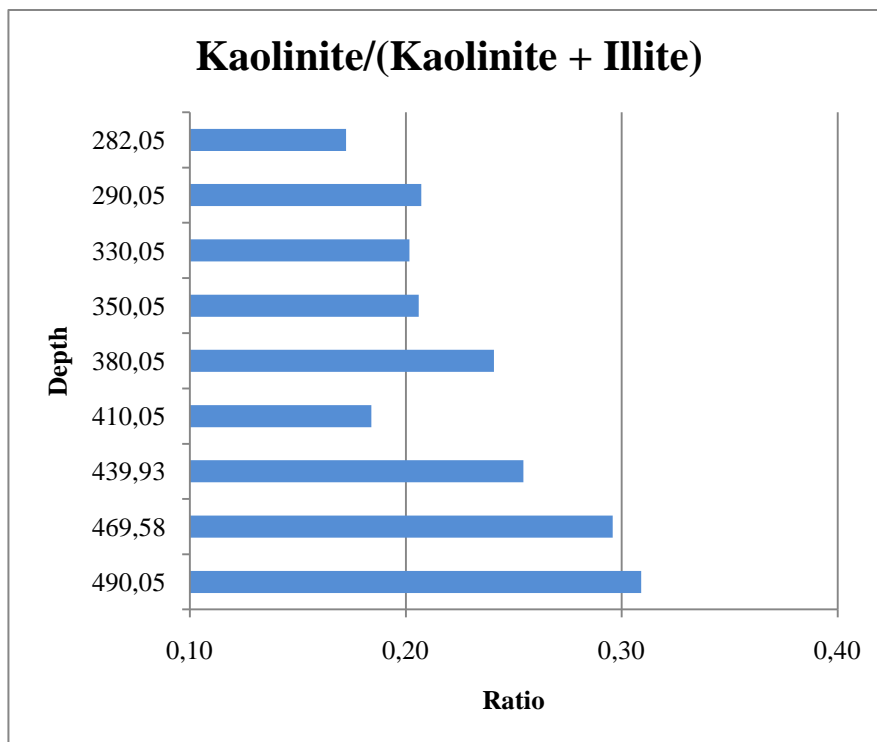


Figure 32: Variations in kaolinite/(kaolinite + illite) ratio in middle Gilsonryggen Member shales.

Siderite appears to have the highest average XRD% content of the carbonates with 6,0, consequently this interval has the highest content of siderite in core BH 9/05. The dolomite and calcite contribution are only slightly higher than in the lower shale interval, with 1,3 and 1,2 XRD%, and no significant variations noted. Pyrite is almost absent through the interval except one large peak at 439,4 m at 18,4 XRD%, bringing the average up to 1,8 XRD%. Besides this peak the pyrite content vary between 0,1 and 0,5 XRD% (Figure 36). The clay minerals are the only minerals which display some variations through this interval, the quartz/(carbonates + pyrite) demonstrate only minor variations.

Upper Gilsonryggen Member siltstones (280,00 – 150,00 m)

One sample (264,59 m) will be discussed separately, as it consists of very coarse material and the siderite content is abnormally high.

This part (280 – 150 m) of the core is mainly made up of siltstones with quartz (35,1 XRD%) and feldspar (18,6 XRD%) (Figure 36). The ratio between the two stays relatively constant, with an average of 0,65.

The most dramatic change in this interval is the increase in illite and chlorite contents, a doubling compared to deeper intervals. Illite show 18,9 XRD% and chlorite 15,7 XRD%, both with the highest values in the middle of the interval (Figure 36). In thin the point

counting large amounts of illitic clay matrix has been detected in this interval (Appendix 3). The kaolinite portion is minor, showing no significant change from the interval below, an average value of 3,2 XRD% (Figure 36). The kaolinite/chlorite and kaolinite/illite display scattered values and no special stratigraphical developments.

Siderite is the most prominent of the carbonates with an average of 5,0 XRD%, followed by dolomite at 2,3 XRD% and 1,1 XRD% calcite. Calcite show a slight decrease compared to levels below, while siderite and dolomite display an upwards increase (Figure 36). This result in a decreasing quartz/carbonates + pyrite trend, even though the pyrite content never exceeds 0,2 XRD%.

The sample at level 264,59 has been analyzed in thin section and a sand layer (5 mm) has been observed. The sample is characterized by a siderite content of 24,5 XRD% and a resulting quartz/(quartz + carbonates + pyrite) ratio of 0,49. The kaolinite/(kaolinite +illite) ratio of 0,28, kaolinite/(kaolinite + chlorite) ratio of 0,43 while the quartz/feldspar does not deviate significant from the other samples, being 0,70 (Appendix 3).

Upper Gilsonryggen Member sandstones (178,00 m – 110,00 m)

This interval represents the upper most part of the studied section and the top of the Gilsonryggen Member. The quartz amounts in this interval are slightly higher than in the siltstones below. The average content is 38,0 XRD%, but it varies from 29,1 to 44,4 XRD%. Feldspar is the second most common mineral with 19,2 XRD%, where plagioclase correspond to 15,6 XRD% and K-feldspar to only 3,6 XRD%. The quartz/feldspar ratio exhibits no obvious tendency, except maybe a slight increase at the top of the interval. The quartz/feldspar ratio is similar to the one observed in point counting (Appendix 3).

Illite is the most common clay mineral, but comprise a smaller portion of the total than in the interval below, with an average contribution of 17,8 XRD%. Chlorite displays a comparable development, having an average value of 13,4 XRD%, a decrease compared to siltstones below. The kaolinite amounts vary between 2,2 XRD% and 5,6 XRD%, which yield the average value of 3,2 XRD%..

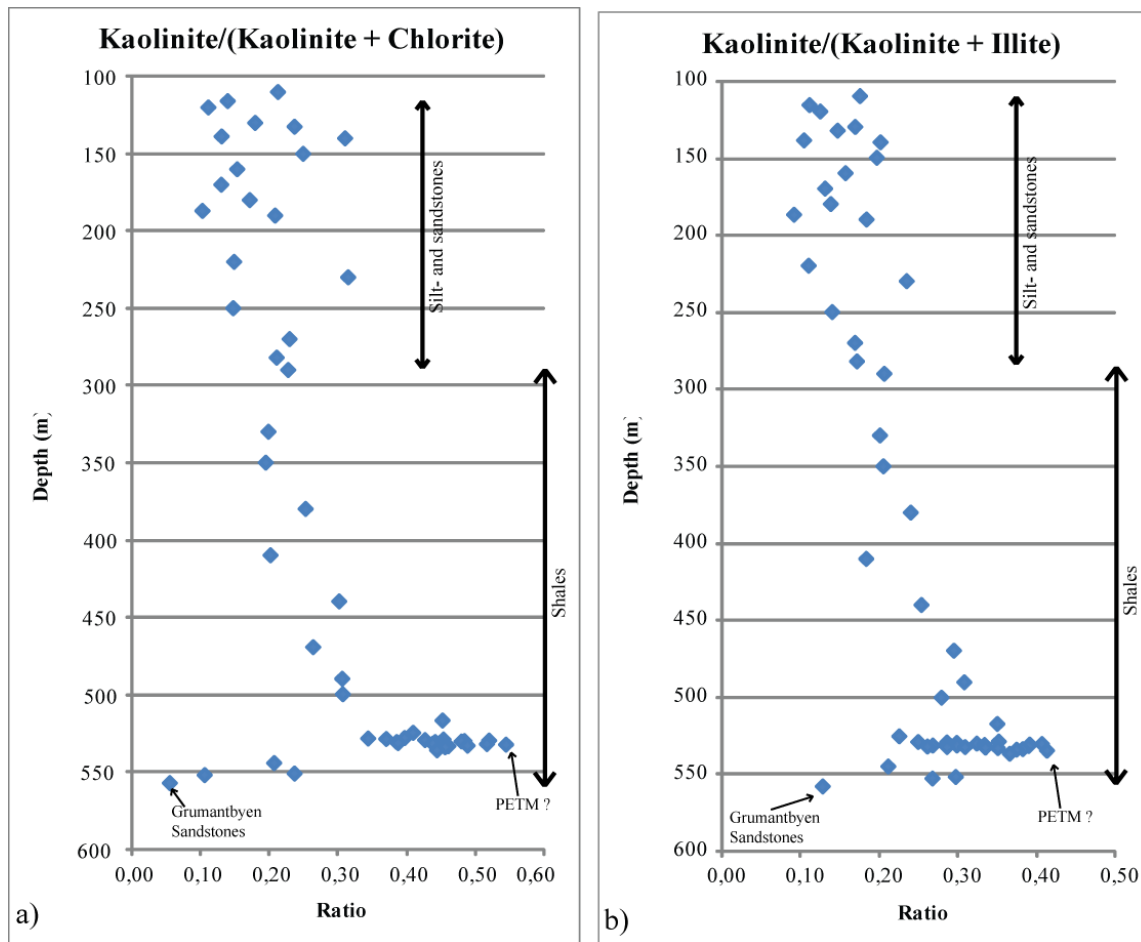


Figure 33: a) Kaolinite/(kaolinite + chlorite) and b) Kaolinite/(kaolinite + illite) variations in BH 9/05

Among the carbonates siderite still occupies the largest portion with 3,5 XRD%, which is a decrease compared the interval below. This is reflected in the relative increase in the quartz/(quartz + carbonates + pyrite) ratio in the sandstones compared to the siltstones. Dolomite and calcite are minor contributors with 2,8 and 1,6 XRD% respectively. Pyrite displays the same values, with an average value of 0,5 XRD%. This value does not reflect the general amount of pyrite in this interval, which is close to neglectable. It is only connected to one peak (138,80) where the pyrite content is 3,0 XRD%. In thin section no pyrite is observed in this silty sample.

General trends

Summation of the general trends observed through the core.

Clay minerals

Figure 34 illustrate the distribution of each of the three clay minerals present in this study. Illite is the most abundant clay mineral on an average. The lowest values are found in the

Grumantbyen sandstones, while the portion of illite display the largest values when moving into the more sandy intervals (220 m and upwards). The increase in illite moving from shale to silt is also displayed in Figure 36. Chlorite is the second most abundant clay mineral. It is present in the coarse grained intervals of Grumantbyen and the siltstones/sandstones of upper Gilsøryggen.

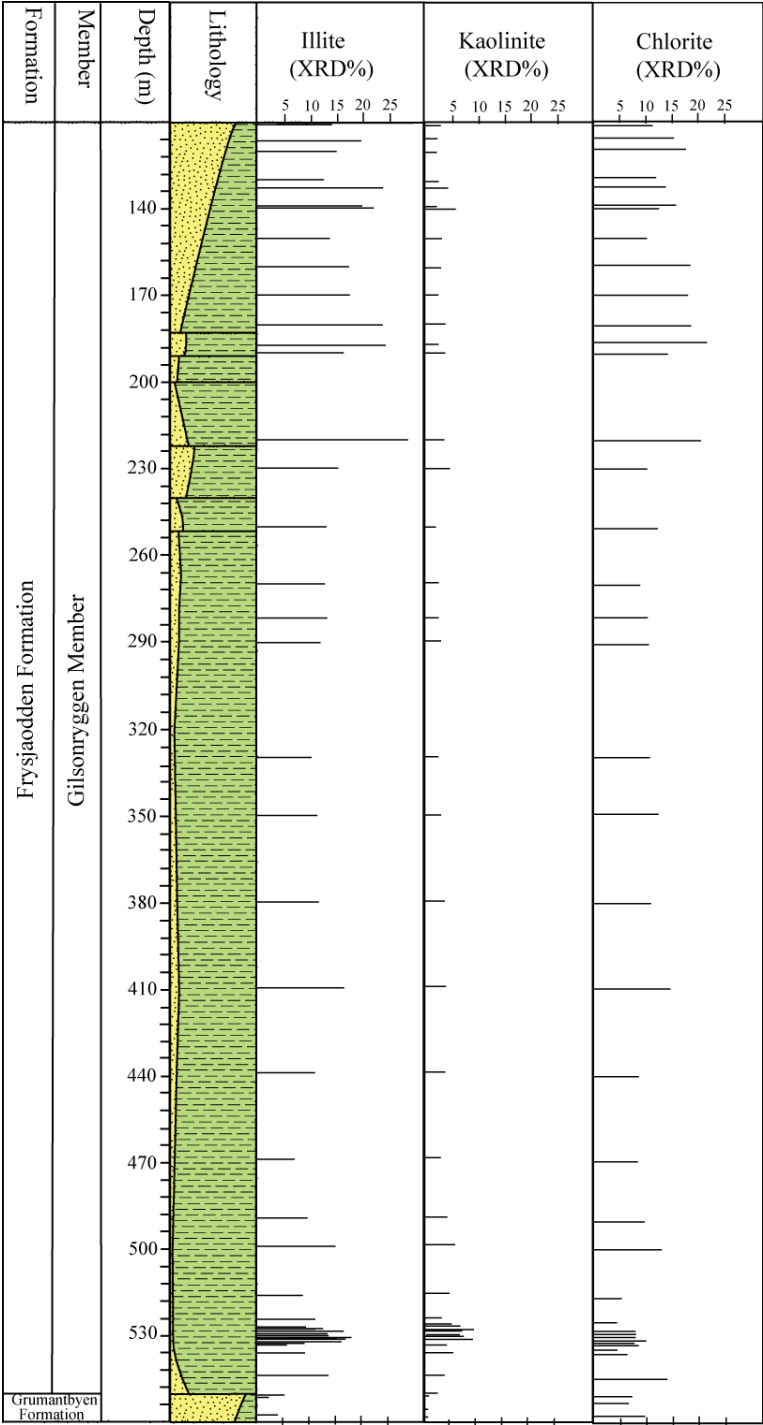


Figure 34: Clay mineral distribution in core BH 9/05

It is also observed in thin sections as part of thin silt layers interrupting the shale deposits in lower/middle Gilsonryggen. The presence of kaolinite is generally low (< 5 XRD%). The highest values are reached in the region of 536 m -520 m, up to 10 XRD% (Figure 34). Figure 35 illustrate how the clay minerals will plot in a ternary diagram, with color codes for each interval. The diagram show that the largest portions of kaolinite are found in the lower parts of Gilsonryggen and the highest amount of chlorite is found in the sandstones of Grumantbyen.

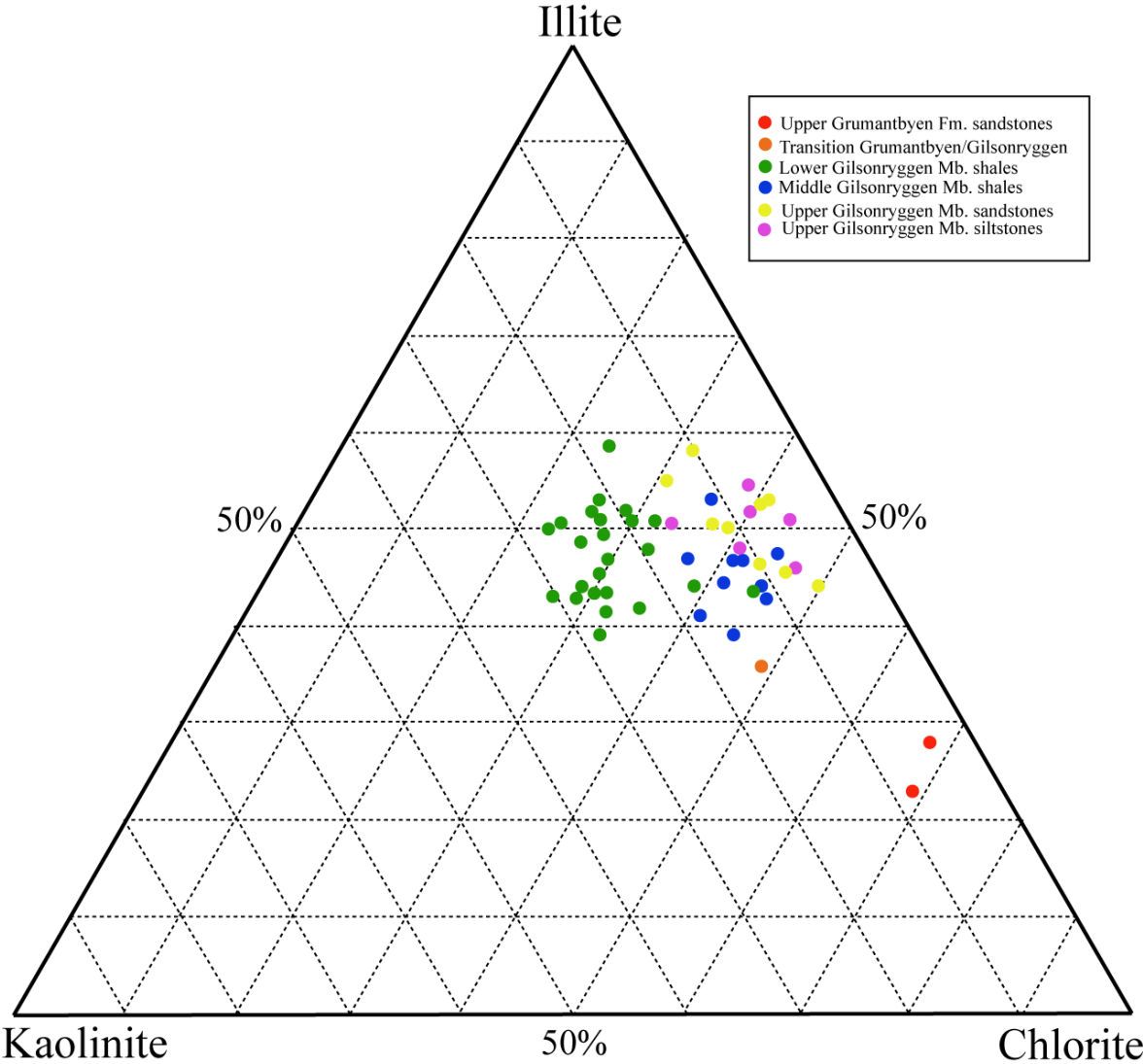


Figure 35: Clay minerals from bulk analysis

In Figure 33 the kaolinite/(kaolinite + chlorite) ratio and kaolinite/(kaolinite + illite) ratio display the same trends. In the Grumantbyen sandstones the ratio is extremely low due to the absence of kaolinite and high content of chlorite in these rocks (Figure 34). In the Frysjaodden Formation the two ratios experience an abrupt increase around 536 m depth and a likewise abrupt decrease in the region of 520 m (Figure 33). Figure 34 show that the reason for this increase is the abundance of kaolinite in the shales of lower Gilsonryggen. Above this interval both intervals will plot close to an imaginary trend line indicating declining values. When reaching the coarser grained interval at around 280 m the ratios will scatter more and deviate from a trend line.

Carbonates and pyrite

The distribution of carbonate minerals (dolomite, siderite and calcite) and pyrite is illustrated in Figure 36 and Figure 37. They are discussed together as they represent an authigenic origin. The authigenic minerals make up relatively low amounts in the sandstones of Grumantbyen Formation. In the lower part of Gilsonryggen Member the content of carbonates and pyrite experience an increase up to maximum values around level 520 m. The authigenic mineral contribution continue to be large up to around 439 m. From this level the combined contribution from carbonates and pyrite seldom exceed 10 XRD%.

Quartz and feldspar

The amounts of quartz and feldspar minerals are displayed in Figure 36 and Figure 37. As mentioned earlier, the Grumantbyen Formation exhibit high content of feldspar compared to quartz. In the Gilsonryggen Member the plagioclase and K-feldspar content will drop considerably and quartz will be the dominant mineral. The ratio between quartz and feldspar will not change noticeable from the lower to upper parts of Gilsonryggen Member.



Figure 36: All minerals from bulk analysis (110 m -490 m).

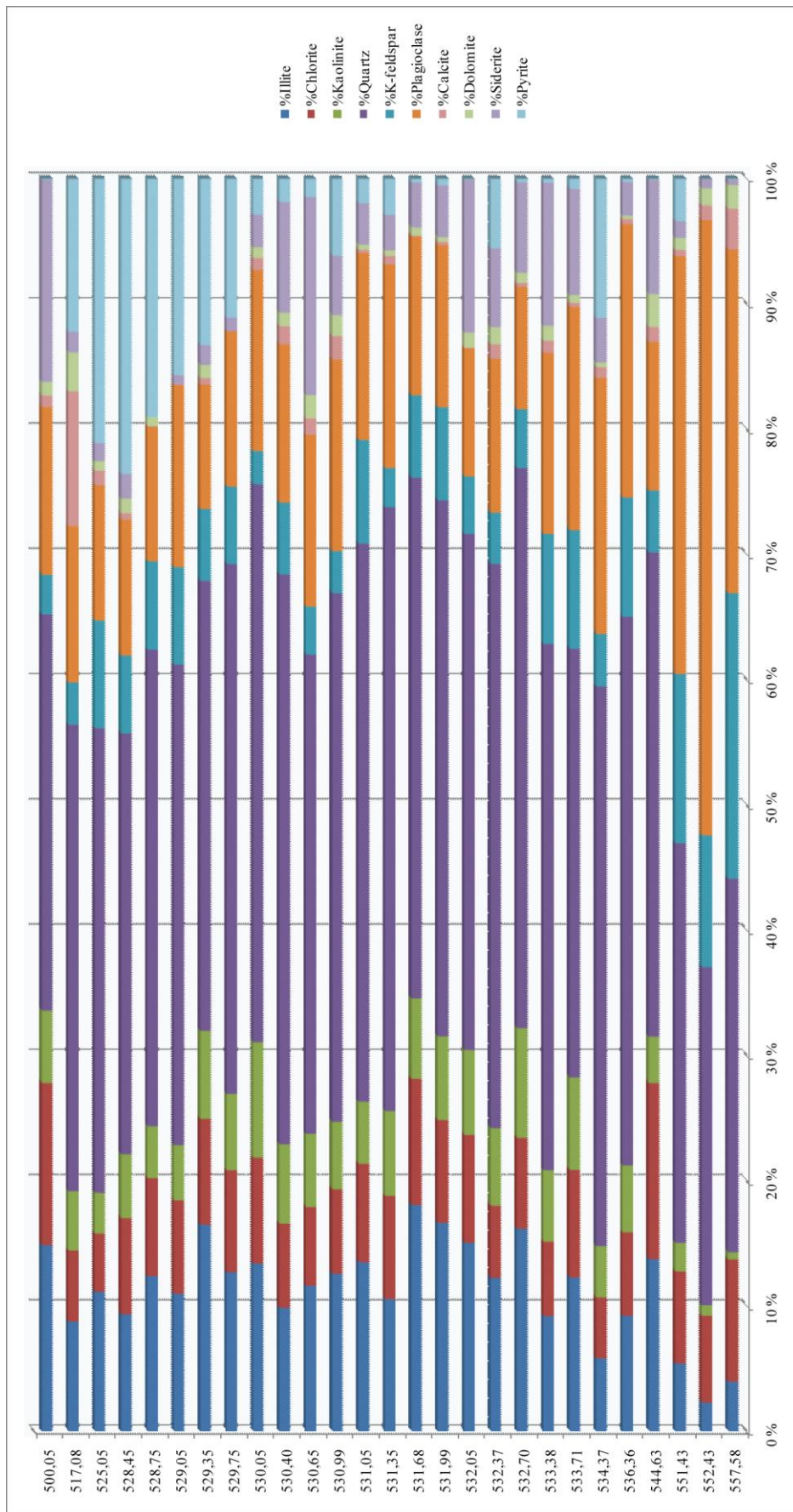


Figure 37: All minerals from bulk analysis (500,05 m – 557,58 m)

6.2.2 Clay separation

Quantification of the 2 μ m-fraction minerals was determined by a least-squares comparison (pseudo-Voigt) of the diffractograms from the EG-saturated samples in Macdiff. The qualitative analysis is based on observations of the diffractograms in air-dried, EG-saturated and heated (550° C) state. Samples which have been subject to clay separation are shown in Table 3.

All samples, except two, are derived from the shales of the lower Gilsonryggen Member. They have been selected to represent the interval spanning, what is thought to be, the entire duration of the PETM. The uppermost two samples represent the shales of the middle Gilsonryggen and are included for comparison.

Table 5: Average values of minerals in the shales of lower Gilsonryggen, plus two comparison values from middle Gilsonryggen shales. See appendix 5 for results of all samples.

Interval/depth	Number of samples	Illite XRD%	Kaolinite XRD%	Chlorite XRD%	Mixed-layered (illite/smectite) XRD%	Siderite XRD%	Pyrite XRD%
Shales of lower Gilsonryggen	19	28,0	26,6	15,5	22,6	5,3	2,0
Comparison	Shale of middle Gilsonryggen (469,58 m)	22,5	15,5	17,5	30,4	14,1	0,0
	Shale of middle Gilsonryggen (350,05 m)	30,3	11,3	28,4	27,9	1,8	0,2

An abnormally low value in the mixed layered minerals is obtained in sample at 529,05 m and thus this sample will stand alone and not contribute to the average values (Appendix 5).

Illite is the most abundant clay sized mineral in the 7,91 m shale section of the lower Gilsonryggen, with an average value of 28,0 XRD%. Its portion increase upwards in the section, with the lowest value (22 XRD%) in the deepest sample (536,36) and the highest values (37,1-36,9 XRD%) in the two shallowest samples (528,75 m and 528,45 m) (Figure 40).

Kaolinite is the second most abundant clay mineral with an average of 26.6 XRD% (Figure 40). The kaolinite/(kaolinite + illite) ratio indicate three phases (Figure 38a). The first phase is the lowest part of the section where the ratio is relatively high (level 533,07), with a peak of 0,61. At 532,05 m a drop down to 0,45 occur and a second upwards increasing trend

develops. This ends at 530,99 m with a peak of 0,52. Then the third and last phase begins with decreasing kaolinite/(kaolinite + illite) ratio. At the top of the section the ratio is as low as 0,35. The average ratio in this section is 0,47. The comparison samples at levels 469,58 m and 350,05 m suggest a decreasing trend of kaolinite relative to illite upwards in the core, with values at 0,41 and 0,27 (Figure 38a).

Chlorite has an average value of 15,5 XRD% through this section, slightly upwards increasing. The average value is relatively low compared to level 350,05 m (28,4 XRD%) (Figure 40). Kaolinite/(Kaolinite + Chlorite) ratio has an average of 0,52. It demonstrates some of the same characteristics as the kaolinite/(kaolinite + chlorite) ratio (Figure 38b). The lowest part of the section is similar to the first phase in the (kaolinite/kaolinite + illite) ratio. The highest ratio is as high as 0,83 (533,07 m), corresponding with the peak kaolinite/(kaolinite + illite) ratio found at the same level. At 532,05 m the ratio drops to 0,61 and only varies slightly, until it exhibit a similar decrease as kaolinite/(kaolinite + illite) ratio in the three upper most samples (0,54, 0,50, 0,53) (Figure 38b).

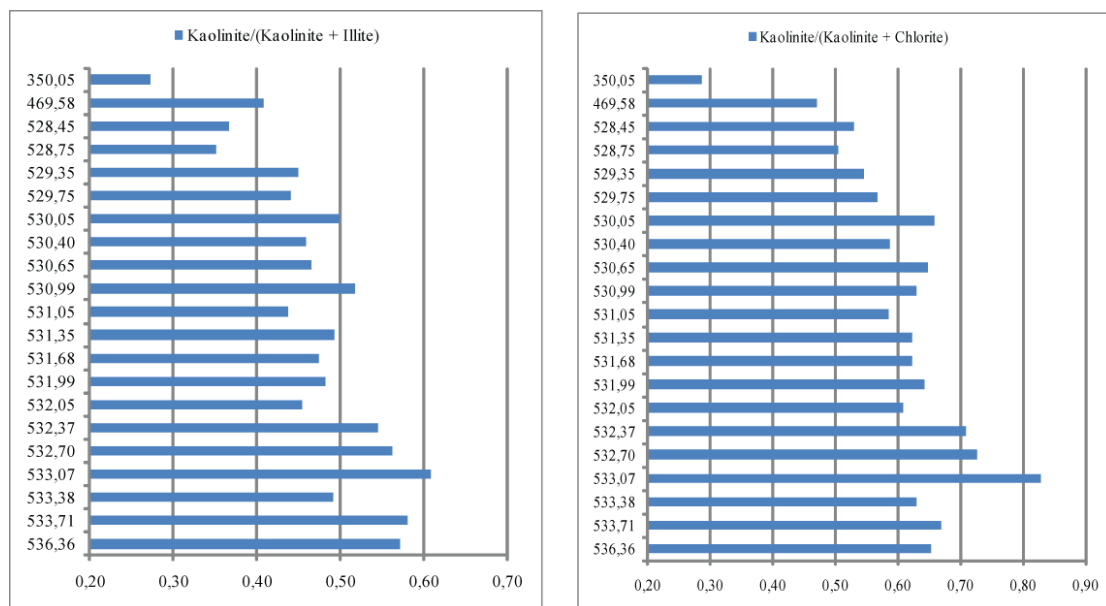


Figure 38:a) The kaolinite/(kaolinite + illite) ratio and b) Kaolinite/(kaolinite + chlorite) ratio across the possible PETM interval. The two uppermost samples are included as comparison.

The mixed-layered clay minerals on average 22,6 XRD%, and do not vary greatly through the section. The mixed-layered minerals content decrease in the two before mentioned samples (533,07 m and 532,05) (Figure 40).

Siderite occupy around 2-3 XRD% of the clay sized minerals. However two samples stand out with respect to the siderite portion. 533,07 m, where 23,0 XRD% constitute of siderite,

and 532,05 with 17,4 XRD% (Figure 40). These two samples coincide with the high value of kaolinite/(kaolinite + chlorite) and kaolinite/(kaolinite + illite) ratio (533,07 m) and where both ratios experience a decrease (532,05 m) .

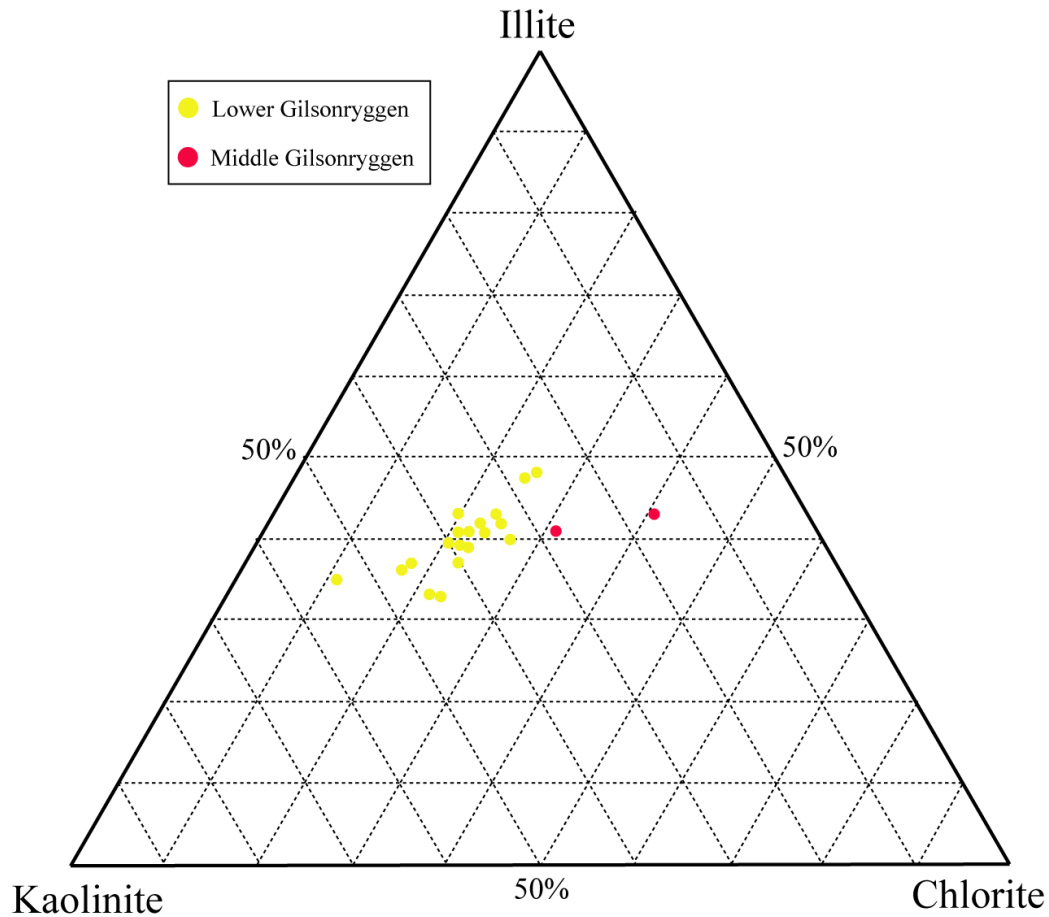


Figure 39: Ternary plot of clay mineral percentages in the clay fraction

The pyrite content is on average 2,0 XRD% , and varies between 0,9 – 4,6 XRD% , a relative high amount compared to the two samples from the shales of the middle Gilsonryggen (0,01 XRD% and 0,2 XRD%) (Figure 40)

Sample 529,05 m, which is not included in the average values has an extremely low portion of mixed layer minerals (5,3 XRD%) (Appendix 5). Its kaolinite/(kaolinite + illite) and kaolinite/(kaolinite + chlorite) ratios however fit in to the decreasing development near the top of the section.

6.2.3 Removal of iron oxide by Na-Citrate:

After removal of possible iron oxide the XRD results revealed the same diffractograms as before, and thus no prominent smectite fraction is present in these samples

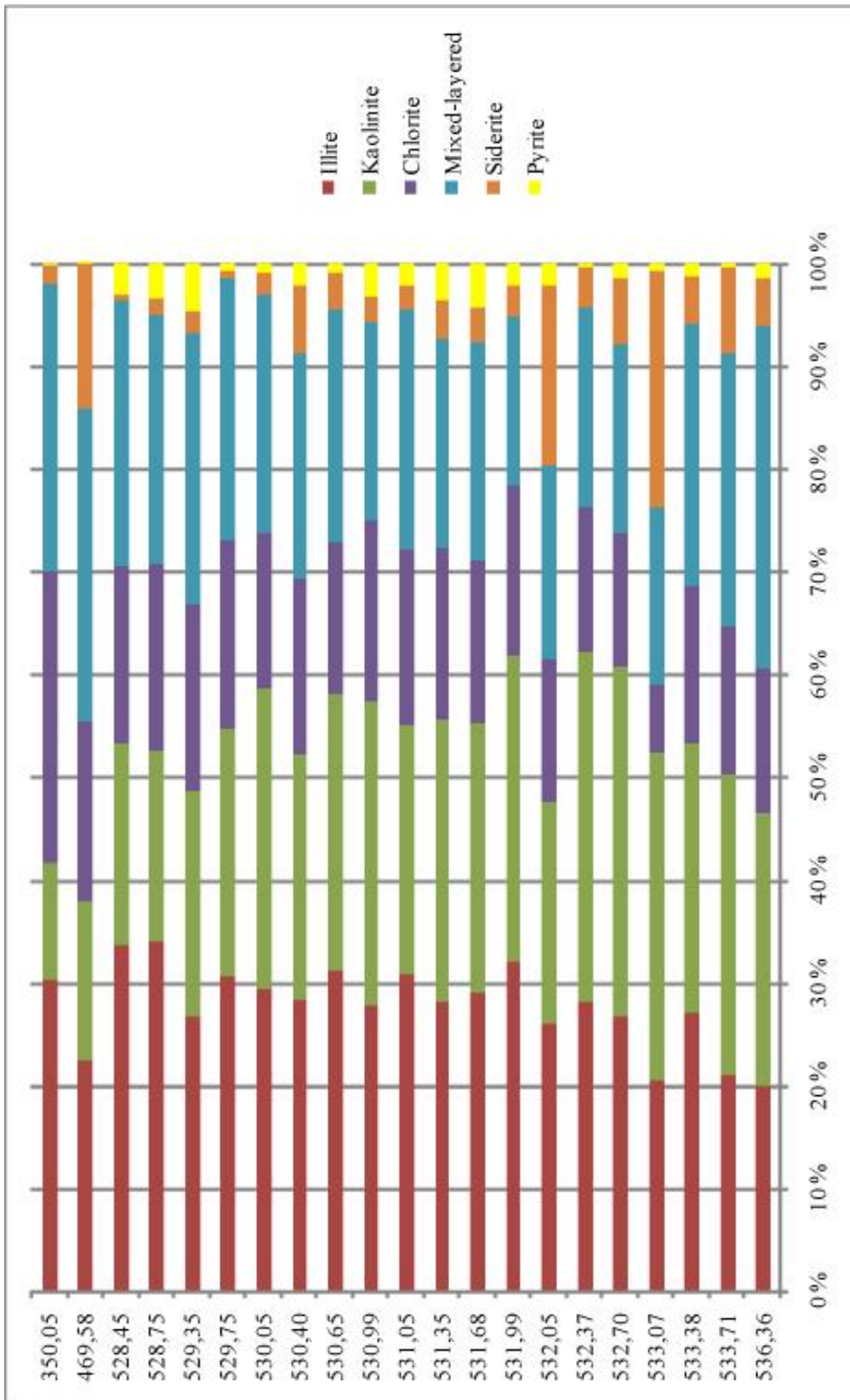


Figure 40: Mineral estimations (XRD%) of the clay fraction

7 Geochemical analysis

This chapter presents the applied geochemical analyses in the reconstruction of burial history (Rock-Eval), characterization of kerogen type (Rock-Eval), amount of organic matter (TOC), CaCO₃ content and evaluation of redox conditions (Th/U ratio).

7.1 Rock-Eval analysis

Thermal maturation history and kerogen typification have roughly been determined on the basis of Rock-Eval parameters discussed in chapter 4.5. The modified van Krevelen diagram (Figure 41) illustrates how the samples plot as a function of hydrogen index and oxygen index. Peters (1986) states that mixtures of kerogen type in rocks are common and will result in samples plotting between major kerogen pathways. In samples from core BH 9/05 plot as a mixture of kerogen type II and III and thus a mixture of organic matter with terrestrial and marine origin (Figure 41). However, if coals of higher plant origin are present, the HI vs. OI diagrams may misrepresent the type of organic matter, plotting them between type II and III when they ought to plot along the type III kerogen pathway. Coals will typically show HI values < below 300 HC/g C_{org} and S₂/S₃ > 5 (Peters, 1986). None of the analyzed samples has higher HI than 218,03 and eight of the samples display S₂/S₃ values greater than 5 (110,05 m, 140,05 m, 509,05 m, 513,05 m, 515,05 m, 525,05 m, 534,37 m, 538,38 m).

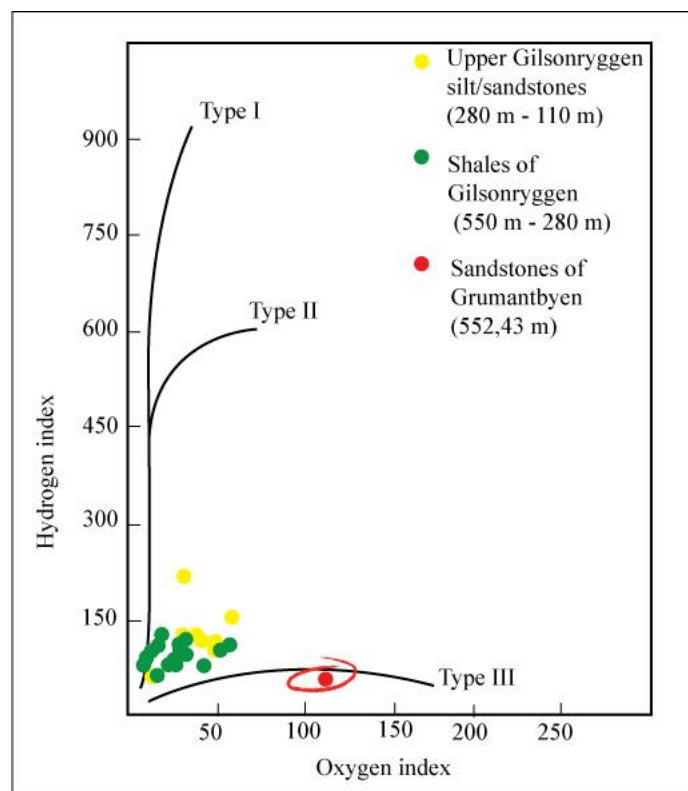


Figure 41: Modified van Krevelen diagram. Based on diagram from Peters and Cassa (1994).

The sandstone sample from the upper Grumantbyen Formation are characterized by the highest OI (111,11 HC/g C_{org}). Together with a low HI value this implies a type III origin of the organic matter in this sample.

Thermal maturation has been estimated based on depth vs. T_{max} and depth vs. production index (PI) charts suggested by Peters (1986) and Peters and Cassa (1994) (Figure 43 and Figure 42). Temperature intervals correspond to the oil window (60° – 150° C) and are based on empirical data from large amounts of wells world-wide. Temperatures are not absolute but are meant to give a rough indication of the degree of maturation experienced by the rock.

There is good correspondence between the two diagrams. Both imply that the upper part of the core has experienced temperatures of about 60°C (top of oil window) and increasing temperatures with deeper burial. The deepest parts have been subject to temperatures about 95° - 110° C, which will correspond to peak oil generation. From level 520 m and stratigraphically upwards the samples plot close to a linear approximation. Samples from 510 m – 550 m deviate from the linear trend in both diagrams (Figure 43 and Figure 42).

The sample from sandstones of upper Grumantbyen Formation (552,43 m) shows a high oxygen index and thus will display a high production index. As a consequence it will plot off the general trend in the depth vs. PI chart, while its position will be as the others in the depth vs. T-max diagram.

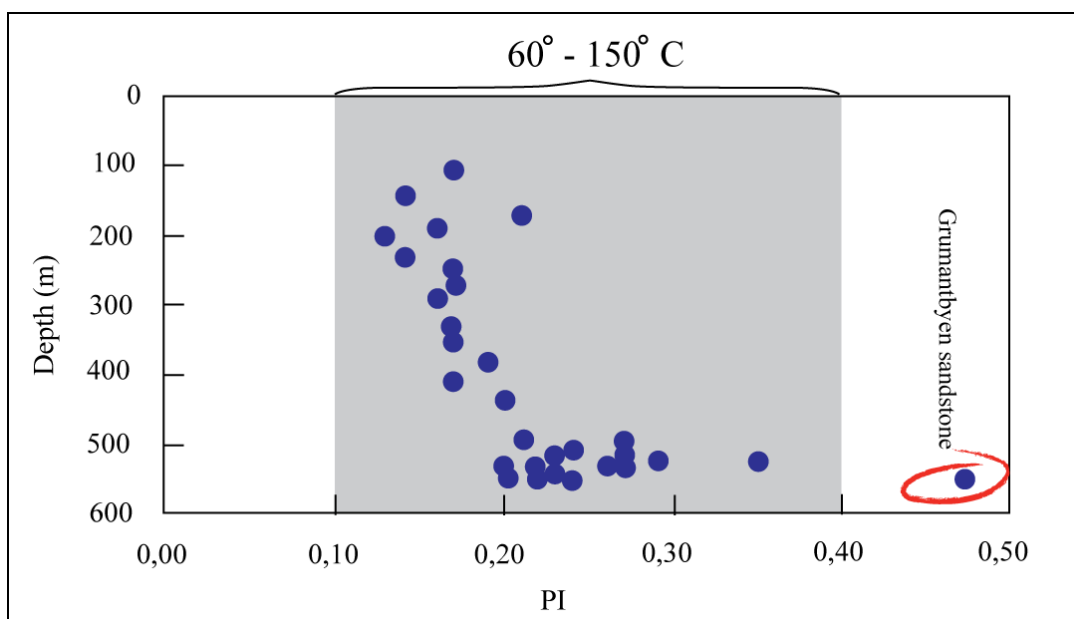


Figure 42: Production index vs. depth as thermal maturation indicator. Temperature interval from Peters (1986)

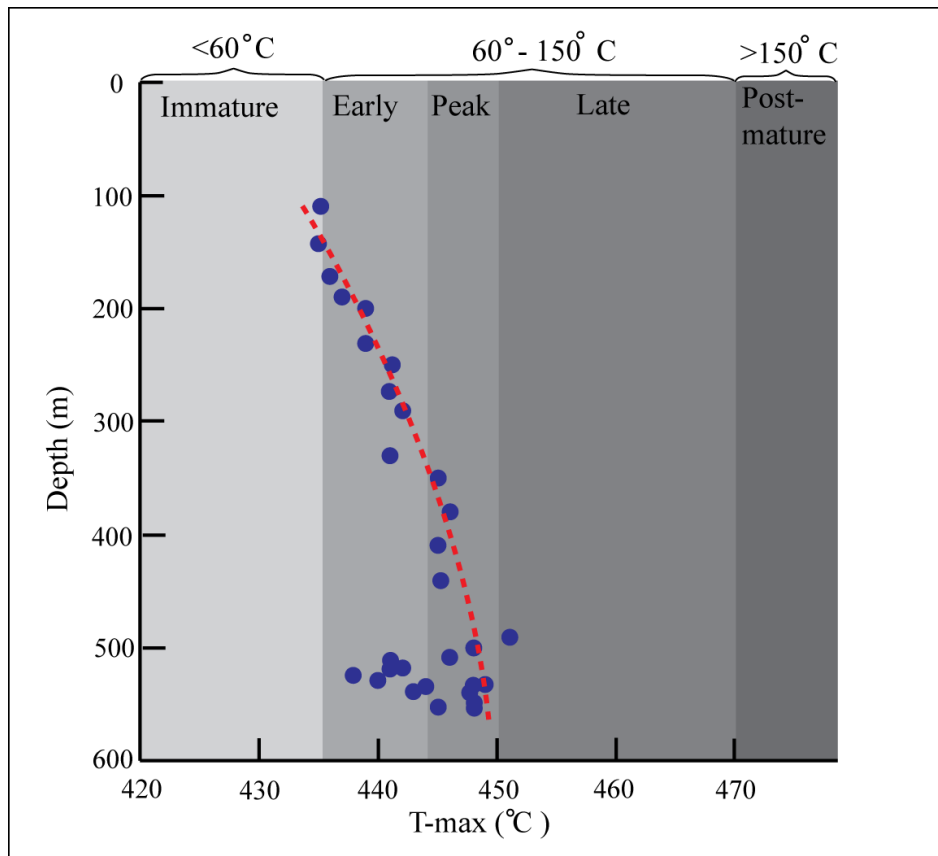


Figure 43: Tmax vs. depth as thermal maturation indicator. Temperature intervals from Peters and Cassa (1994)

7.2 TOC, CaCO₃ and Th/U analysis

7.2.1 CaCO₃

There are no clear-cut patterns to be seen in the CaCO₃ distribution other than a possible slight increase in the youngest formation (Figure 44). In Grumantbyen Formation the content is extremely low with an average of 0,4 %. Four values stand out: 12,7 % at 546,73, 14,9 % at 511,05m, 17,5% at 508,75 and 14,0% at 190,05.

7.2.2 TOC

The TOC level is relatively low in the entire core (Figure 44). Peak values are reached between 538,38 m and 534,37 m (2,30%, 2,94% and 2,92%). Through the rest of the core values vary between 0,75% and 1,5%.

7.2.3 Th/U

The Th/U ratio expresses a general upwards increasing trend (Figure 44). A special feature is the major drop occurring between levels 527,05 m and 508,05 m. This drop is due to a doubling of the Uranium content from around 2 ppm to around 5 ppm in this interval. A small reduction in the ratio is also observed around 360 m, related to a drop in Thorium content.

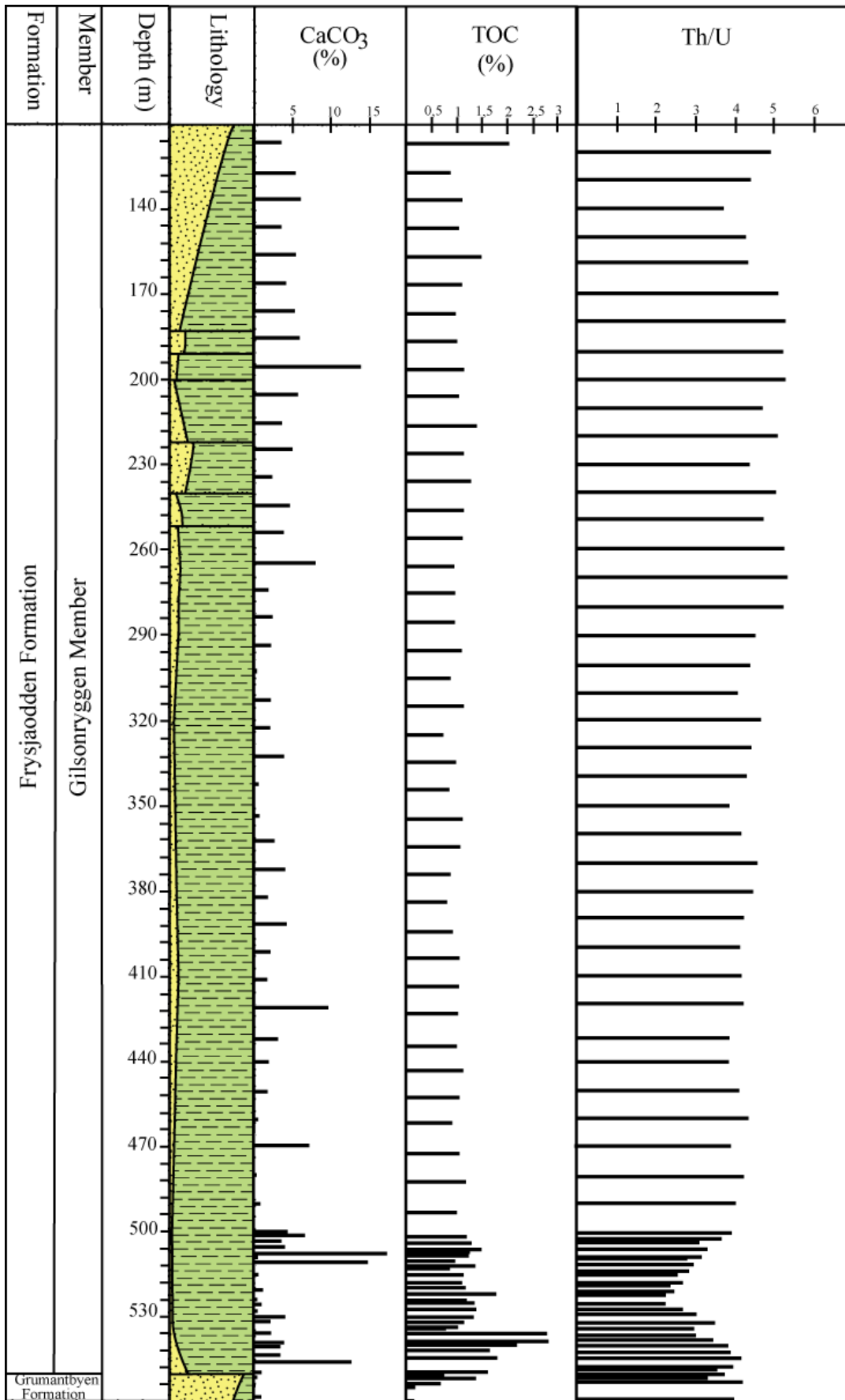


Figure 44: TOC and CaCO₃ content and Th/U ratio.

8 Discussion of data and reconstruction of depositional environment

Sediments and sedimentary rocks are the result of continuing weathering and reworking of rocks and sediments, transportation and finally the deposition. Weathering represents the alteration of rocks and minerals to more stable forms, according to the conditions of the different areas. The two main forces responsible of disintegration of rocks are physical and chemical weathering (Birkeland, 1984). Boggs (2006) define physical weathering as the process of breaking up rocks into smaller fragments by different causes without significant alteration of chemical and mineralogical composition. Chemical weathering, on the other hand, are the processes which can alter both the chemical and mineralogical composition of the rock and occurs as a consequence of disequilibrium between rocks and minerals and near-surface waters, temperatures and pressures (Birkeland, 1984).

Weathering products include all grain sizes, but in this study argillaceous rocks make up 90%, with the last 10% of fine grained sandstones.

The lithological characteristics of shales are highly linked to the oxygen conditions under which they were formed (Potter et al., 2005). Some significant factors which are controlled by the oxygen level at the sea bottom: content of organic matter, color, lamination, bioturbation, pyrite content, Th/U ratio, etc. (Potter et al., 2005).

Clay-sized material in sedimentary rocks is mainly composed of phyllosilicates (clay minerals) and Fe-hydroxides. The phyllosilicates commonly comprise illite, muscovite, biotite, chlorite and various mixed-layered minerals, with kaolinite, vermiculite, smectite often make up a smaller portion (Bergaya et al. 2006). The composition of clay minerals may reflect different sediments sources, e.g.: 1) clay minerals may form as a direct precipitation from water solutions (neof ormation), 2) detrital clay minerals have inherited their composition from provenance area (inheritance), 3) weathering of primary rocks result in degraded clay minerals and 4) composition change during diagenesis (aggradation) (Dypvik et al., 2003). Hence, the clay mineralogy reflects factors such as: primary rock composition, rate of erosion, temperature (burial history), precipitation, vegetation and porosity/permeability in sedimentary rock (Bjørlykke, 2001).

Kaolinite is typically developed as a weathering product in areas with abundant rainfall, good drainage and acid waters which is characteristics of tropical and subtropical climate conditions (Potter et al., 1980). Kaolinite may be the result of early diagenetic dissolution of

feldspar: $K(Na)AlSi_3O_8 + 2H^+ + 9H_2O = Al_2Si_2O_5(OH)_4 + 4H_4SiO_4$. This process can only be driven if reaction products are removed by e.g. flushing of (meteoric) water (Lanson, 2002). Direct kaolinite precipitation (neof ormation) is common in sandstone pores during diagenesis (Bergaya et al., 2006).

Illite, chlorite and random mixed-layered clay minerals generally forms from immature soils which have not undergone chemical weathering but they may also be formed by physical weathering of primary rocks. Illite and chlorite are characteristic of cold regions with little rainfall where chemical weathering rates are very low (Robert and Kennett, 1994). Illite may also form during diagenesis through the transformation chain of smectite → mixed-layered illite-smectite → illite → muscovite (Bergaya et al., 2006) and through replacement of dissolved kaolinite below 3,7 – 4,0 km burial depth (Bjørlykke, 1998). Bjørkum and Gjelsvik (1988) state that illitization of kaolinite may happen at temperatures as low as 50° C if K-feldspar is present. Authigenic chlorite may also be formed as result of transformation of smectite and kaolinite during diagenesis (Bergaya et al., 2006).

Smectites generally form as result of intense chemical weathering in sub-tropic to tropic areas, but unlike kaolinite, in poorly drained areas (Robert and Kennett, 1994). Smectite is also an alteration product of volcanic ash deposits (bentonites) (Potter et al., 1980). In this study smectite has not been identified in diffractograms. The interval in X-ray diffractograms between the chlorite 001 and illite 001 reflection may, according to Moore and Reynolds (1997), be occupied by the mixed-layered minerals. In the XRD analysis of clay-separated samples this interval experience changes in the diffraction pattern after EG treatment, and a reflection is visible in the region near 16 -17,7° 2θ in all samples. Hence illite/smectite is the most probable identity of the mixed-layered minerals (Moore and Reynolds, 1997).

In order to use clay minerals as a proxy of (provenance/climatic/weathering)factors mentioned above, a critical aspect in shale studies will be to identify whether mineral composition originate from processes occurring before deposition (detrital) or in situ (authigenic). This may be done directly by observing minerals in a scanning electron microscope (SEM). In porous sediments authigenic kaolinite often grows in pore spaces and appears in SEM as small booklets (Pe-Piper et al., 2005). Authigenic illite can be recognized as elongated, filamentous crystals (Lanson et al., 2002). An indirect approach will be by analyzing depositional environment and burial history and thus be able to deduce the probabilities of favorable conditions in authigenic origin of clay minerals. In this study

detrital illite has been observed at several positions in thin sections and SEM (Figure 24). Both authigenic and detrital kaolinite have been observed at position 530,99 m (probable PETM localization) (Figure 24) and hence the question is in what proportions they are present. To answer this question an indirect approach has been utilized. The successions at this level consist of shale and hence meteoric flushing probably was of minor influence. Neoformation of kaolinite is therefore less likely due to the absence of efficient pore space and permeability. In the deeper and more porous sandstones of Grumantbyen Formation kaolinite has not been observed in neither XRD-analysis nor SEM and thus neoformation of kaolinite has probably not taken place. Taking these factors into account it seems likely that authigenic kaolinite found at this level (530,99) is the exception rather than the rule, and that its peculiar booklet shape made it easier to spot in the SEM (Figure 24).

Illite has only been spotted as detrital and an authigenic origin seems unlikely also from an indirect evaluation. Early vitrinite analysis suggested a burial depth of less than 1500 m (Thronsen, 1982). The Rock-Eval analysis in this study gives a T_{max} in the deepest parts close to 448 ° C. Converted to vitrinite reflectance: $R_0 \approx 1$ (Bordenave et al., 1993). The relationship between R_0 , T_{max} and depth is not fixed, but the results from this study might suggest that burial depth have been somewhat higher than what was proposed by Thronsen (1982). Even though burial depth is higher than 1500 m it has not been as much as 3.5 – 4 km and hence illitization of kaolinite seems highly improbable.

Below follows a discussion of the results presented in chapter 5,6 and 7. Reconstruction of depositional environment will be placed in a sequence stratigraphic setting, explained in chapter 4.6. A separate discussion regarding a possible candidate for PETM will also be proposed.

8.1 Lowstand systems tract (560 m - 551,60 m)

8.1.1 Sandstones of Grumantbyen Formation (560,00 m -551,60 m)

The upward coarsening succession of sandstones is interpreted to be a regressive phase cumulating in a 5 cm non-erosive conglomerate layer. The absence of well defined structures in the formation is interpreted as a result of immense bioturbation. Large burrows, as bottom conditions (Frey and Pemberton, 1985). The burrows illustrated in Figure 11d show similarities to the trace fossil *Ophiomorpha*. This trace fossil belong to the Skolithos ichnofacies, typically developed in sandy, shallow marine environments (Savdra and Bottjer, 1987).

The sandstones of the Grumantbyen Formation are rich in glauconite. McRae (1972) states that conditions favorable of glauconite enrichment are shallow marine environments (water depths ranging from 15 m – 500 m) with low or even negative sedimentation rate, a view supported by Shaw (1985). A shallow marine depositional environment fits with the observations made in thin sections indicating a grain size of very fine sand and examples of wood particles. The kerogen present in upper Grumantbyen has been identified as type III by Rock-Eval analysis (Figure 41). Type III kerogen originates from land plants, lacking the waxy substance (lipid) found in kerogen type I and II (Peters and Cassa, 1994). This underline the possible major terrestrial input to the sandstones of Grumantbyen Formation.

Grain size, grain shape, sorting and quartz/feldspar ratio are all to some extent maturity controlled factors (Boggs, 2006) and in the Grumantbyen sandstones all factors point to an immature sandstone deposition.

From both the thin section analysis (chapter 6.1) and XRD analysis (chapter 6.2) a high chlorite concentration is apparent in these sandstones. SEM and optical microscopy observations reveal the detrital nature of these chlorites. With chlorite not being particularly resistant to weathering and transport (Ehrmann et al., 1992) a proximal setting of these depositions are probable. The low kaolinite/(kaolinite + chlorite) ratio (on average 0,08) most likely reflect predominantly mechanical weathering of the source rocks and thus a relatively cool and dry climate (Robert and Kennett, 1991). Quantitative analyses also reveal a quartz/(quartz + feldspar) ratio in the region of 0,4, with plagioclase being the most abundant of the feldspars. From the observation of high feldspar and plagioclase contents three aspects are deduced: 1) Provenance area is rich in plagioclase: this could coincide with volcanic source rock which is rich in plagioclase (Boggs, 2006). 2) Transport and deposition have been favorable of plagioclase rich sand. Feldspars are generally less resistant to weathering than quartz and thus a short transportation distance is likely (Boggs, 2006). 3) Meteoric water flushing has not been active. If these sandstones had been subject to meteoric water flushing one would assume the plagioclase content to be lower. As a direct result, authigenic kaolinite could precipitate (Lanson, 2002). The kaolinite content is only 0,7 XRD% in these sandstones and hence only modest dissolution of plagioclase into kaolinite have taken place. Meteoric water flushing can be prevented by either a distal shelf setting lacking the opportunity for contact with meteoric water (Bjørlykke, 1998) or if the rock is sufficiently impermeably to resist flushing (Lanson, 2002). Although these sandstones have poor permeabilities and only moderate porosities, this may be a result of compaction and both may have been better at the

time of deposition. However, poorly sorted, “unclean” sandstone, as these, will reduce the permeability and resist meteoric flushing. Hence a distal location is not necessary to explain the absence of authigenic kaolinite.

The sandstones Grumantbyen Formation end in a 5 cm thick conglomerate (Figure 12a). The transition between sandstones and conglomerate is non-erosive and forms a well defined boundary. A non-erosive contact has been cited in support of deposition by other forces than density currents (Dalland , 1976). No signs of subaerial exposure are observed suggesting a subaqueous deposition. Possible transport mechanisms are discussed in detail by Dalland (1976), with the author concluding transport of pebbles and gravel by ice rafting as the most reasonable hypothesis. When it comes to deposition of such large quantities of coarse material, without eroding the underlying layer, the plausible explanation is that material has been dropped from above by a medium capable to carry coarse material in large amounts. Ice rafting as the mechanism is fitting both those criteria. The problem with this explanation is the need for temperatures to drop below freezing point, at least in the winter season and this contradict the studies by e.g. Schweitzer (1982). In that regard another mechanism, also discussed by Dalland (1976); transport by kelp or algal mats seems more plausible.

From observations made in petrographic microscope and SEM, mechanical compaction looks to be the dominant porosity reducing factor. Prevalence of concavo-convex and long contacts indicates physical compaction and little impact by chemical compaction (McBride, 1991). The existence of dissolved feldspar grains, however points to some effect of chemical compaction (Figure 20). The burial depth of the Grumantbyen Formation has been proposed to be around 1500 m by palynological analysis (Thronsen, 1982). Rock-Eval data from this study only comprise one single, sample from the Grumantbyen Formation sandstones. This one sample display different maturity in Tmax vs. depth and PI vs. depth diagrams (Figure 43). However, the trend line is indicating a maturity within the peak oil window, with temperatures in region of 100° - 110° C, using values from Peters and Cassa (1994). The temperatures from Peters and Cassa (1994) are average values from a large data set with local variations depending on lithology, burial rate, etc. Using these average values suggest a deeper burial than 1500 m suggested by Thronsen (1982). The absence of filamentous illite and authigenic kaolinite in SEM observations support burial depths far above 3-4 km.

8.2 Transgressive systems tract (551,60 m –500 m)

8.2.1 Shales of Gilsonryggen Member

The shales of Gilsonryggen Member can be divided into three separate parts, representing different depositional environments. From 551,60 – 535,00 there is clear fining upwards development while the 535 – 532 interval show upwards coarsening shales. The maximum flooding surface can be found somewhere between level 532 -500, but a precise boundary between the transgressive and regressive phase is difficult to locate. From around level 500 m to the siltstones at level 280 m the shale succession displays an upwards coarsening trend. In the following these different parts of the Gilsonryggen Member will be discussed.

Shales of lower Gilsonryggen (551,60 m – 532,00 m):

The boundary between sandstones of Grumantbyen Formation and shales of Gilsonryggen Member is marked with the conglomerate at 551,60 m. In reality a transition zone of upwards fining siltstones rapidly changing into a claystone are present between the conglomerate at 551,60 m and another conglomerate at 548,40. The quartz/(quartz + feldspar) ratio is also shifting in favor of upwards increasing amounts of quartz. Either a change in transportation and depositional environment or a new provenance area could explain this. Since the feldspars content are gradually declining and quartz content is gradually increasing followed by a mutual decrease in grain size, a change to a more distal environment seems to be most likely. The conglomerate at 548,40 has a distinct basal boundary which is possibly eroding and consists of subangular clasts within a clay rich matrix. From these characteristics the deposition by mass flow seems likely (Tripsanas, 2008). The short transition from sandstones to dark shales suggests that a rapid transgression has taken place.

Above the conglomerate a medium gray shale, non-laminated and moderately bioturbated occupies the region from 548 m to 535 m (Figure 12b). Glauconite grains and fossils are present. The appearance of bioturbation, the medium gray color and the relatively low content of pyrite and lamination suggest that bottom conditions must have been fairly well oxygenated (Myrow, 1990, Savdra and Bottjer, 1987 Wignall, 2005).

Thin (1-2 cm) upward fining, silty shale sequences are observed in this interval. The upward fining trend indicates a possible turbiditic origin (Stow and Shanmugum, 1980). The existence of small mudclasts within the sequence is interpreted as being the result of erosion of the underlying shales by a current flowing on the sea floor, which is commonly found in turbidites. Tracing the source of these sequences is difficult based on the data from this study

alone. Steel et al., (1981) suggested that the first deposits of Frysjaodden Formation represented a shift from a transtensional to a transpressional regime. According to Steel and Worsley (1984) a possibly north/ north-eastern source could be present in early Eocene.

From Rock-Eval analysis the kerogen type found in the shales of lower Gilsonryggen Member are mainly characterized by Type II kerogen implying a marine source (Peters and Cassa, 1984). Because of the relative high kerogen maturity in this study, most of the samples cluster in the left corner of the modified van Krevelen diagram (Figure 41). This makes it difficult to characterize of kerogen in detail for some of the samples.

Short episodic regression: (535 m – 532 m)

From 535 m to 532 m, there is a short interval representing an upwards coarsening development, moderate/highly bioturbated and siderite rich claystone. The siderite in this interval is present both as concretions and frequently occurring bands (1-2 cm). Siderite is an authigenic formed mineral (Pearson, 1979). The existence of siderite has been used as an indication of decreased oxygen levels in bottom waters as an intermediate stage between glauconite enrichment (oxic environments) and pyrite enrichment (anoxic environments) (Potter et al., 1980). But siderite may also occur in homogenous, bioturbated shale indicating less reducing bottom waters (Morris, 1979). It is tempting to correlate this sequence with results of Burca (2008) and R  ther (2007) and interpreting this as a distal part of the Hollenderdalen formation. The stratigraphical position fits, and if sediments were brought into the basin from north/north-west it would explain why the formation is present at Nordenski  land (position of Burca (2008) and R  ther (2007)) and absent or possibly vaguely present in BH 9/05(Figure 1).

Based on the presented data a massive change in depositional environment occurred from the deposits of Grumantbyen Formation to the Gilsonryggen Member. The lower shales of Gilsonryggen can be interpreted to represent the first stage of a transgressive phase. The fining upwards development from silty shale to shale suggest depositional environment change gradually from what is thought to be a proximal shelf towards a distal shelf environment. At the top of this interval there is a short period of coarser material being deposited. This might be due to tectonics occurring north/north-west of the basin being responsible for the marginal development of the Hollenderdalen Formation.

Maximum flooding zone (532 – 500)

The interval from 532 to 500 m consists of dark gray, laminated shales with high pyrite content.

This interval displays several signs suggesting restricted oxygenation. The most apparent is the dark gray to black color and well developed lamination which indicate absence of bottom dwellers (Myrow, 1990, Morris, 1979). Between level 529,75 m and 517,08 the pyrite content is extremely high compare to the rest of the core. This observed both in thin sections, SEM and from the XRD-analysis. A less extreme, but obvious change occurs in the Th/U ratio which experienced a drop between levels 527,05 m and 508,05 m (Figure 44). The TOC is relatively low in the entire core, but the highest values are found ten meters deeper than the Uh/U kick (538,38 m – 534,37) (Figure 44).

The maximum flooding surface (MFS) (Figure 9) is difficult to pinpoint. Instead a maximum flooding zone (MFZ) is suggested, within this one or several maximum flooding surface candidates are possible. This zone is underlain by a regradational parasequence (551 m -532 m) set and overlain by a progradational parasequence set (500 m -110 m). The presence of the most homogenous shales and anoxic conditions are common in the lower portion of maximum flooding zones (Emery and Myers, 2006). From the log it is evident that the finest grained sediments are positioned in this interval (Figure 11a). As mentioned above, several factors point to anoxic conditions in the interval between 529,75 m – 508,05 m, which narrow the interval slightly. Enrichment of CaCO_3 is also a common feature of MFZ (Emery and Myers, 2006). The highest CaCO_3 in the core is found at 508,05 m (Figure 44). Together these factors lead to the conclusion that the MFS probably lie within this interval.

PETM

The identification of a possible candidate for PETM has been conducted by $\delta^{13}\text{C}$ ratios, and the onset is positioned at about 531 m (Cui et al., unpublished data). Preliminary work indicate roughly an age of 55,6 Ma at this level (Charles, pers. com. 2009.) . Earlier work from the Lomonosov ridge indicates the onset of PETM \approx 55 Ma (Sluijs et al., 2006). Brinkhuis et al. (2006) showed that an intensified hydrological cycle was induced in the Arctic due to warm greenhouse conditions. As a result of increased precipitation exceeding evaporation, the Paleogene Arctic Ocean had generally low surface water salinities. Foraminifera studies conducted by David Jargvoll (Jargvoll, 2009) on core BH 9/05 have

unveiled the absence of calcareous species during the suggested PETM interval, which indicate fresh or brackish waters. It has also become evident that the number of benthic species is reduced during this interval. The number of benthic species are reduced from 11 to 5 in the interval between level 534 and 530,99 m (Jargvoll, 2009). A similar benthic extinction has been observed in the Antarctic at the Paleocene/Eocene boundary (Kennett and Stott, 1991). Observations made during core logging implied the occurrence of laminated dark shales beginning almost exactly on the proposed onset of PETM. A similar observation has been made by Sluijs et al. (2006) in core 32X from Lomonosov ridge.

In this thesis one of the aims has been to see if clay mineral assemblages change in the region of a possible climatic event. As discussed at the beginning of this chapter, it has been suggested that an authigenic origin of clay minerals at this level is unlikely and hence the further discussion will be carried out presuming a detrital origin.

Different environmental conditions have been discussed earlier as responsible for the amount of detrital illite, chlorite and kaolinite in the sedimentary record. And thus the kaolinite/(kaolinite + illite) and kaolinite/(kaolinite + chlorite) ratios will reflect changing relations between temperature and precipitation. From the bulk XRD analysis kaolinite/(kaolinite + illite) ratio and kaolinite/(kaolinite + chlorite) both illustrate the same trend (Figure 31)

There is a well defined peak in ratios just around the 531 m depth, coinciding with the proposed PETM. Both ratios also express a steady decrease when moving stratigraphically upwards from the 531 level, suggesting a transition from a humid climate towards a cool and dry climate. When observing the region near 531 m in detail it becomes clear that the peak is broad and spans the area from 536 m to 525 m (Figure 38 and Figure 39). From the bulk samples it even looks like kaolinite decreases slightly exactly at around 531 and have the greatest values just before and after. This phenomenon is less prominent in the clay separated samples where the ratios are slightly higher just before 531 m and then decrease moving upwards. Hence it's difficult to pinpoint the onset of PETM strictly based on clay mineral assemblages. From the foraminifera analysis the presence of only three species at level 527,05 is the strongest indication of the PETM (Jargvoll, 2009). In heinseit the clay separated samples should ideally have covered a broader interval in order to illustrate the PETM peak better. Only two samples were selected outside the PETM interval and they both display significant lower ratios than inside the interval. Future studies should take into consideration

the duration of the PETM-interval and span a larger region. Detrital kaolinite is not only a climatic indicator. Due to the often larger grain size of detrital kaolinite compared to illite and chlorite it may be a good indicator of nearshore depositional environment (Potter et al., 2005). This might explain why Burca (2008) observed larger kaolinite/illite and kaolinite/illite ratios than in this study. Presuming a north/north-western source will locate the Nordenskiöld section of Burca (2008) study closer to the shore.

8.3 High stand systems tract (500 m-110 m)

8.3.1 Shales of middle Gilsonryggen Member (500 m -280 m)

The shales of middle Gilsonryggen Member comprise the aggradation phase with an intermediate transgressional period.

Aggradation phase (500 m- 409 m)

From the fine laminated, dark shale there is a transition into a lighter, siderite rich shale similar to the one found from 535 m-532 m. It is characterized by shales with bioturbated, thin silt layers. In the thin sections an increased content of larger grains (>0,2 mm) and polycrystalline quartz has been observed (Figure 25). The origin of these thin silt layers can be disputed due to the fact that most structures have been destroyed by bioturbation. Some of the silt layers show signs of being upwards fining, indicating a possible turbiditic suspension current origin. But considering a distal shelf environment storm deposits are also a possibility. Episodic supply of material from shallower water will bring oxygenated H₂O to the bottom (Potter et al., 2005), and thus create conditions favorable of benthic organisms. From the factors discussed above, this interval is interpreted to be the initial aggradation characterizing the beginning of a highstand system tract.

Based on the data from this study it is difficult to determine the source of the coarse grained material. It could be sourced from the western Spitsbergen mountain chain, which according to Steel et al., (1985) is beginning to form in early Eocene. Another possibility is a more northerly source, which was suggested for the Hollendardalen Fm. The observations of high frequency of slickensides in this core interval interval could be an indication of increased tectonic activity (Phillipson, 2003), which might be linked to the formation of a nearby mountain chain. But this might also be effects of differential compaction (Phillipson, 2003). A change in water salinity is also suggested by the observation of subaqueous shrinkage structures (Burst, 1965) around 426 m depth (Figure 16).

Upwards decreasing kaolinite/(kaolinite +chlorite) and kaolinite/(kaolinite +illite) ratios suggest either colder climate or erosion into rocks richer in illite/chlorite compared to kaolinite. The steady transition from high to lower kaolinite values corresponding with a climatic transition fits with the earlier work discussed in chapter 3, moving from greenhouse conditions in the Cretaceous to icehouse conditions in the Neogene (Savin et al., 1975, Corfield, 1994, Zachos et al., 1993) .

Intermediate transgressive phase (409 m -330 m)

In the interval between 409 m – 330 m there are factors pointing towards an episode of increased transgression within a larger high stand system tract cycle. The main evidence is the absence of bioturbation and the observation of dark gray, laminated shale. The pyrite content and Th/U ratio do not change notably indicating fairly well oxygenated bottom conditions (Figure 44). Also no significant change in clay mineral composition occurs during this phase.

Aggradation phase (continue) (330 m – 280 m)

The last fifty meters of shale in the core continues the aggradational, upwards coarsening development which started before the transgressive phase. Near the top of this, the occurrences of silt layers are increasing in frequency and in thin erosional contacts are observed towards the underlying shale. Mud clasts are commonly found along the base of the siltstones. These are indications of an increased energy regime.

8.3.2 Siltstones of upper Gilsonryggen Member (280 m -150 m)

The siltstones of upper Gilsonryggen Member represent the first progradational deposition.

Progradation phase (280 m -110 m)

This interval is characterized by a moderate/heavy bioturbated, upwards coarsening, soft-sediment deformed siltstone. The boundary between shales and siltstones is a gradual one, rather than a sharp contact, but for practical reasons a boundary has been placed at 150 m.

Soft-sediment deformation structures are common in siltstones and fine sandstone deposits. High rates of deposition, low permeability and low shear strength of these sediments maximize the deformation (Mills, 1983). In this interval several soft-sediment structures have been observed, representing different conditions under which they are produced; when a silt layer is deposited above clay layer a reverse density gradient is established due to different porosities (Sandstone≈45%, Clay≈70-90%). These differences may produce a metastable

arrangement leading loading casts and flame structures (Figure 18b). Most often these forms occur when there is a differential loading such as under thickened ripple crest (Mills, 1982) (Figure 18c). The occurrences of loading structures are frequent in this interval. In some siltstone vague ripple lamination has been spotted, where the sediment deformation is minor. The observation of ball- and pillow structures also suggests deformation by unequal surface load; caused by rapid deposition and relatively high supply of coarse grained material.

Other mechanisms may also produce soft-sediment deformation. One is the bed shear produced by flowing water which deforms sediments with low shear strength. Such sediments are unconsolidated, newly deposited and liquefied mud (Mills, 1982). The resulting structure of this mechanism is what is known as convolute lamination (Figure 14b). Convolute lamination is defined as distorted stratification forming laterally alternating convex- and concave- upward morphologies, producing a complex pattern of broad synclines and anticlines (Rossetti, 1999). Convolute lamination is a common feature of this interval, possibly indicating a drag of passing currents across newly deposited mud.

The structures discussed above may occur in different environments ranging from shallow-marine to deep marine (Mills, 1982). In these deposits the high frequency of siltstone beds over approximately 150 m might indicate shallow-marine storm events to be responsible bringing out coarse grained sediments. This interpretation is also supported by the occurrence of glauconite grains. The foraminiferal analysis by Jargvoll (2009) also indicates this interval as a transitional zone between a distal to a more proximal setting.

The kaolinite/(illite + kaolinite) and kaolinite/(chlorite + kaolinite) ratios are low, only half the value they were around the proposed PETM, and the steady decrease is continuing. This suggests that the change in climatic conditions persists.

8.3.3 Sandstones of upper Gilsonryggen Member/Lower Battfjellet Formation (150 m – 110 m)

From around level 150 m and upwards the majority of grains are in the sand fraction. This interval displays a rapid progradation with sand content increasing from around 40% at the beginning to almost 90% at the top. Characterizing this interval is high degree of reworking, low-cross and through-cross stratified rocks and an increasing amount of organic matter. The boundary between Gilsonryggen and Battfjellet has been defined as where the shales become subordinate to the sandstones (Helland-Hansen, 1990).

Structures observed in this interval imply a storm-dominated shelf environment. Low-angle ripple lamination is common in many shallow-water environments affected by oscillatory waves (Fielding et al., 2006). Low-angle ripple lamination may also be produced by unidirectional currents associated with large storms (Dumas and Arnott, 2006). Hummocky cross-stratification (HCS) is believed to be preserved in the offshore-transition zone (Figure 45). Below storm wave base energy is too low to produce the hummocks and above fair-weather wave base the structures will be destroyed by normal wave actions (Reading, 1996). Water depths between 13-50 m are ideally for the formation of HCS (Dumas and Arnott, 2006). The presence of large quantities of organic fragments might be explained by transportation from the shoreface to the transition zone during storms (Figure 18d). The planar bedding identified near the top implies moving into the shoreface environment (Reading, 1996).

Spreiten, identified in thin section (Figure 28), reflect the activity of *Rhizocorallium* type trace fossil which are characteristic of the *Glossifungites* ichnofacies (Frey and Pemberton, 1985). The distribution of *Glossifungites* ichnofacies is restricted to firm but unlithified

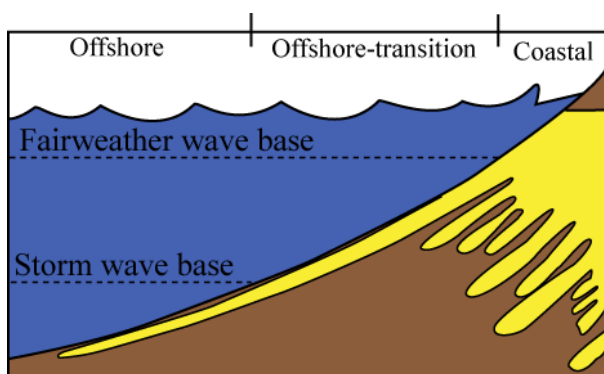


Figure 45: Proximal-distal trends (modified from Reading (1996))

substrates often at the transition between nearshore/offshore or along the shelf edge (Frey and Pemberton, 1985).

In thin section, at level 130,05 m depth, a possible fluid-escape structure is observed.

Such structures are believed to have formed as a result of spontaneous water loss during quick deposition of silt or sand grains (Mills, 1982).

The mineralogy of these uppermost sandstones differs significantly from the sandstones observed in Grumantbyen Formation. The main difference is the proportions of quartz and feldspars. In Grumantbyen Formation sandstones the feldspar content was almost twice as high as quartz. In the sandstones of upper Gilsonryggen Member/lower Battfjellet Formation the quartz content is almost twice as high as that of feldspar. The sandstones of Grumantbyen Formation and upper Gilsonryggen Member/lower Battfjellet sandstones are sourced from different provenance areas, which may explain the difference in quartz/feldspar ratios. The difference may also be the result of a higher maturation and reworking of sediments caused

by a more distal source in the uppermost sandstones. The kaolinite content is 5 times higher than in the Grumantbyen sandstones suggesting a higher degree of early feldspar dissolution (Appendix 3).

9 Conclusion

Grumantbyen Formation sandstones

Steel and Worsley (1984) suggest that in Paleocene, Tertiary basin of Svalbard was closed on three sides. The uplift on the north/north-eastern side of the basin by either the peripheral bulge suggested by Bruhn and Steel, 2003 or by transtensional mechanisms (Steel et al., 1985) provided sediments to the basin. Core BH 9/05 represent the eastern side of the Tertiary basin, and the characteristics of Grumantbyen Formation imply a nearby source to the deposits these sandstones. This sandstone deposition marks the maximum regression from east to west (Figure 47). The presence of glauconite suggest rather slow sedimentation rate and can be interpreted as a result of a more gentle relief caused by erosion of the peripheral bulge. A depositional model similar to the one proposed by Steel and Worsley (1984) fit reasonably well with observations made in this study (Figure 46a).

The grain size and close to total destruction of most sedimentary structures by bioturbation indicates a possible shoreface deposition; possibly lower (Müller and Spielhagen, 1990).

Shales of Gilsonryggen Member

The first part of the shales is interpreted to represent a transgressional phase and a shift in sediment input from north-east to north-west. The maximum flooding zone is indentified between 529,75 m – 508,05 m. The increased supply of sediments from the nearby formed West Spitsbergen mountain chain (Steel et al., 1985) is interpreted to be the main factor of the long term regressional trend beginning at around 500 m (Figure 47). Proposed depositional environment of these shales are a distal shelf setting (Figure 46b).

The interval between 536 m – 529 m show evidence of being deposited during a period of increased temperature and precipitation, based on kaolinite/(kaolinite + chlorite) and kaolinite/(kaolinite + illite). Together with a large extinction of benthic forams (between 534 – 530,99 m) and the stratigraphic position of this interval in the stratigraphic column suggests a highly probable candidate to the PETM. Based on shale characteristics such as color,

lamination and pyrite content and geochemical analyses (Th/U, CaCO₃) place the maximum flooding surface somewhere in the interval 529,75 – 508,05 m (Figure 47).

Gilsonryggen Member/Lower Battfjellet Formation siltstones and sandstones

These sequences represent a rapid regression and a transitional zone from distal shelf setting to a shoreface setting (Figure 47). The upper two meters of the core show evidence of being deposited in a lower shoreface environment. Clay mineralogy reflects differences which may indicate different provenance area and/or colder climate and less precipitation compared to the first parts of Gilsonryggen Member. Figure 46c propose a possible scenario of the infilling of the Tertiary basin from west to east.

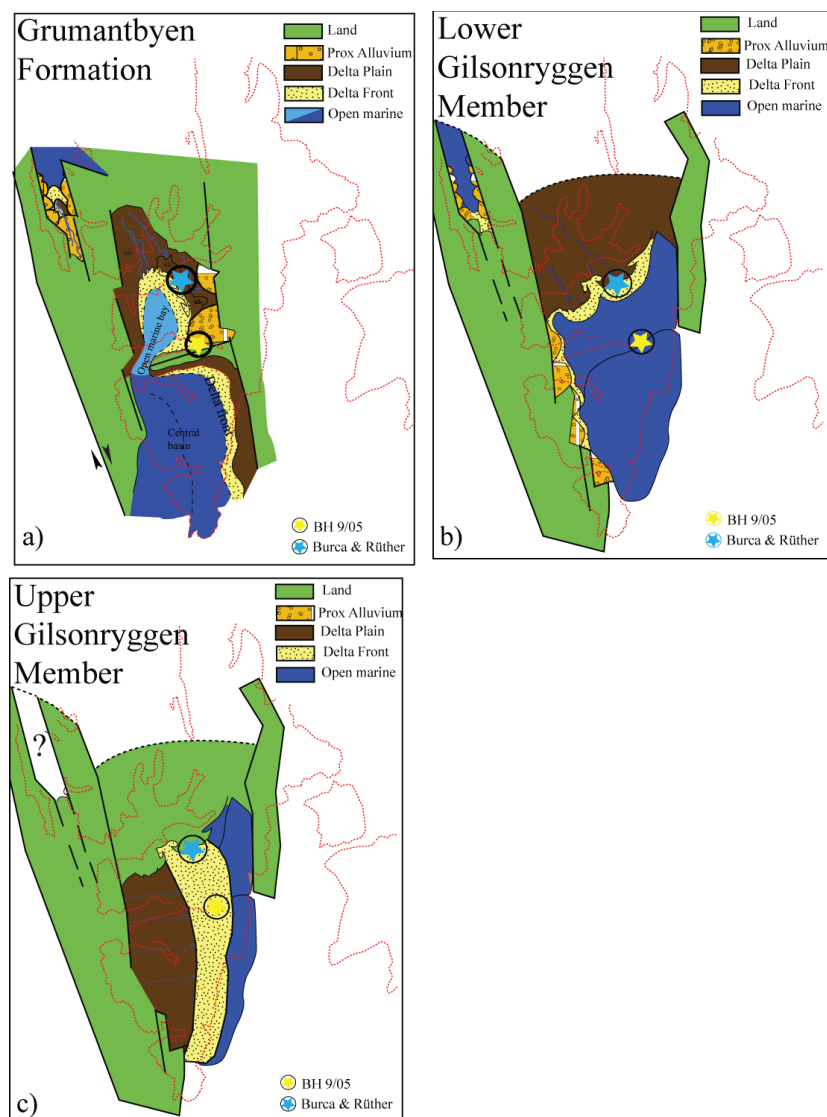


Figure 46: Depositional environment of the a) Grumantbyen Formation sandstones, b) Lower Gilsonryggen Member and c) Upper Gilsonryggen Member. Localities of drill site of BH 9/05 and field logging conducted by Burca (2008) and R  ther (2007) are marked (modified)

Nordenskiöldfjellet 1 + 2
(Burca (2008))

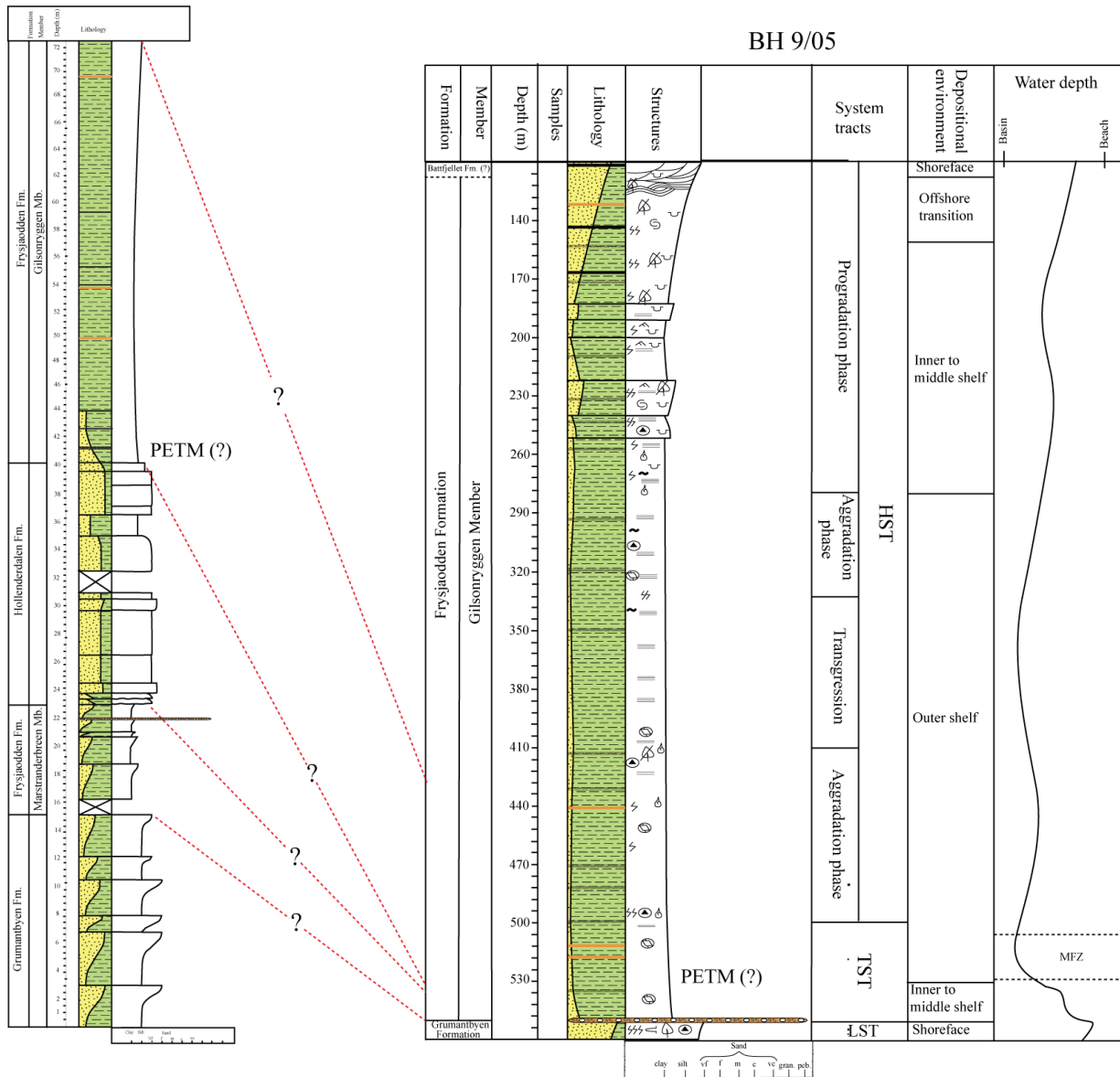


Figure 47: Correlation between Nordenskiöldfjellet and BH 9/05. Note the presence of three bentonite beds in both sedimentary logs above the PETM. In core BH 9/05 sequence stratigraphic interpretation and water depth have been interpreted based on this study and micro paleontology (Jargvoll, 2009)

References

- Anderson, R.F., Fleisher, M.Q., and LeHuray, A.P., 1989, Concentration, oxidation-state, and particulate flux of Uranium in the Black Sea *Geochimica Et Cosmochimica Acta*, v. 53, p. 2215-2224.
- Bains, S., R. M. Corfield, and R. D. Norris, 1999, Mechanisms of climate warming at the end of the Paleocene: *Science*, v. 285, p. 724-727.
- Bergaya, F., Theng, B.K.G., and Lagaly, G., 2006, *Handbook of clay science*: Amsterdam, Elsevier, XXI, 1224 s. p.
- Berger, A., 1988, Milankovitch theory and climate: *Reviews of Geophysics*, v. 26, p. 624-657.
- Birkeland, P.W., 1984, *Soils and geomorphology*: New York, Oxford University Press, xiv, 372 s. p.
- Bjørkum, P.A., and Gjelsvik, N., 1988, An isochemical model for formation of authigenic kaolinite, k-feldspar and illite in sediments *Journal of Sedimentary Petrology*, v. 58, p. 506-511.
- Bjørlykke, K., 1998, Clay mineral diagenesis in sedimentary basins - a key to the prediction of rock properties. Examples from the North Sea Basin: *Clay Minerals*, v. 33, p. 15-34.
- Bjørlykke, K., 2001, *Sedimentologi og petroleumsgnologi*: Oslo, Gyldendal yrkesopplæring, 334 s. p.
- Boggs, S., 2006, *Principles of sedimentology and stratigraphy*: Upper Saddle River, N.J., Pearson Prentice Hall, XIX, 662 s. p.
- Bordenave, M.L., 1993, *Applied petroleum geochemistry*: Paris, Éditions Technip, XI, 524 s. p.

- Brinkhuis, H., Schouten, S., Collinson, M.E., Sluijs, A., Damste, J.S.S., Dickens, G.R., Huber, M., Cronin, T.M., Onodera, J., Takahashi, K., Bujak, J.P., Stein, R., van der Burgh, J., Eldrett, J.S., Harding, I.C., Lotter, A.F., Sangiorgi, F., Cittert, H.V.V., de Leeuw, J.W., Matthiessen, J., Backman, J., Moran, K., and Expedition, S., 2006, Episodic fresh surface waters in the Eocene Arctic Ocean: *Nature*, v. 441, p. 606-609.
- Burca, F. 2008. Palaeogene depositional environments of the Frysjaodden and Hollendardalen formations in central Spitsbergen, University of Oslo (Unpublished master thesis)
- Burst, J.F., 1965, Subaqueously formed shrinkage cracks in clay *Journal of Sedimentary Petrology*, v. 35, p. 348-353
- Bruhn, R., and R. Steel, 2003, High-resolution sequence stratigraphy of a clastic foredeep succession (Paleocene, Spitsbergen): An example of peripheral-bulge-controlled depositional architecture: *Journal of Sedimentary Research*, v. 73, p. 745-755.
- Calvert, S.E., and Pedersen, T.F., 1993, Geochemistry of recent oxic and anoxic marine sediments - implications for the geological record *Marine Geology*, v. 113, p. 67-88.
- Clyde, W.C., and Gingerich, P.D., 1998, Mammalian community response to the latest Paleocene thermal maximum: An isotaphonomic study in the northern Bighorn Basin, Wyoming: *Geology*, v. 26, p. 1011-1014.
- Corfield, R. M., 1994, Paleocene Oceans and Climate – An Isotopic Perspective: *Earth-Science Reviews*, v. 37, p. 225-252.
- Dalland, A., 1976. Erratic clasts in the Lower Tertiary deposits of Svalbard - evidence of transport by winter ice. *Årbok - Norsk Polarinstitut* 1976, p. 151 - 165.
- Dallmann, W.K., 1999, Lithostratigraphic lexicon of Svalbard: review and recommendations for nomenclature use : Upper Palaeozoic to Quaternary bedrock: Tromsø, Norsk polarinstitut, 318 s. p.

- Dickens, G.R., Oneil, J.R., Rea, D.K., and Owen, R.M., 1995, Dissociation of oceanic methane hydrate as a cause of the carbon-isotope excursion at the end of the Paleocene: *Paleoceanography*, v. 10, p. 965-971.
- Dumas, S., and Arnott, R.W.C., 2006, Origin of hummocky and swaley cross-stratification - The controlling influence of unidirectional current strength and aggradation rate: *Geology*, v. 34, p. 1073-1076.
- Dypvik, H., Ferrell, R.E., and Sandbakken, P.T., 2003, The clay mineralogy of sediments related to the marine Mjølner impact crater: *Meteoritics & Planetary Science*, v. 38, p. 1437-1450.
- Ehrmann, W.U., Melles, M., Kuhn, G., and Grobe, H., 1992, Significance of clay mineral assemblages in the Antarctic Ocean *Marine Geology*, v. 107, p. 249-273.
- Emery, D., Myers, K., and Bertram, G.T., 1996, *Sequence stratigraphy*: Oxford, Blackwell Science, V, 297 s. p.
- Espitalie, J., Laporte, J.L., Madec, M., Marquis, F., Leplat, P., Paulet, J., and Boutefeu, A., 1977, Rapid method for source rocks characterization and for determination of petroleum potential and degree of evolution *Revue De L Institut Francais Du Petrole*, v. 32, p. 23-42.
- Fielding, C.R., Bann, K.L., Maceachern, J.A., Tye, S.C., and Jones, B.G., 2006, Cyclicity in the nearshore marine to coastal, Lower Permian, Pebbly Beach Formation, southern Sydney Basin, Australia: a record of relative sea-level fluctuations at the close of the Late Palaeozoic Gondwanan ice age: *Sedimentology*, v. 53, p. 435-463.
- Frey, R.W., and Pemberton, S.G., 1985, Biogenic structures in outcrops and cores. 1. Approaches to ichnology *Bulletin of Canadian Petroleum Geology*, v. 33, p. 72-115.

- Harland, W.B. (1969: Contribution of Svalbard to the evolution of the North Atlantic region.- In: MCKAY (ed.), North Atlantic Geology and Continental Drift. Am. Ass. Petrol. Geol. Mem. v. 12, p. 817-857.
- Helland-Hansen, W., 1990, Sedimentation in Paleogene foreland basin, Spitsbergen Aapg Bulletin-American Association of Petroleum Geologists, v. 74, p. 260-272.
- Helland-Hansen, W., 1992, Geometry and facies of Tertiary clinothems, Spitsbergen: Sedimentology, v. 39, p. 1013-1029.
- Higgins, J.A., and Schrag, D.P., 2006, Beyond methane: Towards a theory for the Paleocene-Eocene Thermal Maximum: Earth and Planetary Science Letters, v. 245, p. 523-537.
- Jargvoll, D., 2009, Microfossil-based depositional environments of a delta-influenced succession in the Paleogene of Spitsbergen, including the PETM, University of Oslo (Unpublished master thesis)
- Kellogg, H.E., 1975, Tertiary Stratigraphy and Tectonism in Svalbard and Continental drift: Aapg Bulletin-American Association of Petroleum Geologists, v. 59, p. 465-485.
- Kennett, J.P., and Stott, L.D., 1991, Abrupt Deep-sea warming, Palaeocenographic changes and Benthic extinctions at the of the Paleocene: Nature, v. 353, p. 225-229.
- Kent, D.V., Cramer, B.S., Lanci, L., Wang, D., Wright, J.D., and Van der Voo, R., 2003, A case for a comet impact trigger for the Paleocene/Eocene thermal maximum and carbon isotope excursion: Earth and Planetary Science Letters, v. 211, p. 13-26.
- Langmuir, D., and Herman, J.S., 1980, The mobility of Thorium in natural wates at low temperatures: Geochimica Et Cosmochimica Acta, v. 44, p. 1753-1766.
- Lanson, B., Beaufort, D., Berger, G., Bauer, A., Cassagnabere, A., and Meunier, A., 2002, Authigenic kaolin and illitic minerals during burial diagenesis of sandstones: a review: Clay Minerals, v. 37, p. 1-22.

- Major, H., and Nagy, J., 1972, Geology of the Adventdalen map area: Oslo, Norsk polarinstitutt, 58 s. p.
- McBride, E.F., Diggs, T.N., and Wilson, J.C., 1991, Compaction of Wilcox and Carrizo sandstone (Paleocene-Eocene) to 4420 m, Texas Gulf-coast: *Journal of Sedimentary Petrology*, v. 61, p. 73-85.
- McRae, S.G., 1972, Glauconite: *Earth-Science Reviews*, v. 8, p. 397-440.
- Mehra, O. P. and Jackson, M.L. 1960. Iron oxide removal from soils and clays by a dithionite-citrate system buffered with sodium bicarbonate: in *Clays and Clay Minerals*, Proc. 7th Natl. Conf., Washington, D.C., 1958, Ada Swineford, ed., Pergamon Press, New York, p. 317-327. Stumm, W. and Morgan, J. J. (1981) *Aquatic Chemistry*.
- Mills, P.C., 1983, Genesis and diagnostic value of soft-sediment deformation structures- A review *Sedimentary Geology*, v. 35, p. 83-104.
- Moore, D.M., and Reynolds, R.C., 1997, X-ray diffraction and the identification and analysis of clay minerals: Oxford, Oxford University Press, xviii, 378 s. p.
- Moran, K., Backman, J., Brinkhuis, H., Clemens, S.C., Cronin, T., Dickens, G.R., Eynaud, F., Gattacceca, J., Jakobsson, M., Jordan, R.W., Kaminski, M., King, J., Koc, N., Krylov, A., Martinez, N., Matthiessen, J., McInroy, D., Moore, T.C., Onodera, J., O'Regan, M., Palike, H., Rea, B., Rio, D., Sakamoto, T., Smith, D.C., Stein, R., St John, K., Suto, I., Suzuki, N., Takahashi, K., Watanabe, M., Yamamoto, M., Farrell, J., Frank, M., Kubik, P., Jokat, W., and Kristoffersen, Y., 2006, The Cenozoic palaeoenvironment of the Arctic Ocean: *Nature*, v. 441, p. 601-605.
- Morris, K.A., 1979, Classification of Jurassic marine shale sequences - Example from the Toarcian (Lower Jurassic) of Great-Britain *Palaeogeography Palaeoclimatology Palaeoecology*, v. 26, p. 117-126.

- Müller, R.D., and Spielhagen, R.F., 1990, Evolution of the Central Tertiary Basin of Spitsbergen – Towards a Synthesis of Sediment and Plate Tectonic History: *Palaeogeography Palaeoclimatology Palaeoecology*, v. 80, p. 153-172.
- Myrow, A New Graph for Understanding Colors of Mudrocks and Shales: A New Graph for Understanding Colors of Mudrocks and Shales., v. 38, p. 16.
- Nagy, J., 2005, Delta-influenced foraminiferal facies and sequence stratigraphy of Paleocene deposits in Spitsbergen: *Palaeogeography Palaeoclimatology Palaeoecology*, v. 222, p. 161-179.
- Olesen, O., Ebbing, J., Lundin, E., Mairing, E., Skilbrei, J.R., Torsvik, T.H., Hansen, E.K., Henningsen, T., Midboe, P., and Sand, M., 2007, An improved tectonic model for the Eocene opening of the Norwegian-Greenland Sea: Use of modern magnetic data: *Marine and Petroleum Geology*, v. 24, p. 53-66.
- Pagani, M., Pedentchouk, N., Huber, M., Sluijs, A., Schouten, S., Brinkhuis, H., Damste, J.S.S., and Dickens, G.R., 2006, Arctic hydrology during global warming at the Palaeocene/Eocene thermal maximum: *Nature*, v. 442, p. 671-675.
- Pearson, M.J., 1979, Geochemistry of the Hepworth Carboniferous sediment sequence and origin of the diagenetic iron minerals and concretions: *Geochimica Et Cosmochimica Acta*, v. 43, p. 927-941.
- Pe-Piper, G., Dolansky, L., and Piper, D.J.W., 2005, Sedimentary environment and diagenesis of the Lower Cretaceous Chaswood Formation, southeastern Canada: The origin of kaolin-rich mudstones: *Sedimentary Geology*, v. 178, p. 75-97.
- Peters, K.J., 1986, Guidelines for evaluating petroleum source rock using programmed pyrolysis: *Guidelines for evaluating petroleum source rock using programmed pyrolysis*, v. 70, p. 318.

- Peters, K. E. and Cassa, M. R.: 1994, 'Applied Source Rock Geochemistry', in Magoon, L.B., and Dow, W.G., 1994, *The Petroleum system: from source to trap*: Tulsa, Okla., American Association of Petroleum Geologists, XIII, 655 s. p.
- Phillipson, S.E., 2003, The control of coal bed decollement-related slickensides on roof falls in North American Late Paleozoic coal basins: *International Journal of Coal Geology*, v. 53, p. 181-195.
- Potter, P.E., Maynard, J.B., and Depetris, P.J., 2005, *Mud and Mudstones: Introduction and Overview*: Berlin, Heidelberg, Springer-Verlag Berlin Heidelberg, 297 s.p.
- Potter, P.E., Maynard, J.B., and Pryor, W.A., 1980, *Sedimentology of shale: study guide and reference source*: New York, Springer, x,306 s .p.
- Reading, H.G., 1996, *Sedimentary environments: processes, facies and stratigraphy*: Oxford, Blackwell Science, XIV, 688 s. p.
- Robert, C., and Kennett, J.P., 1994, Antartic subtropical humid episode at the Paleocene-Eocene boundary - Clay mineral evidence: *Geology*, v. 22, p. 211-214.
- Röhl, U., Bralower, T.J., Norris, R.D., and Wefer, G., 2000, New chronology for the late Paleocene thermal maximum and its environmental implications: *Geology*, v. 28, p. 927-930.
- Rossetti, D.D., 1999, Soft-sediment deformation structures in late Albian to Cenomanian deposits, Sao Luis Basin, northern Brazil: evidence for palaeoseismicity: *Sedimentology*, v. 46, p. 1065-1081.
- Rüther, C. D. 2007. Delta influenced Paleogene depositional environments of the Frysjaodden and Hollendardalen formations, University of Oslo (Unpublished Master Thesis).

- Savdra, C.E., Bottjer, D.J. 1987. Trace fossils as indicators of bottom-water redox in ancient marine environments. In: Bottjer, D.J. (Ed.), *New concepts in the use of sedimentary structures for paleoenvironmental interpretations*. SEMP Pacific Section Special Publication, p. 3-26.
- Savin, S.M., Douglas, R.G., and Stehli, F.G., 1975, *Tertiary Marine Paleotemperatures: Geological Society of America Bulletin*, v. 86, p. 1499-1510.
- Schweitzer, H.J., 1980, *Environment and climate in the early Tertiary of Spitsbergen Palaeogeography Palaeoclimatology Palaeoecology*, v. 30, p. 297.
- Shaw, H.F., 1985, *Clays and their effects in source and reservoir rocks: 17-19 June 1985: London, Joint Association for Petroleum Exploration Courses*, v. 1 b, p. 50.
- Sluijs, A., Schouten, S., Pagani, M., Woltering, M., Brinkhuis, H., Damste, J.S.S., Dickens, G.R., Huber, M., Reichert, G.J., Stein, R., Matthiessen, J., Lourens, L.J., Pedentchouk, N., Backman, J., and Moran, K., 2006, *Subtropical arctic ocean temperatures during the Palaeocene/Eocene thermal maximum: Nature*, v. 441, p. 610-613.
- Sluijs, A., Röhl, U., Schouten, S., Brumsack, H.J., Sangiorgi, F., Damste, J.S.S., and Brinkhuis, H., 2008, *Arctic late Paleocene-early Eocene paleoenvironments with special emphasis on the Paleocene-Eocene thermal maximum (Lomonosov Ridge, Integrated Ocean Drilling Program Expedition 302): Paleoceanography*, v. 23.
- Steel, R.J., Dalland, A., Kalgraf, K., Larsen, V., 1981. *The central Tertiary basin of Spitsbergen—sedimentary development in a sheared margin basin*. In: Kerr, J.W., Fergusson, A.J. (Eds.), *Geology of the North Atlantic Borderlands*, Memoir Canadian Society of Petroleum Geologists, v. 7, p. 647– 664.
- Steel, R.J., Gjelberg, J., Helland-Hansen, W., Kleinsphen, K., Noettvedt, A., Rye Larsen, M., 1985. *The Tertiary strike-slip basins and orogenic belt of Spitsbergen*. In: Biddle, K.T., Christie-Blick, N. (Eds.), *Strike-Slip Deformation, Basin Formation and Sedimentation*, Special Publication Society of Economic Paleontologists and Mineralogists, v. 37, p. 339– 359.

- Steel, R. J. and Worsley, D. 1984. Svalbard's post-Caledonian strata – an atlas of sedimentational patterns and palaeogeographic evolution. In: North European Margin, S., Petroleum geology of the North European margin: proceedings of the North European Margin Symposium (NEMS '83), *in* Spencer, A.M.,ed.:London, Published by Graham & Trotman for the Norwegian Petroleum Society, p. vii, 436 s.p.
- Stow, D.A.V., and Shanmugam, G., 1980, Sequence of structures in fine-grained turbidites - Comparison of recent deep-sea and ancient flysch sediments *Sedimentary Geology*, v. 25, p. 23-42.
- Svensen, H., Planke, S., Malthes-Sorensen, A., Jamtveit, B., Myklebust, R., Eidem, T.R., and Rey, S.S., 2004, Release of methane from a volcanic basin as a mechanism for initial Eocene global warming: *Nature*, v. 429, p. 542-545.
- Talwani, M., and Eldholm, O., 1977, Evolution of the Norwegian-Greenland Sea: *Geological Society of America Bulletin*, v. 88, p. 969-999.
- Thronsen, T. 1982: Vitrinite reflectance studies of coals and dispersed organic matter in Tertiary deposits in the Adventdalen area, Svalbard. *Polar Research* v. 2, p. 77-91.
- Tripsanas, E.K., Piper, D.J.W., Jenner, K.A., and Bryant, W.R., 2008, Submarine mass-transport facies: new perspectives on flow processes from cores on the eastern North American margin: *Sedimentology*, v. 55, p. 97-136.
- Weijers, J.W.H., Schouten, S., Sjuifs, A., Brinkhuis, H., and Damste, J.S.S., 2008, Warm arctic continents during the Palaeocene-Eocene thermal maximum (vol 261, pg 230, 2007): *Earth and Planetary Science Letters*, v. 268, p. 243-243.
- Whiticar, M.J., 1999, Carbon and hydrogen isotope systematics of bacterial formation and oxidation of methane: *Chemical Geology*, v. 161, p. 291-314.
- Wignall, P.B., Newton, R., and Brookfield, M.E., 2005, Pyrite framboid evidence for oxygen-poor deposition during the Permian-Triassic crisis in Kashmir: *Palaeogeography Palaeoclimatology Palaeoecology*, v. 216, p. 183-188.

Zachos, J.C., Lohmann, K.C., Walker, J.C.G. and Wise, S.W. 1993. Abrupt climate change and transient climates during the Paleogene: A marine perspective. *Journal of Geology* 101, 191-213.

Zachos, J., Pagani, M., Sloan, L., Thomas, E., and Billups, K., 2001, Trends, rhythms, and aberrations in global climate 65 Ma to present: *Science*, v. 292, p. 686-693.

Appendices

Appendix 1: Logging Sheet

SHEET NO: _____

	SCALE: SECTION: FORMATION	ORB scale	REMARKS, DESCRIPTION AND INTERPRETATION
	1	1	
	2	2	
	3	3	
	4	4	
	5	5	
	6	6	

METRES A. B.	LITHOLOGY	GRAIN SIZE AND SEDIMENTARY STRUCTURES	COLOURS
1.6 1.2 0.8 0.5 0.25 0.125 0.0625	CLAY (SILT) VF F M C I VC F M	SAND VF F M C I VC F M	PEBL F M
1.6 1.2 0.8 0.5 0.25 0.125 0.0625	CLAY (SILT) VF F M C I VC F M	SAND VF F M C I VC F M	PEBL F M

DATE: _____ BY: _____

Appendix 2: Thin section description

Formation/ member	Depth	Lithology	Dominating framework configuration	Predominant structures	Average grain size (mm)	Most common grain shape	Sorting	Remarks
Frysaodden Formation Gilsonryggen Member	110,05	Sandstone	Grain supported	Bedding	Very fine	Angular/Subangular	Moderate	Parallel bands of organic matter. Moderate porosity.
	115,90	Silt	Grain supported	Cross lamination	Silt	Subangular	Moderate	Contains organic matter. Elongated grains follow the bedding. Upwards coarsening
	120,05	Sandstone	Grain supported		Very fine	Subangular/Subrounded	Moderate	Contains organic matter.
	130,05	Sandstone	Grain supported	Non-parallel bedding due to (possible) water escape.	Silt	Subrounded	Poor	Two upwards fining sequences. Rip-up mud clasts. Spreiten trace fossil.
	138,80	Sandstone	Grain supported		Very fine	Subrounded	Moderate	Upwards coarsening with rip-up mud clasts. Polycrystalline quartz. >10 grains are larger than 0,5 mm
	140,05	Sandstone	Grain supported	Bedding, bioturbation	?	Subangular		Upwards fining and contains organic matter. Rip-up mudclasts oriented obliquely to bedding.
	150,05	Silt	Matrix supported	Reworking and moderate bioturbation.	Silt	Angular	Moderate	Coarse grained silt layer with rip-up mud clasts and loading. Some organic matter.
	160,05	Shale	Matrix supported	Reworking and bioturbation	Clay → Silt	Subangular	Moderate	Upwards fining. A thin coarse grained layer eroding into the shale. Rip-up mud clasts and some organic matter.
	170,05	Shale	Matrix supported	Parallel lamination	Clay	Subrounded	Good	Elongated grains following the bedding. Two thin layers of silt disrupting the shale.

Formation/member	Depth	Lithology	Dominating framework configuration	Predominant structures	Average grain size (mm)	Most common grain shape	Sorting	Remarks
Frysaodden Formation Gilsøryggen Member	180,05	Shale	Matrix supported	Reworking and bioturbation	Clay→Silt	Subangular	Poor	>30 grains larger than 0,2 mm. Homogenous clay layers being disrupted by thin upwards fining silt layers containing agglutinated foraminifera and organic material.
	187,00	Silt	Matrix supported	Cross bedding	Silt	Angular/Subangular	Moderate	Homogenous silt. Elongated grains have a preferred direction.
	190,05	Shale	Matrix supported	Alternating clay and silt/sand layers. Moderate bioturbation	Clay	Angular/Subangular	Moderate	Well cemented upwards fining silt/sand layers disrupting the background shale. Loading and rip-up mud clasts. Elongated grains follow the bedding.
	220,05	Shale	Matrix supported	Alternating clay and sand layers. Reworking	Clay → Very fine	Subrounded	Good	Clay layer eroded by upwards fining sand layer. Loading and rip-up mud clasts. Organic matter in sand layer.
	230,05	Shale	Matrix supported	Heavy bioturbation.	Clay	Subangular	Moderate/Good	Some very thin silt layers interrupting the background clay sedimentation.
	250,05	Shale	Matrix supported	Heavy bioturbation	Clay	Subangular → subrounded	Moderate	Upwards fining, with some lamination at the top. Chert pebble.
	264,59	Shale	Matrix supported	Heavy bioturbation. Reworking	Clay → Very fine	Angular/Subangular	Moderate	Upwards fining sand layer disrupting clay sedimentation. Elongated grains do not have a preferred direction.
	270,05	Shale	Matrix supported	Moderate bioturbation.	Clay	Subangular	Poor → Moderate	Polycrystalline quartz and chert pebbles. Agglutinated foraminifera. Elongated grains obliquely oriented in relation to bedding.

Formation/member	Depth	Lithology	Dominating framework configuration	Predominant structures	Average grain size (mm)	Most common grain shape	Sorting	Remarks
Frysaodden Formation Gilsønyggen Member	282,05	Shale	Matrix supported	Reworking and heavy bioturbation.	Clay	Subangular → subrounded.	Moderate	Thin silt layer eroding into the shale. Rip-up mud clasts. Agglutinated foraminifera.
	290,05	Shale	Matrix supported	Reworking and moderate bioturbation	Clay	Subangular	Moderate	Alternating clay and upwards fining silt layers. Polycrystalline quartz.
	330,05	Shale	Matrix supported	Heavy bioturbation	Clay	Subangular	Moderate	Three upwards fining shale layers. Angular polycrystalline quartz grain (d=0,25 mm)
	380,05	Shale	Matrix supported	Poor bioturbation and parallel lamination	Clay	Subangular	Moderate	Listric normal fault
	410,05	Shale	Matrix supported	Moderate bioturbation and bedding.	Clay	Subrounded	Moderate	Alternating layers with finer and coarser material. Some organic matter and agglutinated foraminifera. >10 grains larger than 0,2 mm. Polycrystalline quartz.
	439,93	Shale	Matrix supported	Moderate bioturbation and lamination.	Clay	Subrounded → rounded	Poor	>5 grains larger than 0,2 mm. Polycrystalline quartz. Upwards fining clay layers.
	490,05	Shale	Matrix supported	Moderate bioturbation	Clay	Subrounded	Poor	Agglutinated foraminifera.
	500,05	Shale	Matrix supported	Heavy bioturbation. Bedding	Clay	Subrounded / rounded	Moderate	Alternating layers of finer/coarser grain size, where bedding is destroyed by bioturbation. Agglutinated foraminifera.
	517,08	Shale	Matrix supported	Parallel lamination	Clay	Subrounded/rounded	Good	Secondary cracks. Framboidal pyrites making up one layers.
	525,05	Shale	Matrix supported	Parallel lamination	Clay	Rounded/subrounded	Good	Circular fossil and pyrites.

Formation/member	Depth	Lithology	Dominating framework configuration	Predominant structures	Average grain size (mm)	Most common grain shape	Sorting	Remarks
Frysaodden Formation Gilsøryggen Member	530,99	Shale	Matrix supported	Bedding	Clay	Rounded	Good	Secondary cracks following the bedding. Rich in pyrite, also framboidal pyrites.
	532,37	Shale	Matrix supported	Moderate bioturbation.	Clay	Rounded	Good	>10 agglutinated foraminifera. Rich in pyrite.
	534,37	Shale	Matrix supported	Heavy bioturbation	Clay	Subrounded	Moderate	Rich in pyrite. >5 grains larger than 0,2 mm.
	544,63	Shale	Matrix supported	Parallel lamination and possible ripple lamination	Clay	Subangular	Poor	Rich in coarse grains. Agglutinated foraminifera and organic matter.
	548,35	Conglomerate	Grain supported	Heterogenic	Medium	Rounded	Moderate	Large amount of clay matrix in between grains. >10 grains larger than 0,5 mm. Chert pebbles, rock fragments and polycrystalline quartz.
	551,43	Silt stone	Grain supported	Moderate bioturbation	Silt	Subangular	Poor	Rich in coarse grains > 0,25 mm.
Grumantbyen Formation	552,43	Sandstone	Grain supported	Heavy bioturbation	Very fine	Subangular	Moderate	Moderate porosity, but no connection between pores. Mud clasts with various orientation.
	557,58	Sandstone	Grain supported	Reworking	Very fine	Angular	Poor	Moderate porosity but no connection between pores. Mud clasts with various orientation.

Appendix 3: Mineral counting in thin sections

	Depth (m)	Mono-quartz	Poly-quartz	Feldspar	Matrix		Organic Matter	Pyrite	Chlorite	Glauconite	Fossils	Fe-oxide	Mica	
					Clay	Illitic clay							Muscovite	Biotite
Sandstones of Gilsønyggen	110,05	38,5 %	2,6 %	25,7 %	2,0 %	23,0 %	1,2 %	0,0 %	0,0 %	0,0 %	0,0 %	0,0 %	8,2 %	0,5 %
	115,90	31,8 %	0,0 %	12,0 %	4,2 %	37,0 %	5,4 %	0,0 %	0,0 %	0,2 %	0,0 %	0,0 %	6,7 %	1,7 %
	120,05	27,0 %	1,8 %	17,8 %	8,0 %	38,5 %	2,5 %	0,0 %	0,5 %	0,0 %	0,0 %	0,0 %	2,5 %	0,0 %
	130,05	14,4 %	0,0 %	17,1 %	14,6 %	44,2 %	3,5 %	0,0 %	4,0 %	0,0 %	0,0 %	0,0 %	2,0 %	0,2 %
	140,05	25,2 %	0,0 %	22,6 %	9,2 %	27,3 %	4,6 %	0,0 %	3,5 %	0,0 %	0,0 %	0,0 %	6,9 %	0,7 %
Siltstones of Gilsønyggen	150,05	17,2 %	0,0 %	6,5 %	41,6 %	20,6 %	7,7 %	0,0 %	0,2 %	0,0 %	0,0 %	0,0 %	5,5 %	0,7 %
	160,05	12,9 %	0,0 %	4,1 %	50,8 %	20,9 %	7,7 %	0,0 %	0,0 %	0,0 %	0,0 %	0,0 %	3,6 %	0,0 %
	190,05	12,5 %	0,0 %	2,8 %	49,3 %	18,8 %	9,8 %	0,0 %	0,0 %	0,0 %	0,0 %	0,0 %	6,3 %	0,8 %
	230,05	13,3 %	0,0 %	9,1 %	64,2 %	8,6 %	2,0 %	0,0 %	0,0 %	1,0 %	0,0 %	0,0 %	1,7 %	0,0 %
Shales of Gilsønyggen	282,05	5,8 %	0,0 %	1,1 %	82,5 %	4,9 %	0,9 %	0,0 %	0,0 %	0,0 %	0,0 %	0,0 %	4,4 %	0,0 %
	330,05	5,5 %	0,0 %	2,0 %	83,8 %	6,5 %	1,0 %	0,0 %	0,0 %	0,0 %	0,0 %	0,0 %	1,3 %	0,0 %
	490,05	1,5 %	0,0 %	0,8 %	88,8 %	7,3 %	0,5 %	0,0 %	0,0 %	0,0 %	0,0 %	0,0 %	1,3 %	0,0 %
	530,99	2,7 %	0,0 %	1,7 %	87,6 %	1,2 %	0,0 %	6,0 %	0,0 %	0,2 %	0,0 %	0,0 %	0,5 %	0,0 %
	551,43	23,0 %	1,4 %	22,0 %	6,7 %	27,5 %	10,0 %	3,0 %	1,7 %	0,4 %	0,0 %	0,0 %	4,0 %	0,1 %
Grumant-byen	552,43	26,1 %	1,2 %	46,4 %	1,5 %	16,9 %	0,2 %	0,0 %	1,5 %	1,7 %	0,0 %	0,0 %	3,7 %	0,7 %
	557,58	23,5 %	4,0 %	49,8 %	7,5 %	7,0 %	3,0 %	0,0 %	2,8 %	1,3 %	0,0 %	0,0 %	1,0 %	0,3 %

Appendix 4: Mineral estimation from XRD

Depth	% Illite	% Chlorite	% Kaolinite	% Quartz	% K-feldspar	% Plagioclase	% Feldspar	% Calcite	% Dolomite	% Siderite	% Pyrite	Kaolinite /chlorite	Quartz/ Feldspar	Kaolinite/ Illite
Sandstones of Gilsonryggen														
110,05	14,3	11,2	3,1	40,8	4,6	14,4	19,0	0,7	5,6	5,1	0,2	0,21	0,68	0,18
115,90	19,8	15,2	2,5	33,1	4,8	17,8	22,6	0,8	3,4	2,3	0,3	0,14	0,59	0,11
120,05	15,2	17,3	2,2	41,7	3,5	13,9	17,4	1,3	2,8	2,0	0,0	0,11	0,71	0,13
130,05	12,9	12,0	2,6	44,4	4,0	12,9	16,9	3,5	3,3	4,3	0,1	0,18	0,72	0,17
132,50	24,2	13,4	4,2	35,9	0,7	17,8	18,5	0,6	0,7	2,3	0,1	0,24	0,66	0,15
138,80	20,0	15,4	2,3	29,1	2,2	17,4	19,6	3,6	3,9	3,0	3,0	0,13	0,60	0,10
140,05	22,1	12,4	5,6	37,2	4,0	12,8	16,7	1,1	1,1	3,6	0,1	0,31	0,69	0,20
150,05	13,9	10,2	3,4	41,6	5,2	17,7	23,0	0,9	1,6	5,2	0,2	0,25	0,64	0,20
<i>Average</i>	<i>17,8</i>	<i>13,4</i>	<i>3,2</i>	<i>38,0</i>	<i>3,6</i>	<i>15,6</i>	<i>19,2</i>	<i>1,6</i>	<i>2,8</i>	<i>3,5</i>	<i>0,5</i>	<i>0,20</i>	<i>0,66</i>	<i>0,15</i>
Siltstones of Gilsonryggen														
160,05	17,6	18,0	3,3	33,1	3,6	15,4	19,0	1,1	2,6	5,3	0,1	0,15	0,64	0,16
170,05	17,7	17,7	2,7	31,0	5,5	13,5	19,0	0,7	4,7	6,5	0,1	0,13	0,62	0,13
180,05	23,9	18,5	3,9	30,1	3,7	11,3	15,0	0,8	3,0	4,7	0,2	0,17	0,67	0,14
187,00	24,4	21,4	2,5	28,6	2,9	12,1	14,9	1,6	1,9	4,7	0,1	0,10	0,66	0,09
190,05	16,5	14,1	3,7	38,2	3,7	15,3	19,0	1,2	2,0	5,2	0,1	0,21	0,67	0,18
220,05	28,6	20,2	3,6	25,6	2,6	13,4	16,0	1,0	1,9	3,2	0,1	0,15	0,62	0,11
230,05	15,4	10,3	4,8	37,9	3,9	20,7	24,6	1,2	1,8	3,8	0,1	0,32	0,61	0,24
250,05	13,2	12,4	2,2	43,1	4,7	14,2	18,9	0,5	1,3	8,3	0,1	0,15	0,70	0,14
270,05	12,8	8,8	2,6	48,7	6,9	13,9	20,8	1,6	1,4	3,0	0,4	0,23	0,70	0,17
<i>Average</i>	<i>18,9</i>	<i>15,7</i>	<i>3,2</i>	<i>35,1</i>	<i>4,1</i>	<i>14,4</i>	<i>18,6</i>	<i>1,1</i>	<i>2,3</i>	<i>5,0</i>	<i>0,1</i>	<i>0,18</i>	<i>0,65</i>	<i>0,15</i>
Shales of middle Gilsonryggen														
282,05	13,2	10,2	2,7	44,2	6,4	12,2	18,6	0,7	1,5	8,3	0,6	0,21	0,70	0,17
290,05	12,1	10,6	3,1	42,5	8,1	15,0	23,1	1,6	0,4	6,1	0,4	0,23	0,65	0,21

Depth	% Illite	% Chlorite	% Kaolinite	% Quartz	% K-feldspar	% Plagioclase	% Feldspar	% Calcite	% Dolomite	% Siderite	% Pyrite	Kaolinite /chlorite	Quartz/ Feldspar	Kaolinite/ Illite
330,05	10,5	10,6	2,6	44,8	8,3	14,5	22,8	1,3	0,7	6,6	0,1	0,20	0,66	0,20
350,05	11,5	12,3	3,0	43,8	8,5	13,3	21,8	2,8	0,4	3,9	0,5	0,20	0,67	0,21
380,05	11,7	10,9	3,7	47,6	7,4	10,9	18,3	0,9	0,3	6,1	0,3	0,25	0,72	0,24
410,05	16,5	14,6	3,7	38,8	4,7	14,3	19,0	1,5	1,5	4,2	0,1	0,20	0,67	0,18
439,93	11,2	8,8	3,8	37,2	5,0	12,0	16,9	0,6	0,0	3,1	18,4	0,30	0,69	0,25
469,58	7,2	8,3	3,0	41,3	8,8	14,7	23,5	0,6	3,0	13,0	0,1	0,27	0,64	0,30
490,05	9,7	9,8	4,4	48,6	5,0	13,9	18,9	1,6	2,1	4,7	0,1	0,31	0,72	0,31
<i>Average</i>	<i>12,4</i>	<i>11,1</i>	<i>3,2</i>	<i>43,0</i>	<i>6,5</i>	<i>13,6</i>	<i>20,1</i>	<i>1,2</i>	<i>1,3</i>	<i>6,0</i>	<i>1,8</i>	<i>0,23</i>	<i>0,68</i>	<i>0,21</i>
Shales of lower Gilsonryggen														
500,05	14,9	12,9	5,8	31,6	3,2	13,4	16,6	0,9	1,1	16,1	0,1	0,31	0,66	0,28
517,08	8,7	5,7	4,7	37,2	3,4	12,5	15,8	10,8	3,1	1,6	12,2	0,45	0,70	0,35
525,05	11,1	4,7	3,3	37,1	8,6	10,8	19,4	1,2	0,7	1,4	21,1	0,41	0,66	0,23
528,45	9,3	7,7	5,1	33,6	6,2	10,9	17,1	0,5	1,2	2,0	23,6	0,40	0,66	0,35
528,75	12,4	7,8	4,1	38,0	7,1	10,7	17,8	0,1	0,7	0,0	19,0	0,35	0,68	0,25
529,05	11,0	7,5	4,4	38,4	7,8	14,5	22,3	0,1	0,0	0,7	15,7	0,37	0,63	0,29
529,35	16,5	8,4	7,0	35,9	5,7	9,9	15,7	0,5	1,1	1,6	13,3	0,46	0,70	0,30
529,75	12,7	8,2	6,1	42,3	6,2	12,4	18,6	0,0	0,0	1,1	11,1	0,43	0,69	0,32
530,05	13,4	8,5	9,2	44,6	2,7	14,5	17,1	1,0	0,8	2,6	2,9	0,52	0,72	0,41
530,40	9,8	6,7	6,4	45,5	5,7	12,6	18,4	1,4	1,1	8,8	1,9	0,49	0,71	0,39
530,65	11,6	6,3	5,8	38,3	3,8	13,7	17,5	1,3	1,8	15,8	1,5	0,48	0,69	0,33
530,99	12,6	6,8	5,4	42,2	3,4	15,3	18,7	1,9	1,7	4,7	6,1	0,44	0,69	0,30
531,05	13,5	7,9	5,0	44,6	8,3	14,9	23,2	0,2	0,4	3,3	2,0	0,39	0,66	0,27
531,35	10,5	8,3	6,8	48,2	3,1	16,3	19,4	0,7	0,4	2,8	2,9	0,45	0,71	0,39
531,68	18,1	10,1	6,4	41,6	6,6	12,7	19,3	0,1	0,7	3,6	0,3	0,39	0,68	0,26
531,99	16,6	8,2	6,7	42,8	7,4	13,0	20,4	0,3	0,4	4,1	0,5	0,45	0,68	0,29
532,05	15,0	8,6	6,8	41,2	4,6	10,2	14,8	0,1	1,2	12,2	0,1	0,44	0,74	0,31

Depth	% Illite	% Chlorite	% Kaolinite	% Quartz	% K-feldspar	% Plagioclase	% Feldspar	% Calcite	% Dolomite	% Siderite	% Pyrite	Kaolinite /chlorite	Quartz/ Feldspar	Kaolinite/ Illite
532,37	12,2	5,8	6,2	45,1	4,1	12,3	16,4	1,1	1,4	6,3	5,6	0,52	0,73	0,34
532,70	16,2	7,3	8,8	44,7	4,7	9,8	14,5	0,3	0,8	7,2	0,3	0,55	0,76	0,35
533,38	9,2	5,9	5,7	42,0	8,8	14,5	23,2	1,0	1,2	11,4	0,3	0,49	0,64	0,38
533,71	12,3	8,6	7,4	34,2	9,5	17,8	27,3	0,3	0,6	8,5	0,8	0,46	0,56	0,38
534,37	5,8	4,9	4,1	44,7	4,2	20,5	24,7	0,8	0,4	3,6	11,1	0,46	0,64	0,41
536,36	9,2	6,6	5,3	43,8	9,5	21,8	31,3	0,4	0,3	2,7	0,3	0,45	0,58	0,37
544,63	13,7	14,1	3,7	38,7	4,9	11,9	16,8	1,2	2,6	9,1	0,1	0,21	0,70	0,21
<i>Average</i>	<i>12,3</i>	<i>7,8</i>	<i>5,8</i>	<i>40,7</i>	<i>5,8</i>	<i>13,6</i>	<i>19,4</i>	<i>1,1</i>	<i>1,0</i>	<i>5,5</i>	<i>6,4</i>	<i>0,43</i>	<i>0,68</i>	<i>0,32</i>
Transition between sandstones of Grumantbyen and shales of Gilsonryggen														
551,43	5,4	7,3	2,3	31,9	13,5	33,4	46,9	0,5	1,0	1,3	3,4	0,24	0,41	0,30
Sandstones of upper Grumantbyen														
552,43	2,3	6,9	0,8	27,0	10,5	49,1	59,7	1,1	1,4	0,8	0,0	0,11	0,31	0,27
557,58	3,9	9,8	0,6	29,8	22,8	27,5	50,2	3,3	1,9	0,4	0,1	0,06	0,37	0,13
<i>Average</i>	<i>3,1</i>	<i>8,4</i>	<i>0,7</i>	<i>28,4</i>	<i>16,7</i>	<i>38,3</i>	<i>55,0</i>	<i>2,2</i>	<i>1,6</i>	<i>0,6</i>	<i>0,04</i>	<i>0,08</i>	<i>0,34</i>	<i>0,20</i>
Anomalous samples														
264,59	18,2	9,4	7,1	26,5	1,9	9,5	11,4	0,6	1,0	24,5	1,3	0,43	0,70	0,28
533,07	6,9	2,3	5,7	25,2	3,4	4,6	8,0	1,0	3,0	47,7	0,1	0,71	0,76	0,45
548,35	5,5	4,0	1,3	61,4	11,7	12,1	23,8	0,9	1,3	1,2	0,6	0,24	0,72	0,19

Appendix 5: Mineral estimations (XRD%) from clay fraction

d-spacing	10Å	7Å	7Å	13-10Å	2,79Å	2,71Å		
Depth	Illite	Kaolinite	Chlorite	Mixed-layered	Siderite	Pyrite	Kaolinite/ (Kaolinite+Chlorite)	Kaolinite/ (Kaolinite+Illite)
Middle Grumantbyen shales								
350,05	30,3	11,3	28,4	27,9	1,8	0,2	0,29	0,27
469,58	22,5	15,5	17,5	30,4	14,1	0,0	0,47	0,41
Lower Grumantbyen shales								
528,45	33,8	19,5	17,3	25,9	0,5	3,0	0,53	0,37
528,75	34,1	18,4	18,2	24,2	1,7	3,4	0,50	0,35
529,35	26,8	21,9	18,3	26,4	2,1	4,6	0,54	0,45
529,75	30,6	24,1	18,4	25,5	0,7	0,6	0,57	0,44
530,05	29,3	29,3	15,1	23,3	2,0	1,0	0,66	0,50
530,40	28,3	24,0	17,0	21,9	6,7	2,1	0,59	0,46
530,65	31,1	27,0	14,7	22,7	3,5	0,9	0,65	0,46
530,99	27,7	29,7	17,5	19,4	2,4	3,3	0,63	0,52
531,05	30,9	24,1	17,2	23,4	2,4	2,1	0,58	0,44
531,35	28,2	27,5	16,6	20,4	3,6	3,6	0,62	0,49
531,68	29,0	26,2	15,9	21,2	3,4	4,2	0,62	0,47
531,99	32,0	29,8	16,6	16,4	3,1	2,2	0,64	0,48
532,05	25,9	21,6	13,9	18,9	17,4	2,2	0,61	0,45
532,37	28,2	34,0	14,0	19,4	4,0	0,3	0,71	0,55
532,70	26,7	34,2	12,9	18,4	6,5	1,4	0,73	0,56
533,07	20,5	31,9	6,6	17,2	23,0	0,7	0,83	0,61
533,38	27,1	26,2	15,3	25,4	4,8	1,2	0,63	0,49
533,71	21,1	29,2	14,5	26,6	8,4	0,3	0,67	0,58
536,36	19,9	26,6	14,1	33,3	4,7	1,5	0,65	0,57
Average	28,0	26,6	15,5	22,6	5,3	2,0	0,61	0,47
Special sample								
529,05	42,3	24,4	22,9	5,3	3,3	1,9	0,52	0,37

Appendix 6: Rock Eval analysis

Depth	S1	S2	S3	TOC	TC	Tmax	S2/S3	HI	OI	PP	PI
110,05	0,27	1,28	0,24	2,13	2,57	435	5,33	60,07	11,26	1,50	0,17
140,05	0,39	2,37	0,32	1,09	1,52	435	7,41	218,03	29,44	2,80	0,14
170,05	0,28	1,03	0,50	1,01	1,67	436	2,06	101,58	49,31	1,30	0,21
190,05	0,35	1,82	0,68	1,19	2,87	437	2,68	153,20	57,24	2,20	0,16
200,05	0,20	1,31	0,33	1,09	1,79	439	3,97	120,40	30,33	1,50	0,13
230,05	0,25	1,55	0,52	1,33	1,61	439	2,98	116,89	39,22	1,80	0,14
250,05	0,26	1,28	0,55	1,16	1,64	441	2,33	110,06	47,29	1,50	0,17
270,05	0,26	1,23	0,36	1,01	1,24	441	3,42	122,02	35,71	1,50	0,17
290,05	0,26	1,34	0,35	1,15	1,42	442	3,83	116,93	30,54	1,60	0,16
330,05	0,22	1,04	0,52	1,03	1,50	441	2,00	101,27	50,63	1,30	0,17
350,05	0,25	1,24	0,31	1,15	1,24	445	4,00	107,64	26,91	1,50	0,17
380,05	0,22	0,91	0,47	0,85	1,07	446	1,94	107,30	55,42	1,10	0,19
410,05	0,20	1,00	0,32	1,08	1,30	445	3,13	92,42	29,57	1,20	0,17
439,93	0,18	0,73	0,18	1,18	1,43	445	4,06	61,76	15,23	0,90	0,20
490,05	0,21	0,81	0,22	1,04	1,14	451	3,68	77,96	21,17	1,00	0,21
500,05	0,35	0,96	0,52	1,26	1,80	448	1,85	76,25	41,30	1,30	0,27
509,05	0,50	1,59	0,26	1,42	1,48	446	6,12	112,29	18,36	2,10	0,24
513,05	0,46	1,23	0,20	1,19	1,25	441	6,15	103,45	16,82	1,70	0,27
515,05	0,34	1,13	0,12	1,16	1,24	441	9,42	97,67	10,37	1,50	0,23
517,08	0,42	1,02	0,16	1,21	1,24	442	6,38	84,30	13,22	1,40	0,29
525,05	0,68	1,29	0,11	1,47	1,53	438	11,73	87,87	7,49	2,00	0,35
527,05	0,65	1,74	0,22	1,41	1,52	440	7,91	123,84	15,66	2,40	0,27
530,99	0,35	1,01	0,28	1,08	1,57	449	3,61	93,43	25,90	1,40	0,26
532,37	0,21	0,83	0,23	0,82	1,01	448	3,61	101,33	28,08	1,00	0,20
534,37	0,65	2,30	0,19	2,92	3,18	444	12,11	78,85	6,51	3,00	0,22
538,38	0,61	2,41	0,28	2,30	2,77	443	8,61	104,74	12,17	3,00	0,20
544,63	0,44	1,45	0,33	1,67	2,09	448	4,39	86,77	19,75	1,90	0,23
548,35	0,17	0,62	0,19	0,79	0,87	448	3,26	78,53	24,07	0,80	0,22
549,75	0,28	0,91	0,22	1,45	1,56	448	4,14	62,76	15,17	1,20	0,24
552,43	0,09	0,10	0,20	0,18	0,23	445	0,50	55,56	111,11	0,20	0,47

Acknowledgments

I would like to express my gratitude to all those who gave me the opportunity to complete this master thesis.

First of all, I thank Professor Henning Dypvik and Professor Jenö Nagy at the Department of Geosciences, University of Oslo. Especially Henning Dypvik deserves big thanks for always being supportive and available (at all times!) for questions and discussions. Thanks to Jenö Nagy for interesting and helpful discussions and all the stories about polar bears.

Thanks to David Jargvoll for good teamwork both during field work at Svalbard and after. Also thanks to SNSK for donating core BH 9/05 to science and letting us use the storage tent for one week.

Berit Løken Berg has been very helpful in the preparation and carrying-out of the XRD-analyses and guiding me through the chaotic world of electron microscopes together with Turid Winje. Thanks to Mofak Naoroz who helped me out with the Na-Citrate treatment.

Thanks to Marit Sørli at the library of Department of Geoscience who has been very helpful.

Lunch breaks and work-outs with the guys at 217 (Dag, Christian and Hans Kristian) have been highly appreciated. Friday lunch cakes will be missed!!!

Thanks to Revolver and Dan Marius. Those beers at “Trivelig tirsdag” were a welcomed break!!

Last but not least, I owe a lot to my family, especially to Kjersti for all love and patience and to my parents for always being supportive.

